THE UNIVERSITY
of EDINBURGH

Formulating an improved *in vitro* hepatic model for drug development and toxicity testing

Frances 'Katie' Morgan

PhD - The University of Edinburgh - 2018

Table of Contents

List of Figures

List of Tables

Declaration of authorship

I hereby declare that the research presented in this thesis and the thesis itself was composed by myself based on work done at the Hepatology Department at The University of Edinburgh. The work done in collaboration has been stated.
This thesis has not entirely or in part been submitted for any other degree or professional qualification, apart from an experimental protocol developed and published in my final year dissertation for my BSc which was subsequently developed further for this thesis. The details of this are clearly stated in acknowledgements and Chapter 3 of the thesis.

Signed:

Frances Katie Morgan

Date: 13/08/18

Abstract

There is a need in the pharmaceutical industry for more informative and functional *in vitro* human models for drug testing as the currently used animal models have poor correlation to their human counterparts. The liver is the main organ of metabolism and xenobiotics detoxification. As such, a human hepatic *in vitro* model with improved metabolic functions similar to primary human hepatocytes (PHHs) could reduce the number of animals needed in pre-clinical testing and enhance the relevance of data obtained for subsequent *in vivo* testing.

Most immortalized hepatic cell lines are derived from carcinomas and do not retain a full range of functional activity *in vitro*. Here we have compared a novel hepatic cell line (HepaRG™), an intrinsic co-culture of hepatocyte and cholangiocyte-like cells, with the commonly used C3A cell line which is a derivative of HepG2 cells, in terms of metabolic competency. We found that the HepaRG™ cells out-perform C3As in a number of metabolic functions that include phase I and II metabolism as well as CYP activity. This makes the HepaRG™ cell line a strong alternative to PHHs for *in vitro* pre-clinical drug testing.

Next, we considered the platform for *in vitro* modelling. There are currently many tissue engineering models available with improved cell culture characteristics such as 3D spheroids, microfluidic models or 3D printing. However, these methods are costly and time consuming. We have used nanopatterned culture plates to develop a cheaper and faster platform that

will produce an enhanced human hepatic culture capable of sustaining a differentiated state for several weeks. Such a model will also allow for multi-experimentation or repeat dosage and would be a significant step towards reducing small animal *in vivo* testing and may correlate better to pre-clinical human trials.

We have specifically selected a nanopatterned and oxygen plasma treated culture system that has shown promise in differentiating other stem-like cells into organ specific cultures without the use of additional chemicals or hormones. By growing HepaRG™ progenitor (HepaRG-P™) cells on these prototype plates, we showed a much earlier differentiation compared with the established HepaRG-P™ cell culture protocols. Improved functionality at this early time point can also be seen in terms of CYP activity and markers of maturation. There is also some evidence to suggest specific zonation of mature HepaRG™s within this model.

Finally, a real-time, label–free monitoring of cell culture fitness, that encompasses a quantitative analysis of cell culture during treatment with a pharmacological agent, is desirable. An electrical cell impedance substrate (ECIS) platform that fulfils the above criteria was validated for real-time, non-invasive, monitoring of the HepaRG™ cell culture. Chlorpromazine (CPZ), a model cholestatic drug, was used to assess its effect on the HepaRG™ cells using ECIS. This study also gave us the opportunity for a more in-depth analysis of CPZ-induced cholestasis by not only analysing tight junctions, adhesion and cell membrane integrity, but also by studying the bile acid and xenobiotic transporters and the inflammatory and adaptive responses to CPZ-induced injury. We have shown disruption of membrane integrity,

changes in bile acid transporters and the regulation of both xenobiotic and phospholipid transporters as well as inflammatory markers.

In conclusion, in this thesis I have demonstrated that by using a novel cell line with novel prototype culture plates (nanopatterned) and a label free technique (ECIS) to measure cellular fitness, a much improved *in vitro* model of drug testing can be developed.

Lay Summary

The liver is the main organ of metabolism of drugs and nutrients. There is currently a need in the pharmaceutical industry for human cell models for use in drug testing as the currently used animal models have poor correlation to their human counterparts. There are two types of liver cells used in drug toxicity testing, immortalised human cells taken from tumours and primary cells from patients undergoing surgery. Primary cells are difficult to obtain and use for experimentation as they only last a few days, while immortalised cells can be kept for long periods within the laboratory and used for repeat experimentation. Though immortalised cells are more reproducible in experimentation they often lack some functions of primary liver cells. A human model using immortalized cells with improved metabolic functions, similar to primary human liver cells, could reduce the number of animals needed in pre-clinical testing and enhance the relevance of data obtained for subsequent pre-clinical human drug trials.

Here we have compared two immortalised lines, the novel liver cell line, HepaRG™, with the commonly used C3A cell line. The difference in these lines lies in the types of cells within each culture. HepaRG™ cells contain both liver cells which carry out major functions of the liver, and biliary cells which are part of the system responsible for moving bile throughout the liver while C3As contain only liver cells. This alone sets the HepaRG™ cell line apart making it more relevant in drug toxicity modelling as it shows potential for evaluating two intrinsic cells of the liver and gives the ability to also study drug transport mechanisms. In terms of metabolism, we found that the

HepaRG™ cells out-perform C3As in a number of metabolic functions and contain more enzymes akin to primary liver cells. This makes the HepaRG™ cell line a strong alternative to primary cells for pre-clinical drug testing.

Next we considered the way cells are grown for use in drug toxicity studies. There are currently many models available which manipulate the cells to improve enzymatic activity, and make them more like primary liver cells, such as growing cells into 3D spheres, using microfluidic models or 3D printing. However, these methods are costly and time consuming. We have used nanopatterned culture plates to develop a cheaper and faster platform that will produce an enhanced human liver cell culture capable of sustaining a mature and functional state for several weeks. Nanopatterned plates are different from traditional plates in that they contain small holes on the surface which may help the cells to adapt to their environment, as it may reflect and be more similar to the internal surface of the liver. Such a model will also allow for multi-experimentation or repeat dosage and would be a significant step towards reducing small animal testing.

By growing HepaRG™ progenitor (HepaRG-P™) cells on these novel plates, we showed that cells can become mature much earlier compared with the established HepaRG-P™ cell culture protocols. Improved functionality at this early time point can also be seen in terms of enzymatic activity.

Finally, the ability to monitor a cell line in real-time and quantify damage caused by drugs would be very beneficial in the pharmaceutical industry. We have used an electrical impedance platform (ECIS) that fulfils the above criteria and has been validated for real-time, non-invasive, monitoring of the HepaRG™ cell culture. Chlorpromazine (CPZ) is a drug used to treat

schizophrenia. It also causes damage to biliary cells which can promote jaundice and other liver diseases in patients. We used this drug and assessed its effect on the HepaRG™ cells using ECIS impedance. Electrical impedance monitoring involves using a small electrical current run underneath the cells to measure their ability to attach or adhere to the surface. Any disturbance to the cell culture caused by environment or chemicals can easily be seen through a loss of impedance. This study also gave us the opportunity for a more in-depth analysis of CPZ-induced toxicity by analysing the tight junctions between cells, the cells' ability to adhere to the culture surface and cell membrane integrity. We also assessed the proteins responsible for expelling toxic compounds out of the cell and found that these proteins were affected and disrupted based on the dose of CPZ. Primarily, the protein responsible for bile acid transport was impaired. Since bile acids are toxic to the cell, this highlights a possible mechanism for CPZ induced toxicity. We also assessed the inflammatory and adaptive responses to CPZ-induced injury and found that the inflammatory response increased as the dose of CPZ increased.

Here we have shown disruption of cell membrane integrity, changes in bile acid transporters and changes in the regulation of transport proteins responsible for expelling fats and drugs from the cell which may give insight into the damage caused by CPZ.

In conclusion, in this thesis I have demonstrated that by using a novel cell line with novel cell culture surfaces (nanopatterns) and a real-time impedance based technique (ECIS) to measure cellular fitness, a much improved *in vitro* model of drug testing can be developed.

Acknowledgements

I would like to dedicate this thesis to my father, Alfred Paul Morgan (January 20 1947-March 24 2016) who gave me the advice and love to overcome many challenges in my life and who taught me I could do whatever I set my mind to.

I would like to thank the many people who made this thesis possible, most importantly my supervisors Professor Peter Hayes and Professor John Plevris for supervision, support and guidance. I would also like to thank Dr Lenny Nelson for his friendship, encouragement and support. I would also like to thank Dr Natalie Homer for her training in LC:MS/MS during my final year as an undergraduate and initial establishment of the LC:MS/MS technique. Part of the comparison between HepaRG™ and C3A cells began in my final year dissertation and continued as part of my PhD. In particular, the experiment in regards to phenacetin turnover has previously been included in my final year dissertation. I would like to thank Kay Samuel for training in flow cytometry, hours of proof reading, coffees and her amazing sense of humour which kept me grounded. I also wish to thank Philipp Treskes for his training, friendship and support, Helen Grant for HPLC, Joanna Brzeszczynka for her help in molecular techniques and her investigation into the genes of interest for chlorpromazine, Marie Craigon, Pierre Bagnininchi for training in ECIS technology and Mai Abd El-Aziz for the comparison of HepaRG and C3A cells using end-point PCR.

Other colleagues and friends I would like to mention and thank; Ana Bryans, Filip Brzeszczynki, Christy Cox, Phillip Evans, Tracy Spears Graber for her

beautiful illustration, Austin Koh, Kelly Kirkpatrick, Jennifer Allan, Ted Wiga, Ada Kozlowska, Patricia Lee, Michael Mabbott, Daniel Soong, Steve Morley, Gareth Mayze and Eric Owens. Special thanks to Wesam Gamal who had a dual role as friend and ECIS advisor.

I would also like to thank my family for their love and support, especially my mother, Kathy McWilliams, my grandmother, Dorothy McWilliams and my Uncle Tom McWilliams. I would also like to thank my stepmother Dawn Morgan for her persistent encouragement. Thank you all for your unconditional love and guidance throughout my life.

I would like also to give heartfelt thanks to Margaret, Glenda, Bill and Peggy Johnson for their inspiration and encouragement, without which I would not have started on this road. Finally, I would like to thank my partner Bob Murphy and son William Smallwood for their tolerance and love throughout this endeavour. Indeed, it's impossible to add a specific thank you to all of the people who have encouraged and supported me throughout. I am very blessed and grateful.

Abbreviations

AC	Alternating Current
APAP	Paracetamol (N-(4-hydroxyphenyl)acetamide)
ATP	Adenosine triphosphate
BSA	Bovine Serum Albumin
C3As	HepG2/C3A cell line
cDNA	Complementary Deoxyribose Nucleic Acid
Ck19	Cytokeratin 19
Cm	Impedance measurement of cell membrane capacitance
CPS	Carbamoyl phosphate synthetase
CPZ	Chlorpromazine
Cq	Cycle
CYP450	Cytochrome P 450 enzyme
Da	Dalton
DILI	Drug induced liver injury
DMSO	Dimethylsulfoxide
DNA	Deoxyribose Nucleic Acid
DSQ	Disordered square array
EBL	Electron Beam Lithography

ECIS	Electric Cell Impedance Sensing
ECM	Extra Cellular Matrix
ELAD	Extracorporeal Liver Assist Device
ESI	Electron Spray Ionization
FBS	Fetal Bovine Serum
GAPDH	Glyceraldehyde 3-phosphate dehydrogenase
GOI	Gene of Interest
GPS	General Purpose Media
GS	Glutamine Synthetase
HBSS	Hanks Balanced Saline Solution
HepaRGs™	HepaRG™ Fully differentiated cell line
HepaRG™ P	HepaRG™ Progenitor cell line
HEX	Hexagonal
HIM	Hepatocyte Induction Media
HNF4α	Hepatic Nuclear Factor 4 alpha
HPLC	High Performance Liquid Chromatography
kHz	Kilohertz
LC:MS/MS	Liquid Chromatography with tandem Mass Spectrometry
m/z	Mass to charge ratio
MEME	Minimum Essential Medium Eagle
MeOH	Methanol

MIQE	Minimum Information for publication of Qualitative real time PCR Experiments
MMM	Maintenance and Metabolism Medium
MSC	Mesenchymal Stem Cell
MTT	3-(4,5-Dimethylthiazol-2-yl)-2,5-diphenyltetrazolium bromidefor
MW	Molecular Weight
NPS	Nanopatterned substrate
OCN	Osteocalcin
OCT	Ocular Coherence Tomography
OMP	Omeprazole
OPN	Osteopontin
PCR	Polymerase Chain Reaction
PDMS	Polydimethylsiloxane
PET	Polyethylene Terephthalate
PGA	Polylactic co-Glycolic Acid
PHHs	Primary Human Hepatocytes
qRT-PCR	Quantitative Real Time Polymerase Chain Reaction
RAND	Random
Rb	Impedance measurement of tight junctions
RBC	Red Blood Cell
RG	Reference Gene
RIF	Rifampicin

RIN	RNA Integrity Number
RNA	Ribose Nucleic Acid
SD	Standard Deviation
SOX9	SRY-Box 9 gene
SQ	Square
TBS	Tris Buffered Saline
TCP	Tissue Culture Plastic
TE	Tissue Engineering
TJ	Tight Junction
TJP	Tight Junction Protein
UoG	University of Glasgow
UP	Unpatterned
UV	Ultraviolet
V	Voltage
VEGF	Vascular Endothelial Growth Factor
W	Wattage
ZO1	Zonula Occludens 1

List of Publications related to this thesis

Abstracts

1. Poster: 'Chlorpromazine disrupts structural integrity of hepatic cell membranes in human HepaRG cells and initiates a pro-inflammatory response'
   K. Morgan[1], N. Martucci[2], A. Kozlowska[1], W. Gamal[3], F. Brzeszczynki[1], K. Samuel[4], P. Treskes[1], P. Hayes[1], L. Nelson[5], P. Bagnininchi[2], J. Brzeszczynska[1] and J. Plevris[1] BASL Conference, York, UK Sept 2018

2. Talk and Poster: 'Chlorpromazine disrupts structural integrity of hepatic cell membranes in human HepaRG cells and initiates a pro-inflammatory response'
   K. Morgan[1], N. Martucci[2], A. Kozlowska[1], W. Gamal[3], F. Brzeszczynki[1], K. Samuel[4], P. Treskes[1], P. Hayes[1], L. Nelson[5], P. Bagnininchi[2], J. Brzeszczynska[1] and J. Plevris[1] IBCA Conference, Edinburgh, UK June 2018

3. Poster: 'TOWARDS UNDERSTANDING THE MECHANISMS OF CHLORPROMAZINE- INDUCED HEPATIC TOXICITY USING A HUMAN HEPARG- BASED MODEL'
   J. Brzeszczynska[1], **K. Morgan[1]**, F. Brzeszczynski[2], K. Samuel[1], P. Hayes[3], J. Plevris[1] EASL Conference, Paris, France 2018

4. Talk/Abstract number 0282 'Directed-nanopatterning promotes earlier liver-specific maturation and outperforms metabolic function of differentiated human hepatic HepaRG progenitor cells on standard tissue culture plastic'
   Katie Morgan, Anna Bryans, Filip Brzeszczynski, Paul Reynolds, Michael Mabbott, Nicole Martucci, Graham Anderson, Steve Morley, John Plevris, Peter Hayes, Nikolaj Gadegaard, Leonard J Nelson eCells and Materials
   ISSN 2522-2350282 eCells and Materials, TERMIS EU Conference Davos, Switzerland 2017

5. Talk/Abstract number 0290 'Nanotopographical features influence derivation and selection of reference genes for progenitor cell differentiation protocols'

Katie Morgan, Filip Brzeszczynski, Joanna Brzeszczynski, Michael Mabbott, Paul Reynolds, Graham Anderson, Steve Morley, John Plevris, Peter Hayes, Nikolaj Gadegaard, Leonard J Nelson ISSN 2522- 2350290 eCells and Materials, TERMIS EU Conference Davos, Switzerland 2017

6. Poster: 'Mechanistic Insight into Chlorpromazine-induced Hepatic Tight Junction Disruption Using a Human HepaRG-based Liverbiochip Impedance,
   A Kozlowska, W. Gamal, **K. Morgan**, P. Treskes, P. C. Hayes, J. N. Plevris, P. O. Bagnaninchi, L. J. Nelson, 2015, UEG Week, October 24-28, 2015, Barcelona – Spain.

Papers

1. **Morgan, K.,** Martucci, N., Kozlowska, A., Gamal, W., Brzeszczynki, F., Treskes, P., Samuel, K., Hayes, P., Nelson, LJ., Bagnaninchi, P., Brzeszczynska, J., and Plevris, J. (2019) Chlorpromazine toxicity is associated with disruption of cell membrane integrity and initiation of a pro-inflammatory response in the HepaRG hepatic cell line. *Biomedicine & Pharmacotherapy,* Vol 111, pages 1408-1416

2. Nelson, L.*, **Morgan, K.*,** Treskes, P., Samuel, K., Henderson, C., LeBled, C., . . . Plevris, J. (2017). Human Hepatic HepaRG Cells Maintain an Organotypic Phenotype with High Intrinsic CYP450 Activity/Metabolism and Significantly Outperform Standard HepG2/C3A Cells for Pharmaceutical and Therapeutic Applications. *Basic & Clinical Pharmacology & Toxicology,120* (1), 30-37.
   ***equal first author**

Chapter 1 Introduction

1.1 The liver

The liver is located below the diaphragm in the right upper quadrant of the abdominal cavity. It is the largest organ in the body, weighing approximately 1.4kg. It is separated into a large right and smaller left lobe by the falciform ligament, and is able to regenerate in response to injury, but can fail when exposed to repeated toxic or metabolic insult.

1.2 Functions of the liver

The liver is responsible for synthesizing and breaking down molecules that are used to support homeostasis. These molecules comprise the main metabolic pathways within the liver. Although the liver is responsible for over 500 different metabolic functions they can be divided into 4, mainly; carbohydrate, lipid and protein metabolism and phase I and II detoxifying metabolic enzymes such as cytochrome P450s.

Carbohydrate metabolism is critical to maintain concentrations of dietary and endogenous glucose in blood within a narrow, normal range. Too much or too little glucose over an extended period of time can lead to pathologies such as diabetes, metabolic syndrome and non-alcoholic liver disease. There are various metabolic pathways that contribute to the control of the

production of glycogen or breakdown of glucose within the liver. However, the initiation of glycolysis or gluconeogenesis is governed by hormones produced within the pancreas.

The pancreas is made up of the islets of Langerhans (Lackie, 2010) containing a variety of cell types. Within the centre of the islet, β cells secrete insulin and amylin in response to blood glucose levels, but also in response to the rate at which the blood glucose levels are changing (Rang and Dale 2007). These β cells are surrounded by α cells which secrete glucagon, and Δ cells which secrete somatostatins (Rang and Dale 2007). Glucagon opposes insulin and somatostatins can inhibit both the secretion of insulin and glucagon. Secretion of these hormones is governed by potassium channels which determine the resting membrane potential of the cell (Rang and Dale 2007). ATP is the molecule which blocks potassium channels in islet cells and works alongside the membrane transporter glut-2 which work in tandem as a 'glucose sensor' (Rang and Dale, 2007). These membrane bound proteins are instrumental in the response to blood glucose levels and release the hormones mentioned above to maintain homeostasis in response to glycolysis or gluconeogenesis which mostly take place within the liver (Rang and Dale 2007).

Gycolysis, or the lysing of glucose to produce energy, takes place in the cytoplasm of cells throughout the body. Glycolysis is a ten step process that uses ATP and NAD to break down a 6 carbon molecule of glucose into 2, 3

carbon molecules of pyruvate. By doing this a net of 2 ATP and 2 NADH are created.

As NAD is needed to fuel glycolysis, NADH donates its hydrogen electron to the electron transport chain creating more ATP and leaving behind NAD+, which is then recycled back into the pathway to fuel glycolysis (Fantin et al., 2006). Pyruvate, as the final product of glycolysis, enters the citric acid cycle after transformation into Acetyl-CoA where it is used for further energy production in a process known as oxidative phosphorylation (Lunt & Vander Heiden, 2011 & Kumari, 2018).

Although glycolysis is present throughout all tissues, gluconeogenesis mainly takes place in the liver though gluconeogenesis can also be seen in the kidney cortex to a lesser extent (Gerich et al., 2001, Lemaigre and Rousseau, 1994). Gluconeogenesis is essentially the reverse of glycolysis as it generates glucose from non-carbohydrate substrates such as glycerol and amino acids (Gerich et al., 2001)(Figure 1.1). However, there are some differences in enzymes which are needed to circumvent the irreversible steps of glycolysis. This allows for the production of a glucose molecule which is readily available and secreted into the bloodstream. The gluconeogenic pathway assists in the maintenance of blood glucose levels through unidirectional enzymes; fructose-1,6-bisphosphatase, glucose-6-phosphatase and Phosphoenolpyruvate carboxykinase which are transcriptionally influenced by the hormones insulin, glucagon and

glucorticoids (Yoon et al., 2001). These hormones are produced in response to significant fluctuations of glucose and dietary need and as such gluconeogenesis is a target therapy for type II diabetes where decreased insulin secretion decreases glucose production and increases uptake of blood glucose by peripheral tissues (Rines et al., 2016).

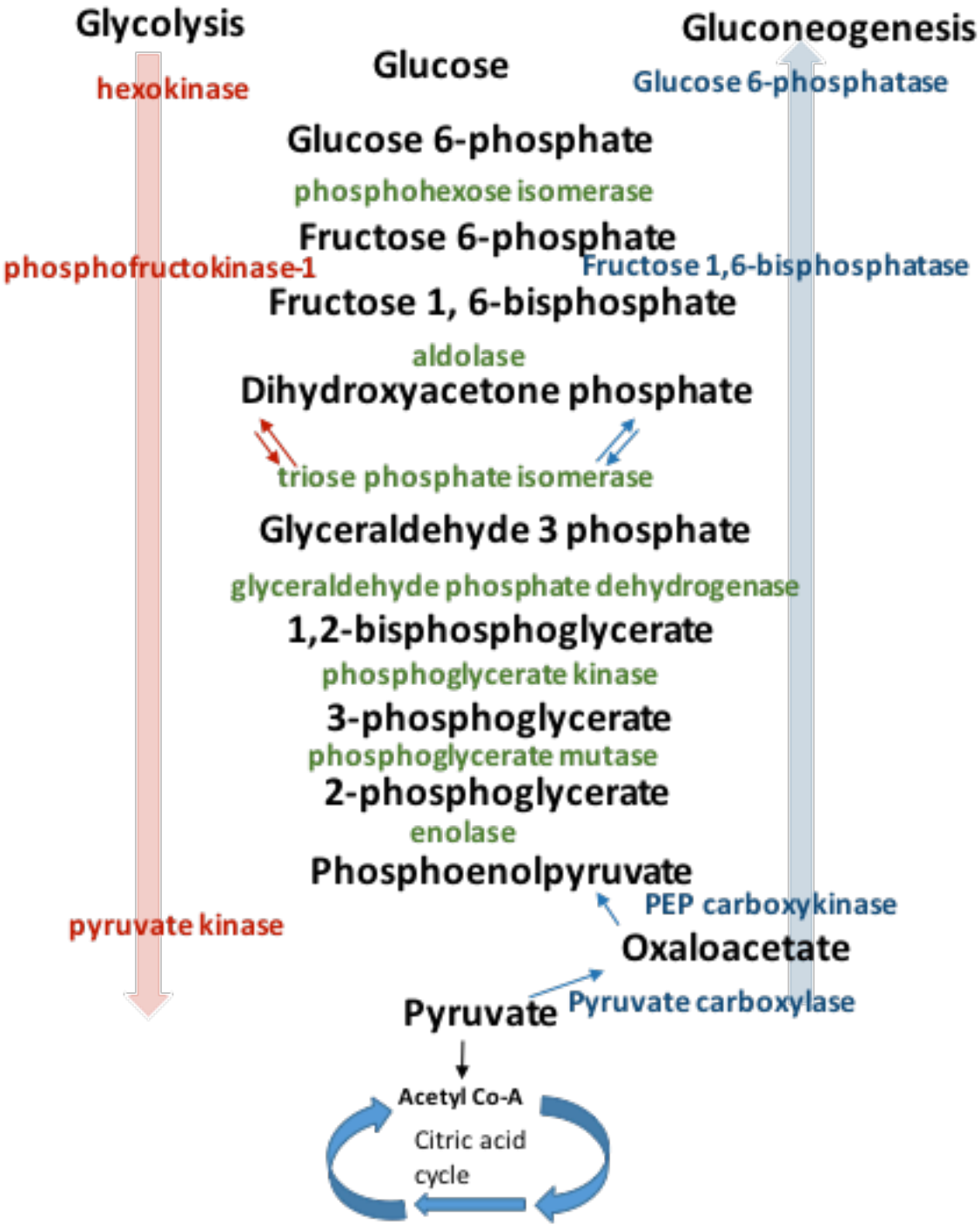

Figure 1.1: **Overview of glycolysis and gluconeogenesis metabolism and their relationship to the Citric Acid cycle.** Substrates are shown in black. Enzymes unique to glycolysis are shown in red while enzymes unique to gluconeogenesis are shown in blue. Enzymes used in both pathways shown in green.

The liver is also responsible for synthesizing around 800mg of cholesterol and phospholipids per day (Berg et al., 2002). These are packaged with lipoproteins and made available to the rest of the body or can be excreted in bile as cholesterol or bile acids

The biliary system is responsible for transporting waste products, bile and bile acids out of the liver. Bile acids emulsify fat by making the surface area of the fat molecule more available for digestion. Unsaturated fatty acids and cholesterol are important precursors for hormone production, while excess carbohydrates and proteins are converted into fatty acids and triglycerides which are then oxidised to produce energy.

Protein metabolism is responsible for deamination and transamination of amino acids, removal of ammonia from the body and synthesis of plasma proteins. Deamination is the breakdown of amino acids within the liver. Ammonia resulting from this process is toxic and therefore requires conversion to urea via the urea cycle, which is then easily excreted via the kidneys. Enzymes involved in deamination/transamination of amino acids are often used as clinical markers to assess liver damage. Alanine transaminase, alkaline phosphatase and aspartate aminotransferase are enzymes which can be used to analyse hepatic transport, damage and blockage of bile ducts. When abnormal concentrations of these enzymes appear in the blood, it can give an indication of liver injury or disease. Understanding how these

enzymes are used within the liver can point to particular pathology when levels of these enzymes in blood are outside normal levels.
The liver also synthesises proteins, mainly albumin which is responsible for maintaining osmotic pressure and transporting substrates, including, cholesterol, calcium, hormones, bilirubin and vitamins, throughout the body.

1.3 Microanatomy of the liver

1.3.1 Cell types within the liver

The liver is comprised of parenchymal hepatocytes and cholangiocytes and non-parenchmal cells including Kupffer cells, sinusoidal endothelial cells, oval cells and stellate cells.

Hepatocytes are responsible for the major metabolic functions of the liver having a role in maintenance of homeostasis, storage, digestion, and bile production. Cholangiocytes are epithelial cells that line and form the bile ducts and are responsible for exchange of bile acids and other molecules excreted by hepatocytes.

The oval cell is considered the hepatic progenitor cell as it retains the capability of differentiating into either a hepatocyte or cholangiocyte lineage (Takiya et al., 2013). This cell exhibits foetal markers such as alpha foetoprotein, but also hepatocyte specific and cholangio- specific markers albumin and cytokeratin 19 (CK19) respectively. Oval cells line the parenchyma and differentiate into hepatocytes or branch into ducts within the

canals of Hering towards the portal vein. The positioning of these cells determines differentiation based on the functions which they are required to perform (Takiya et al., 2013).

Also found in the liver are Kupffer cells which are part of the innate immune system and clear microorganisms, cellular debris and aged erythrocytes from the blood, while stellate cells are responsible for transport and storage of retinoids.

1.3.2 Structure of the liver and microanatomy

The liver is predominately made up of the right and left lobes divided by the falciform ligament. These lobes can be further devolved into 4 adding the caudate and quadrate lobes as anatomical markers or could be portrayed as 8 sections which are used as anatomical and surgical landmarks as each segment has its own vasculature and biliary drainage (Germain et al., 2014) (**Figure 1.1**).

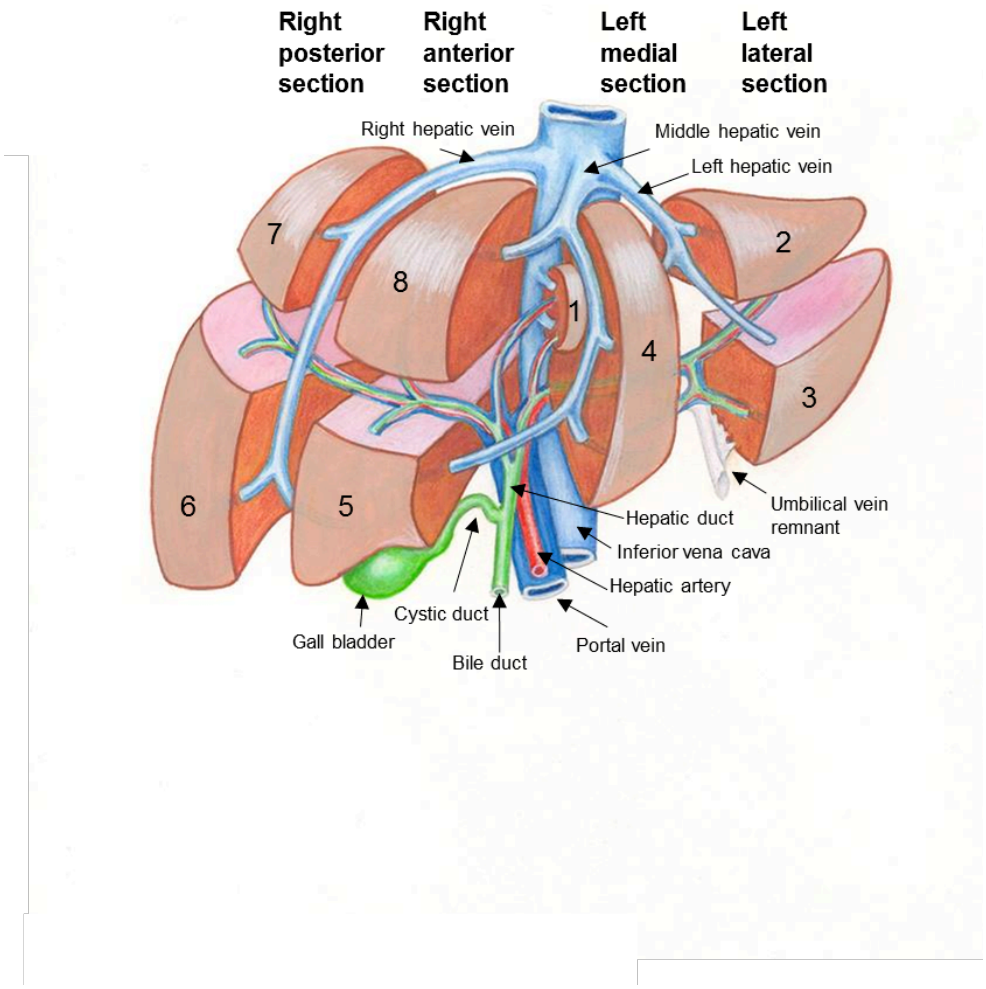

Figure 1.2: Depiction of the main quadrants and segments of the liver in correlation to vasculature: The right and left lobes of the liver can be divided into 8 sections each with their own vasculature. Here the vasculature of the liver is also represented in the form of the portal vein, hepatic artery, bile duct and hepatic vein. (Adapted from image © Spears-Graber, T. and reprinted with the permission of the illustrator)

The lobes of the liver are comprised of microscopic units referred to as lobules. Each lobule is hexagonal and has at its centre the central vein, whilst the portal triads (made up of the portal vein, hepatic artery and bile duct) can be seen at the periphery joined to the central vein by sinusoids (**Figure 1.2**). Hepatocytes form cords between sinusoids of the liver lobule. Cholangiocytes form the biliary ductules at the portal triad and thereafter the bile ducts.

The concept of the liver acinus was proposed in terms of delineating zones of specific liver function by shifting the focus of the central vein to the portal triad (Rappaport, 1958). Within the acinus the portal triad is central and 3 zones are delineated by function along the sinusoids culminating at the central vein (**Figure 1.2**)

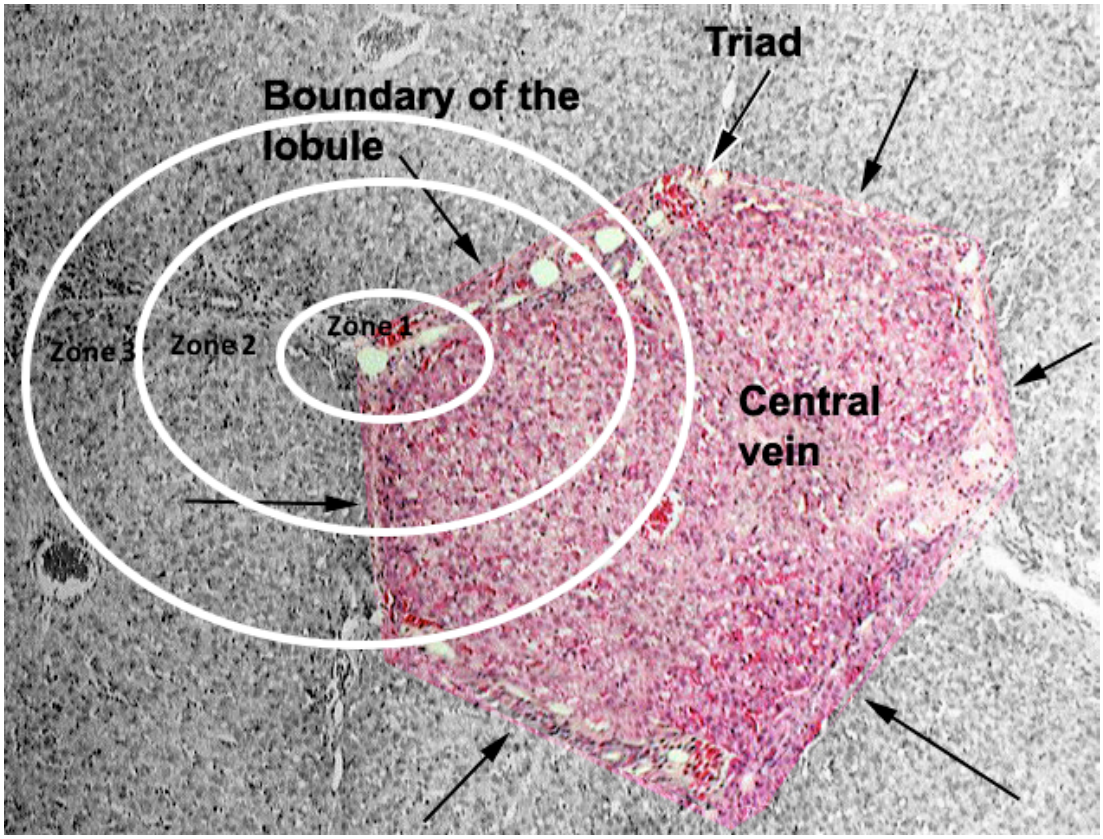

Figure 1.3: The liver lobule with specific zonation of the acinus: Histology slide depicting the hexagonal liver lobule with central vein and portal triad as well as representing the 3 zones of liver zonation which centre around the portal triad as proposed by Rappaport . (Figure modified from Caceci, T.www.doctorc.net/Labs/Lab20/LAB20.HTM)

The portal triad enables blood supply of the acinus via the portal vein and hepatic artery and supports the concurrent counter flow of bile. Oxygen gradient within the acinus is thought to be one of the most important regulators of the 3 zones (Keitzman, 2017). Zone 1 is located near the portal triad where oxygenated blood enters the liver. A gradient of oxygenation then occurs through zone 2 culminating in poor oxygenation in zone 3. Various pathways have been studied in an attempt to further categorise and understand liver zonation (Wnt/β-catenin, hedgehog). However, these pathways are often modulated by hypoxia (Keitzman, 2017). The concept of oxygenation in zonation will be discussed further in Chapter 4.

The sinusoids within the acinus are lined predominately with hepatocytes and cholangiocytes. However, oval cells, Kupffer cells and stellate cells are also found along the acinus.

1.4 Detoxification within the liver

1.4.1 Liver zonation

The acinus is split into 3 functional zones which are relative to their distance from the arterial blood supply. These zones are defined by a gradation of enzymes and functions as blood, metabolites and drugs pass through the sinusoids before entering the central vein. Within the gradient of the acini, each cell expresses the same genes, but the expression level of these genes

is determined by the position of the cell and function along the gradient. For example, cytochrome P450 enzymes (CYPs) needed for drug detoxification are located in the perivenous region, the last cell population which can detoxify blood before it is recirculated.

While this zonation is present *in vivo*, it is currently not possible to mimic liver zonation *in vitro*. Developing an *in vitro* model capable of *in vivo*-like metabolism that could represent one or more of the specific zones of the liver could be beneficial in drug toxicity testing and could further inform drug development.

1.4.2 Phase I/II/III metabolism

Metabolism within the liver involves enzymatic conversion of a substrate into various small molecules known as metabolites. Metabolites can be hydrophobic or hydrophilic. Hydrophobic compounds are not excreted by the kidneys so must undergo further metabolism into hydrophilic (or polar) compounds before they can be excreted in urine (Rang and Dale 2007).

The enzymes responsible for metabolism of drugs are found mostly in the liver. The main type of enzymes responsible for drug metabolism are cytochrome P450 enzymes. These enzymes are haem proteins categorized by the letters CYP and a further sequence of numbers and letters to distinguish specificity (Rang and Dale 2007). CYP enzymes metabolise drugs as well as exogenous compounds such as steroids, bile acids and

prostaglandins and are involved in cholesterol production (Zanger and Schwab, 2013).

Specific CYP enzymes can be induced by chemicals and therefore are important in understanding specific metabolic pathways and can be used in the study of liver zonation as most CYPs are highly expressed in the perivenous region of the acinus (Oinonen and Lindros, 1998). As such CYP enzymes differ between species and also within a human population and therefore can be a source of variability in DILI studies (Zanger and Schwab, 2013). It is also possible for more than one CYP enzyme to metabolise a particular substrate. For instance, CYP2E1, CYP3A4 and CYP1A2 all metabolise paracetamol (Tonge et al., 1998).

There are 3 main phases of drug metabolism. Phase I reactions are catabolic and often produce toxic products by way of oxidation, hydroxylation, deamination or hydrolysis (Rang and Dale, 2007). Phase II reactions usually follow on from phase I and involve conjugation of the products of phase I into more polar, or hydophillic, molecules making them less toxic (Rang and Dale, 2007). However, depending on the rate of the enzymatic reactions and availability of anti-oxidants, toxic products may not always be conjugated into less harmful metabolites and can cause damage leading to disease (Daly, 2007, Ma et al., 2017).

As phase II metabolites pass back into the small intestine the antiporter system, found within the liver and on the tips of the villi of the small intestine, move phase II metabolites out of the hepatocytes and mediate their excretion through the intestinal tract. This efflux system containing proteins such as P-glycoproteins and multidrug resistance associated proteins can be referred to as phase III metabolism and is crucial in the understanding of enterohepatic circulation (Xu et al., 2005).

1.5 Current hepatic models in drug development

There are three main stages of drug toxicity testing within the context of drug development. Initially, *in vitro* human cell lines are used to give an indication of toxicological effects of drugs. This is normally carried out on primary cells, immortalized cell lines or tissues from donors. After assessment of *in vitro* models, drugs and new pharmaceutical compounds are tested on small animals. Around, 79% of candidate drugs still enter clinical trials when liver toxicity has been shown in rodent and non-rodent experimentation (Ballet, 2015). This is because animals are used solely to determine the target organ, and not necessarily the level of toxicity, due to the interspecies differences in metabolism.

Initially, the target organ of toxicity is identified and toxic and therapeutic doses are established. Once a non-toxic, but therapeutic dose is determined, the compound can be tested further in large animal models before moving to

the third phase, clinical trials in humans. New compounds commonly fail at this stage due to metabolic differences between animals and humans. It is estimated that it takes 9 years for a new drug to be tested, validated and accepted (Chapman et al., 2013). False positives of liver toxicity are one of the major causes of drugs being withdrawn before pre-clinical human testing. While a holistic approach to drug toxicity is used in animal models, it is often due to the interspecies differences of CYP enzymes within the liver which mean that there can be no correlation between an animal and human model. A human hepatic *in vitro* model replicating *in vivo* CYP activity, capable of phase I-III metabolism would be beneficial in identifying the mechanisms behind liver toxicity in drug trials by helping to identify toxic metabolites at an early stage in toxicity testing. A model capable of real time assessment of hepatic cells would give an immediate indication of toxicity and show a profile of cell health before and after the addition of the test compound. Such a model may reduce the amount of animals needed and provide a better indication of how a compound will perform in the third stage of clinical trials. Within this chapter, the disparity of current models used for drug development will be discussed alongside ways of improving these models to ensure a more *in vivo* like hepatic construct. Platforms using hepatic cell lines in toxicity testing will also be investigated, highlighting pros and cons. Finally, a full model comprising cell type, platform and techniques of investigation will be put forward and tested in future chapters.

1.5.1 Disparity of current models

There are several issues with the current *in vitro* and *in vivo* models used within drug development. Firstly, most cell lines used are immortalized lines derived from carcinomas and do not retain a full range of functional activity *in vitro*. Secondly, small animals do not always mimic the same conditions that may be seen in human trials (Jemnitz et al., 2008). One main reason for this is the disparity CYP enzymes, especially in small animal models. This often leads to false positives and false negatives when used in clinical trials. Within the pharmaceutical industry, evaluation of new compounds and pharmaceuticals requires use of regulated animal models before passing on to pre-clinical human studies. This regulates the safety aspect of a new compound by testing specific organ toxicity and identifying compounds likely to be toxic to humans. However, animal models, large and small, used in prediction of human safety should regularly be reviewed, in light of these interspecies variations (Ballet, 2015). For instance, it has been shown that CYP450 enzymes in mice are structurally and functionally different from those of humans or that mice can be devoid of certain CYP enzymes altogether. (Ballet, 2015, Martignoni et al., 2006, Turpeinen et al., 2008). Therefore, it is not certain in rodent/murine models, that their metabolism of drugs or their model of drug induced liver injury (DILI) will be directly comparable with that of humans.

As scientific understanding and technology advances, *in vitro* models of drug toxicity should be considered as a way to bridge the gap between inter

species variations and understand the mechanistic pathways involved in individual drug toxicity studies.

Earlier use of appropriate hepatic *in vitro* models in the drug development process would ensure a more relevant use of animals saving both time and money reducing the possibility of pre-clinical attrition.

1.5.2 The need for better *in vitro* models in drug development

Considering the complications and limitations around drug withdrawl from the market, there is currently a need to improve the lengthy and costly process of developing therapeutics and make it more likely that they will be used at the bedside. The UK government is committed to ensuring the licenses granted under the Animals for Scientific Procedures Act (1986) must comply with the ethos of the 3R's. The 3R's consist of replacement, reduction and refinement of the use of animals within research. While there are rigid and detailed rules for the use of animals in experimentation, the model is still lacking in screening potential therapeutics and arriving at safe and effective compounds for general use.

1.6 Establishing an improved hepatic model of *in vitro* drug testing

A good hepatic *in vitro* toxicology model should have three key aspects.

1. A cell line that represents, as closely as possible, the *in vivo*, human hepatic conditions.

2. A platform for cell culture which is accessible, promotes best conditions for growth, maturation and viability and is cost effective.

3. Techniques to assess toxicity encompassing a variety of methods which consider aspects of cellular health and viability, timely measurements of toxicity to gain insight into possible mechanisms of action and assessment of molecular markers and protein translation.

1.6.1 Cell lines commonly used in hepatic drug/toxicity testing

1.6.1.1 Primary Human Hepatocytes (PHHs)

PHHs have been considered the 'gold standard' within toxicological and therapeutic research. Although this provides a human model without the inter-species issues described above, there are inevitably intra-species differences. Within a given human population, the level of CYP enzymes used in drug metabolism differ between individuals based on age, race, lifestyle and genetics. PHHs are difficult to obtain and can be derived from individuals already undergoing a procedure for liver disease suggesting the cells may not always represent a healthy population. However, it is possible to use hepatocytes from healthy donors. While this is preferable, there is still the issue of reproducibility as PHH represent one phenotype within a given population. Although using various phenotypes of PHH in drug toxicity testing may be advantageous and more representative of a population, it is perhaps

not ideal at faithfully proving the initial toxicity of a compound. In the early stages of toxicity testing reproducibility of toxicity and dose response on a stable culture is preferred. In addition, PHHs are expensive to produce, and difficult to culture. Most PHHs survive only days in culture as opposed to immortalized cell lines which can survive for weeks (Nelson et al., 2015). Therefore, a model based on PHHs is not sustainable for repeated experimentation due to the quantity of cells being finite, while using PHHs from different donors within a drug study will adversely affect reproducibility of results as even minor genetic variations can cause drug metabolism to vary, and complicate dosing regimes.

An alternative that is both comparable to human physiology and robust enough to remain viable *in vitro* for several weeks at a time is needed for many forms of liver research to continue, especially in light of current legislation to reduce animal testing across Europe and throughout the world.

1.6.1.2 Immortalized cell lines

Hepatic cell lines are commonly obtained from patients with hepatocellular carcinoma. These cell lines have been transformed by the molecular changes caused by the carcinoma and are immortal, meaning they can be maintained *in vitro* for many generations, allowing for reproducibility and high throughput experimentation. In the past, such cell lines have been found to be genetically unstable. There are a variety of immortalised human hepatic cell lines available including Huh-7, Fa2N-4, HepG2/C3A, Hep3B and HepaRG™. Numerous studies have compared these lines to PHHs showing

that many exhibit lower hepatic functionality and CYP activity. While each of these cell lines has a niche for *in vitro* work they fall short in overall interrelation to PHHs. For example, Huh-7 cells are known for their ease of transfectability and have been used extensively in Hepatitis C experimentation (Gomez-Lechon et al., 2010), Fa2N-4 cells display highly inducible CYP enzyme expression, though they are not always as high as PHHs (Hariparsad et al., 2008) The next section will focus on the most widely used cell lines, the HepG2/C3As and the HepaRG™.

1.6.1.2.1 HepG2/C3A

In recent years, the cell line of choice has been HepG2 and their derivative culture, C3As.

HepG2/C3As have been a favoured line because they are transfectable and can be induced to increase CYP expression (Lu and Cederbaum, 2008). As extensive work and characterization has been done within the Hepatology laboratory with the HepG2/C3A cell line it will serve as a standard cell line for comparison with emerging hepatic cell lines.

However, HepG2/C3A cells still show differences compared to PHHs. For example, it has been observed that even when grown in 3D hydrogel, polarity in HepG2 cells is less evident than in other cell lines (Bhattacharya et al., 2012). Furthermore, to establish acceptable levels of CYP activity within the C3A cell line, transfection, co-culture and metabolic pre-conditioning (Filippi et al, 2004) have to be routinely used to force these cells into an acceptable phenotype for drug toxicity studies. C3A cells have also been shown to be

deficient in terms of hepatic polarity and also phase II and III metabolism, making them unsuitable for many *in vitro* applications (Nelson et al., 2017).

1.6.1.2.2 HepaRG™ cell line

The human organotypic HepaRG™ cell line was isolated from a female in her 30's who had grade I differentiated hepatocellular carcinoma, concurrent to hepatitis C (Gripon et al., 2002). The HepaRG™ cells are unique in that they are a bipotent line, which can be differentiated to generate an intrinsic co-culture of hepatocytes and cholangiocyte-like cells. This culture shows stability for 4 weeks and beyond, by retaining differentiated characteristics, which presents HepaRG™ cells as a viable model for drug toxicity testing. They are comparable in phenotype and function to PHHs, and can also be used for repeat experimentation (Nelson et al., 2017).

One of the main reasons for their functionality could be attributed to their plasticity as a bipotent adult progenitor/hepatoblast cell line. HepaRG™ cells can be taken through a formal differentiation program which provides researchers with a tool for *in vitro* study of early hepatic development and possibly also hepatocyte dedifferentiation in response to injury or metabolic challenge

In contrast to other hepatic cell lines, fully differentiated HepaRGs™ are a unique co-culture of cholangiocyte-like and hepatocyte-like cells, which makes them a useful model for drug transporter studies and for use in cholestatic models such as cholestasis, fibrosis and cirrhosis (**Figure 1.3**) (Le Vee et al., 2013)(Szabo et al., 2013).

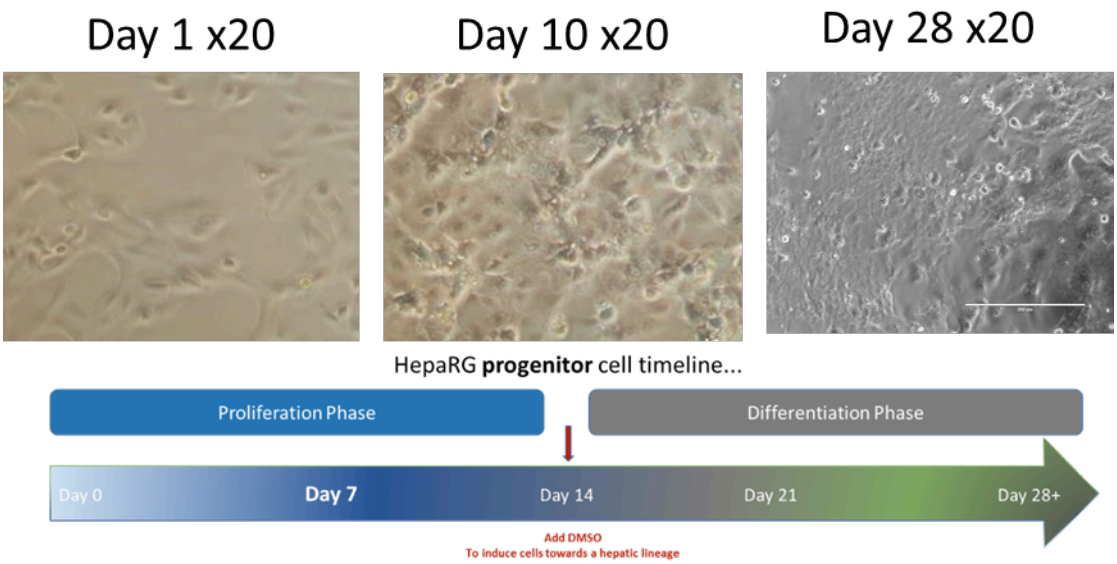

Figure 1.4 HepaRG™ progenitor (HepaRG-P) time line: Phase microscopy showing a typical HepaRG-P cell culture at days 1, 10 and 28 and timeline of proliferation and differentiation phases. HepaRG-P cells go through two distinct phases of proliferation and differentiation over a period of 28 days. DMSO is added at day 14 to induce and maintain differentiation and a co-culture of hepatocytes and cholangiocytes is seen at day 28. Scale bar at day 28 represents 200μm.

Spectral karyotyping of HepaRG's™ has revealed a stable and unique phenotype which is still consistent after several passages. Only 2 abnormalities have been seen after 40 mitoses. All samples tested, have shown evidence of an additional chromosome located at chromosome 7 and a translocation between chromosome 22 and 12, though no reported loss of sequence is evident (Gripon et al., 2002). (**Figure 1.4)** Even taking these two anomalies into consideration, HepaRG™ cells display a robust phenotype after multiple passages lending confidence to their repeated and extensive use in pre-clinical drug testing. (Guguen-Guilliozo, 2014).

HepaRG™ cells are also available in a progenitor (HepaRG™-P) culture. These cells have de-differentiated into a hepatoblast-like cell and although bipotent, still retain a plasticity not seen in the fully differentiated HepaRGs™. These cells eventually differentiate into a co-culture of hepatocytes and cholangiocyte-like cells after 4 weeks following the introduction of dimethylsulfoxide (DMSO) to the media at day 14. The advantages of this line over the fully differentiated HepaRG™s is the ability to study developmental and maturation markers under a variety of conditions. The HepaRG™-P cells differentiation capacity allow the study of various tissue engineering platforms, taking advantage of their plasticity by culturing them on scaffolds and various surface substrates that may give rise to an improved phenotype and may provide a more realistic biochemical basis for future drug discovery and toxicity testing.

HepaRG™ cells have been widely reported as a surrogate to PHH. Since 2002 many studies have characterised HepaRG™s in terms of its use in DILI studies, CYP activity, urea cycle, expression of membrane bound transporters, viral infectibility, spheroid production and uses within tissue engineering. Table 1 highlights advantages and disadvantages highlighted within this chapter.

Table 1: Characteristics of HepaRG™ co-culture

Advantage	Disadvantage
Co-culture of Hepatocytes and cholangioccytes (Cerec et al., 2007)	Cost (cost of cells and specialised media)
Ability to transdifferentiate through a bipotent progenitor culture which shows plasticity relevant to PHH (Cerec et al., 2007)	Derived from human hepatocellular carcinoma.
Longevity in culture (up to 4 weeks) (Guillouzo et al., 2007)	Limited nitrogen fixation and presence of Carbomyl Phosphate Synthetase through urea cycle (Moedas et al., 2017)(Lubberstedt et al., 2011)

Functional sinusoidal and canalicular drug transporters similar to PHH (OCT1, OATP-B, OATP-C, NTCP, MRP2, MRP3, BSEP and P-glycoprotein) (Le Vee et al., 2006)(Guillouzo et al., 2007)	Glutathione transferase M3 gene less expressed than other hepatic cultures (Gerets et al., 2012)
Supports infection with Hepatitis B (Gripon et al., 2002)	Poor CYP2D6 expression (Gerets et al., 2012)
Higher levels of albumin than PHH (Lubberstedt et al., 2011)	Cells not as predictive for induction/DILI studies (Gerets et al., 2012)(Sison-Young et al., 2017)
Higher CYP activity than HepG2/C3A. CYP levels comparable to PHH for main CYPs such as; CYP3A4, CYP1A2, CYP2C9, CYP2C19 and CYP4B1 (Nelson et al., 2015)(Gerets et al., 2012)(Guillouzo et al., 2007)	
Phase I, II and III enzymes along with nuclear receptors CAR PXR and AhR (Gerets et al., 2012)(Aninat et al. 2006)(Guillouzo et al., 2007)	

3D spheroids viable for several weeks in culture which maintain high functionality compatible with high throughput analysis (Martucci et al., 2018)(Leite et al., 2012)(Shin et al., 2018)	

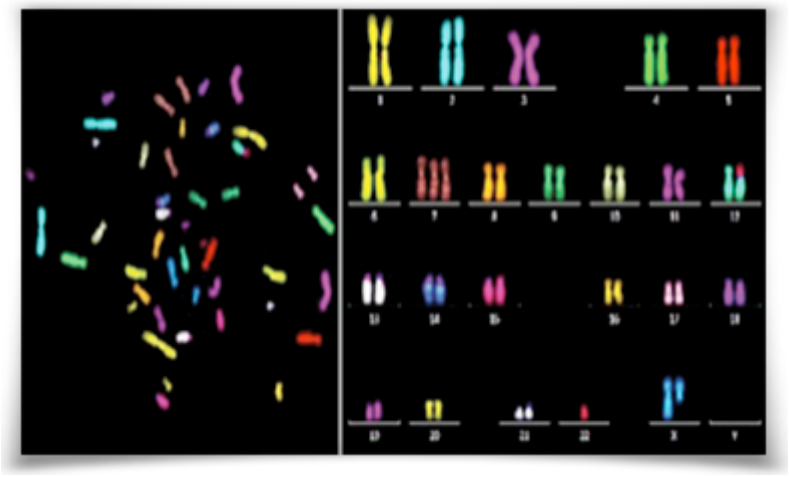

Figure 1.5 Karyotype of fully differentiated HepaRG™ cells shown at passage 12. Karyotyping of fully differentiated HepaRG ™ cells shows a stable karyotype for up to 20 passages. A translocation is present between chromosomes 22 and 12 and there is evidence of an additional chromosome located at chromosome 7. No loss of sequence is evident and cells remain viable after 46 mitosis.(Figure obtained from Biopredic International https://www.heparg.com/rubrique-features 2018)

1.6.1.3 Improvement of current models by altering phenotype using tissue engineering techniques

It is known that surface topography in cell culturing impacts proliferation, adhesion, phenotype, gene expression and function of cells (Dalby et al., 2007)(Schernthaner et al., 2012)(Galli et al., 2012)(Kim et al., 2013). The interactions of cells with their environment is central to many biological processes, and it is well known that cells respond to environmental, chemical and topographical cues *in vivo*. This interaction can be exploited with the use of tissue engineering techniques by culturing cells on various synthetic materials, substrates and scaffolds, including 3D scaffolds, to manipulate cells into a desired response (Martucci et al., 2018) prompting earlier differentiation through environmental cues. One way to create an altered surface topography is with the application of 'roughness' to traditional cell culture substrates (Wei et al., 2013) Various types of sandpaper, polymers and chemicals have been used to create rough surfaces that enhance cell adhesion (Wang et al., 2016) (Lin et al.,2014). However, it is difficult to get accurate reproducibility as this is a manual technique applied to the surface of culture plates and varies with each application.

Grooves, pores, nodes and other notches and depressions are found within the basement membranes of cells/tissues in the body. Various types of nanotopography have been employed to mimic the *in vivo* basement

membranes and to provide a more relevant cell culture for *in vitro* experimentation (Micholt et al., 2013).

1.6.1.3.1 Nanopatterning

Nanopatterning has been used to create an uneven surface of pits, either random or patterned, within the surface of the tissue culture plastic, which has been shown to have an effect on cell adhesion and migration (Qian and Wang, 2010).

1.6.1.3.2 Origins of nanopattern substrates

Textured substrates have been used for more than 100 years in cell culture and *in vitro* applications (Qian and Wang, 2010). In recent years the use of nanopatterned substrates (NPS) has gained popularity in applications such as orthopaedics where Dalby's (2007) use of nanopatterns with mesenchymal stem cells promoted a spontaneous differentiation into osteoblasts without the use of specialized media.

Nanotopography has been increasingly used in the assessment of cellular adhesion, proliferation and function of stem-like and progenitor cell lines. To mimic the *in vivo* effect of pattern or pores, multiple cell types such as mesenchymal stem cells, fibroblasts, smooth muscle cells and endothelial cells have been exposed to NPS or nanopits to assess their adhesion, migration, differentiation and function (Yim et al 2005).

The benefit of using a pattern over techniques such as roughness is the reproducibility for experimentation. Using electron beam lithography,

templates can be created to imprint the same pattern on multiple cell culture slides, making them highly reproducible.

Cellular migration is controlled by two cues; internal phenotypic cues and external mechanical cues (Qian and Wang, 2010). Internal cues are usually governed by integrin mediated adhesions, formation of attachments (which includes altered actin organisation), and the ability to contract and detach from the substrate (Qian and Wang, 2010). While external cues pose a structure for the cell to grow around (as in the case of scaffolds) or constrain the cell culture in terms of space causing a change in cell behaviour (Dorcemus et al., 2017). It has been shown in various experiments with different cell types that cells grown on nanopatterns exhibit filopodia (Qian and Wang, 2010). This is an example of internal cues causing conformational changes to cell structure resulting in altered cell function, i.e. on a molecular level.

To illustrate deeper the molecular changes caused by patterned substrates, we can consider the translocation of β catenin which is a multifunctional protein regulating cell adhesion and gene transcription (Schernthaner et al., 2012). Schernthaner et al., (2012) showed a difference in translocation of β-catenin between cells cultured on flat, nano rippled and nano walled surfaces. On flat polyethylene terephthalate (PET) β-catenin was mainly localised around cell-cell adhesions. However, on PET surfaces with nanostructured foils and ripples, β-catenin was seen primarily in the nucleus (Schernthaner et al., 2012).

This shows a type of molecular/nuclear activation induced following culture of cells on nanopatterned substrates. Taking into consideration that further initiation of transcriptional programs such as β-catenin is usually destroyed in the cytosol, and does not migrate to the nucleus if there is absence of Wnt signalling, it is logical to presume an activation of Wnt signalling in the cells grown on nanopatterned ripples, as β-catenin was found predominantly in the nucleus (Schernthaner et al., 2012). These are just some examples of the morphological and molecular changes that can be seen in an established culture when grown on nanopatterned surfaces.

1.6.1.3.3 Nanopattern manufacturing techniques

The two main methods of nanopatterning used today are soft lithography and electron beam lithography. Soft lithography is a technique that uses a polydimethylsiloxane (PDMS) stamp to transfer patterns by micro-contact printing (Qian and Wang, 2010). The surface is coated with a photoresist film and exposed to ultraviolet (UV) light on a silicon support. A mask can be applied and the photoresist dissolved leaving a master pattern around the original mask (Qian and Wang, 2010). At this point, functional proteins and molecules can be added to enrich the nano-environment for cells. This form of nanopatterning is popular due to its cost effectiveness, flexibility and wide application.

Electron beam lithography (EBL) is a positive printing method that has been used to create ordered arrays (Vieu et al., 2000) Within this model a mould is produced using a set pattern and can be repeatedly used to print this pattern into a heated polymer. This polymer is then coated with either oxygen plasma or a corona surface treatment that allows cells to adhere in culture. However, the nanotopography of the extracellular matrix ECM *in vivo* is not as uniform or ordered as these arrays and therefore it can be hard to extrapolate similarities and differences between EBL topography and *in vivo* ECM conditions. This method is usually more costly than other methods, but is the most reproducible (Qian and Wang, 2010).

The initial mould development is both time consuming and expensive, and therefore not convenient for prototype production. However, the use of pre-existing moulds is more affordable and enables high through-put production (Stormonth-Darling and Gadegaard, 2012). The University of Glasgow (UoG) have developed a nanopattern manufacturing protocol that, once established, reduces the cost of electron beam lithography (EBL) and facilitates high throughput manufacturing of NPS using injection moulding for biological applications. (Stormonth-Darling and Gadegaard, 2012). This technique is also more reproducible and expedient than focused ion beam or laser ablation and provides a platform on which a variety of inlays can be used in different configurations to replace the need for multiple tools (Stormonth-Darling and Gadegaard, 2012).

1.6.1.3.4 Cell types used in nanopatterned cultures

There are many examples of different tissues which have been cultured successfully on nanopatterned substrates under a variety of experimental conditions. Using the human fibroblast h-tert cell line, Curtis et al. (2004) compared the orientation of cell culture on hexagonal or orthogonal patterns, plated in such a way that low adhesion and cell-cell interactions would not interfere with measurement of orientation. At 24 hours, cells grown on orthogonal patterns showed a disposition of 90 degree separated orientation while those grown on hexagonal patterns showed a 120 degree orientation indicating that surface pattern affects cell growth (Curtis et al., 2004).

This work also showed that adherence to ordered NPS is low when compared to unpatterned planar controls (UP), while adherence to random patterns is not dissimilar to UP. They further demonstrated that after 24 hours growth on NPS, cells appear more organised as compared cells grown on tissue culture plastic (TCP) (Curtis et al., 2004).

Dalby et al., (2007) used ordered and disordered nanopits to examine how mesenchymal stem cells (MSCs) adhere to nanotopography and whether surface topography could direct their differentiation toward an osteoblastic lineage. Their plates were embossed with nanopits of 120nm in diameter and 100nm in depth, arranged in 5 different topographies; an ordered square array (SQ), hexagonal array (HEX), disordered square array (DSQ) with pits

displaced at 50nm apart, disordered square array (DSQ50), and a disordered array with pits displaced at 20nm apart (DSQ20) and a random placement of pits (RAND). Ordered nanopits had negligible effect on MSC adhesion or differentiation, whereas, MSCs grown on disordered nanopits displayed improved adhesion and differentiation in the absence of supplements that normally drive differentiation. MSCs grown on DSQ50 showed an aggregated cell population with early formation of nodules containing osteopontin (OPN) and osteocalcin (OCN) positive regions. Extending culture to 28 days, minearlization within discrete nodules was observed. It is important to note that cell aggregation, expression of OPN and OCN and evidence of mineralization was only seen on DSQ50 (disordered array with pits displaced at 50nm apart). To further confirm osteoblastic formation, osteospecific macroarrays were used to analyse mesenchymal stem cell (MSC) differentiation across all 5 nanotopographies. This confirmed that MSCs cultured on DSQ50 exhibited up-regulation of osteogenic markers required for osteoblast adhesion, differentiation and collagenous matrix formation.

1.6.1.3.5 Applications of nanotopography

Medical implant devices are now being manufactured to promote increased adhesion of native cell populations which will aid in patient recovery. This is most notably being applied in orthopaedics where implants treated with chemicals to induce a ‘roughness’ aid in joint replacement by promoting adhesion of innate cells (Zareidoost et al., 2012)

Most notably, this technique also provides the ability to assess bacterial adhesion to medical implants. One of the drawbacks of medical implants such as knee, hip and shoulder replacement namely, is the ability of bacteria to form biofilms which can become resistant to antibiotic intervention. It has been shown that using specific patterns and types of roughness can discourage the growth of bacteria and improves cellular adhesion of healthy tissue while remaining biocompatible with bone regeneration and innate tissue response (Jaggessar, et al., 2017).

Nanotechnology is also useful in other areas, for example on biocompatible titanium in vascular stents where it reduces platelet adhesion, increases nitric oxide and enhances viability (Mohan et al., 2012), thus reducing the likelihood of late stent thrombosis sometimes seen when using unpatterned metallic stents.

Other applications have included investigating the effect of nanotopography on cell cycle.

Skeletal stem cells showed variation in cell cycle which affected growth and renewal when grown on specific patterns similar to those used in previous studies on MSCs (Lee et al., 2017). In this instance, transcriptomic and western blot analysis was used to monitor pathways involved in cell cycle regulation and to elucidate the mechanisms of cellular renewal (Lee et al., 2017)

While nanotopography shows promise in terms of regulating cellular differentiation, highlighting pathways involved in regeneration and in the advancement of medical implants, there are drawbacks with this technology. First, there is currently an aspect of 'trial and error' when assessing NPS for use in specific tissue. What is optimal for one cell type, may not be optimal for another. Introducing a new cell type requires analysis on many different types of nanopatterns, to investigate if changes are occurring. Secondly, current models operate on a 2D surface which does not completely mimic the highly structured 3D extra cellular matrix. These drawbacks, alongside the cost of producing nanotopographical substrates, will need to be overcome to accentuate the usefulness of this technology.

1.6.1.3.6 Surface treatment of cell culture plates

While nanotopography plays a key role in regulating adhesion, proliferation and differentiation, surface chemistry may also be important. All cell culture plates (NPS or TCP) are coated in some way to create an environment promoting cellular adhesion (Ramsey et al.,1984). Hydrophillic surfaces allow proteins in media to adhere to the substrate and form a layer whereby cell adhesion is supported. If cell culture surfaces are not treated, they remain hydrophobic and cells will not attach. There are two main types of surface chemistry, each having pros and cons for manufacture and cell growth.

1.6.1.3.6.1 Oxygen plasma:

One technique used to create an adhesive surface is oxygen plasma coating. Uncoated plates are placed in a vacuum chamber containing only oxygen.

Application of a charge across inductive electrodes produces a plasma yielding ozone that coats the plate. The type, or description, of oxygen plasma treatment is determined by wattage and time of exposure. For example, a plate could be treated at 40W for 30s or 80W for 60s or any variation of time and wattage. However, this process needs to be optimized for individual cell lines or applications as cellular adhesion differs from one cell line to another. A high wattage for a long period of time could have implications on the physical surface of the culture plate while a short low watt treatment may not be sufficient for cellular adhesion (Nedela, Slepicka and Svorcik, 2017).

1.6.1.3.6.2 Corona treatment:

A corona treatment is currently used in many industry standard tissue culture plates. Plates are coated on the bench using a discharge of high voltage to create a corona plasma that ionizes the air around a conductor. In contrast to oxygen plasma, both oxygen and nitrogen are used in coating plates (Izdebska, 2015).

1.6.1.3.6.3 No treatment:

It is also important to mention untreated cell culture grade plastic. Untreated plates are hydrophobic, and are used when adhesion is not wanted or necessary such as the study of cells in suspension or within microbiology applications (Krasowska and Sigler, 2014).

Considering the plasticity of the HepaRG™-P cells we will assess this culture on a variety of NPS based on Dalby et al's (2007) technique and prototype NPS. We will aim to assess whether NPS accelerates differentiation and maturation of HepaRG™-P cells without the addition of DMSO and compare to standard cultures grown on TCP.

While some laboratories use a technique of measuring the angle of a water drop to assess adhesive properties of a rough or patterned surface, we will be assessing adhesion of cells by comparing treated vs untreated plates (Martines et al., 2005, Olin et al., 2013). This is again is to improve reproducibility and possible contamination of the model. Water angle measurements can be influenced by temperature, humidity, ambient airflow and other variables on the day of analysis. Whereas, assessing adhesive properties of plates is better regulated as both treated and untreated plates can be handled and assessed at the same time and under the same conditions. By growing cells on plates (treated and untreated) and assessing morphology and viability we will compile a more complete and reproducible picture of the effects of surface treatment.

1.6.2 New techniques: real time impedance-based assays

1.6.2.1 Improving current models of drug toxicity analysis using a real-time impedance-based assay

While tissue engineering, in the form of substrate manipulation, plays a role in attempting to reproduce a more *in vivo*-like environment, it can only be visually assessed through changes in morphology or quantitatively assessed through assays. As most assays are end-point, they only provide a snapshot of how a drug or compound has affected the cell culture after it has been administered. A real time assessment of a culture before, during and after administration of a compound would be beneficial to informing the pharmaceutical industry.

1.6.2.1.1 Impedance based assays

Currently, there are a number of assays available to measure aspects of cellular health before and after administration of a drug or compound. Some are end-point assays such as the Promega Cell titer-glo™ which measures total ATP in total cell lysates. By comparison, non-lytic assays like PrestoBlue™, can be used repeatedly on the same cell culture to give an indication of the rate of change in cell viability through the reducing capability of the cell. However, PrestoBlue™ still only gives an indication of cellular health at specific time points in culture. At best, you can create a series of snapshots rather than an end-point result as from the ATP assay.

A high throughput, real time, label-free means of measuring the cellular effects of drug toxicity would be beneficial to the pharmaceutical industry as it would supply a way to assess the effects of new compounds in real time.

The use of electrical impedance-based monitoring of cell cultures has gained credence within the last decade and there are now a number of systems available for use in toxicology and wound healing models. Impedance based assays are capable of giving a real time assessment of cell culture health by growing cells on electrodes and using a small electrical current to assess cellular adhesion, tight junctions and overall membrane capacitance through measurements of impedance.

1.6.2.1.2 Electric Cell impedance sensing (ECIS)

There are various different platforms available to measure cellular impedance (TEER, CNBIO, xCelligence™, CellKey™ and Bionas Discovery™). However, none of these systems are capable of the mathematical modelling and sensitivity of the AB Biosciences ECIS Zθ™. This system is capable of measuring total impedance over time and then deconvolving this data into biologically relevant components measuring specifically: tight junctions (Rb), adhesion (α) and overall membrane integrity (Cm). This is achieved by measuring impedance on a multiple frequency setting which can identify the different pathways the current can take. By alternating the frequency of the current between low (<10kHz) and high (>40kHz) you can determine where

there are gaps within your cell culture. At 10kHz and below, the current flows under and in between the cells. This allows for a measurement which indicates how well cells have adhered to the substrate as well as a measurement of cell-cell interaction or tight junctions. At higher frequencies, >40kHz, the current moves through the cells which exposes any compromise of cell membrane integrity as well as giving an indication of intracellular processes (Wegener, Keese & Giaver, 2000, Giaver & Keese, 1991).
One consideration when analysing ECIS data is sensitivity. While this is a benefit, one must be aware that changes in temperature, pH, media composition and even the opening of the incubator door will appear as background noise or disruption of impedance. However, this level of sensitivity can be very beneficial in terms of providing insight into a number of variables in culture and could inform drug testing in terms of time of toxicological event and also indicate where a pathway of damage is occurring (eg. total impedance, TJ, adherence, or over all membrane capacitance)

The ECIS model first reported by Nobel prize laureates Ivor Giaever and Charles Keese (1984) is a real-time, non-invasive, label free method of monitoring cell behaviour throughout the course of an experiment. Through their particular mathematical modelling of impedance, it is possible to render a measurement of cellular confluence and detect motion on the ECIS gold electrode array (Giaever and Keese, 1984) (**Figure 1.5**). This gives the option of measuring a baseline of the cell culture (an internal control), before

addition of a substance or introducing a wounding assay, and recording and monitoring the outcome in real time.

Within the ECIS model, cells are grown on a gold electrode through which an alternating current (AC) at a low voltage (V) of 1V is applied through a series resistance of 1MOhm to produce a small non-invasive current of 1microAmp. Impedance is the measurement of the resistance of this alternating electrical current as it meets opposition, caused in this case by the cell membrane acting as an insulator (Giaever and Keese, 1984). As cells grow to confluency, this increases the impedance of the low AC current (**Figure 1.6**). The current must therefore go under, around or between cells.

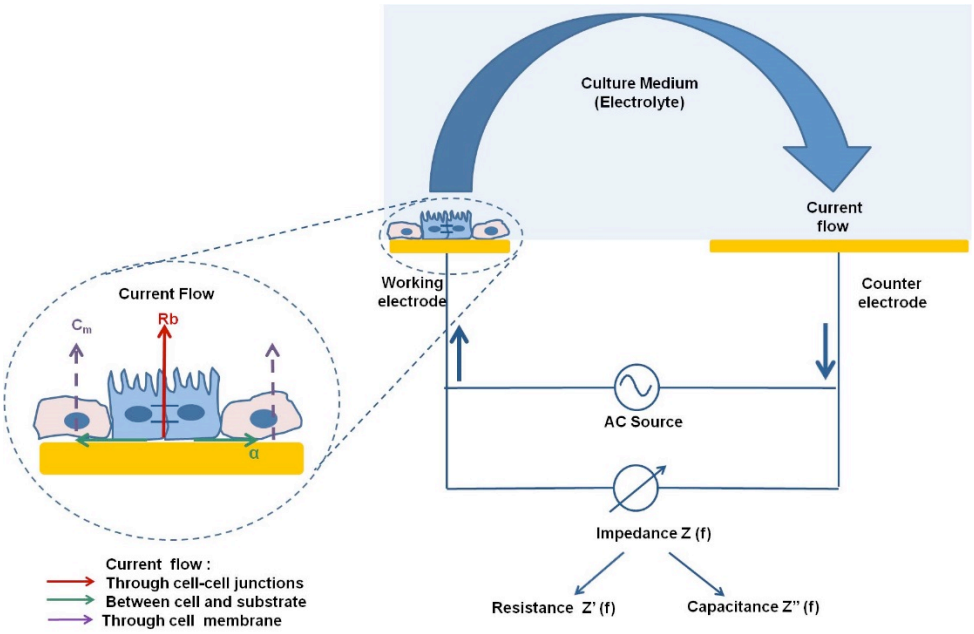

Figure 1.6: Schematic representation of current flow from ECIS Z theta system. Large scale representation of AC current flow within the ECIS theta system with magnification of cells grown on electrode. Cells are grown on working electrodes through which AC current flows under working electrode. AC current can flow under cells showing; adhesion (α), through cell membrane showing capacitance (Cm), and between tight junctions of cells (Rb). Alterations in current can give an indication of these three parameters of cellular health. (Figure reproduced with permission from the author Gamal, W., 2015.)

Changes in impedance are then measured in real time giving a graphical read-out of impedance versus time. This measurement of total impedance in Ohms can then be deconvolved to give a prediction of the flow of current between cells (tight junctions/Rb), under cells (membrane capacitance/Cm) and through cytoplasm (transcellular current/alpha). Impedance measurement has been used in a variety of ways and is a very simple indicator of confluence and health of a cell culture. Any variance to the culture which causes injury or death to the cells is immediately visible as a decrease in impedance (**Figure 1.7**).

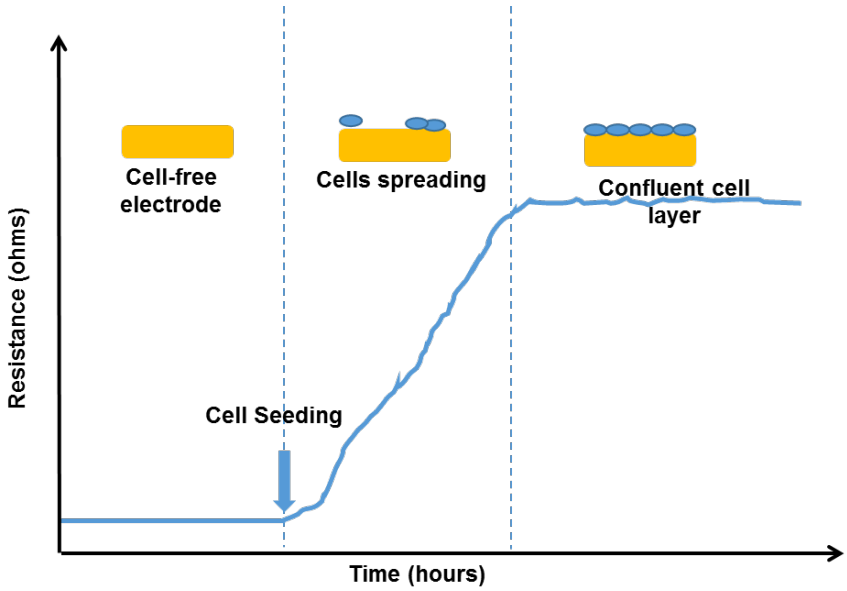

Figure 1.7: Graphical example of measurement of impedance over time. This graph shows a low baseline of impedance just after seeding of cell culture and how impedance rises as cells become more confluent. Once cells are spread over an electrode the impedance measurement plateaus indicating confluency and cell synchronization (Figure reproduced with permission from the author Gamal, W., 2015.)

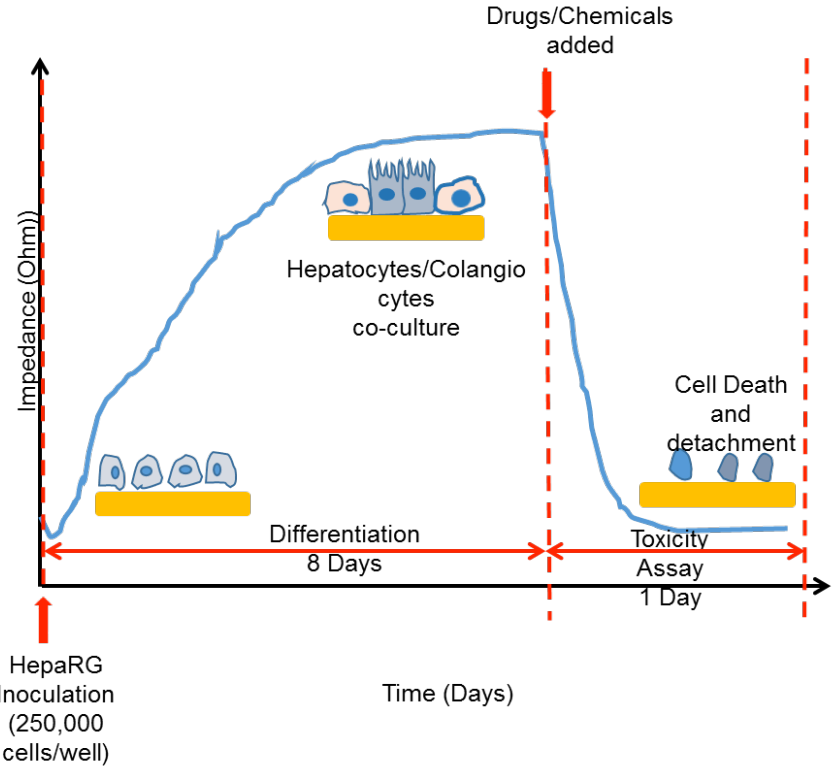

:

Figure 1.8: Graphical example of loss of impedance due to addition of a compound Graphical representation showing impedance over time where total impedance rises to plateau before the addition of drug/compound. After addition of a drug or compound a drop in impedance can be measured and interpreted as a disturbance of electrical current caused by changes or damage to cell culture**.** (Figure reproduced with permission from the author Gamal, W., 2015.)

ECIS can simultaneously monitor cell adhesion, tight junction integrity, and overall cell membrane integrity, this offers a comprehensive, non-invasive, depiction of cellular integrity that cannot currently be accomplished by other impedance-based assays.

Other applications of this system include the ability to reversibly permeabilize the cell membrane using a small electric field which causes electroporation (Stolwijk et al., 2011). This can be useful when delivering molecules into the cytoplasm of living cells. As this process is reversible, it can then trap compounds or molecules within the cell. Since this is a real-time model, the cell can be monitored before electroporation, during and after, providing an initial baseline before treatment and allowing post treatment monitoring.

1.6.2.1.3 ECIS tissue cultureware

A variety of tissue culture wells can be purchased to give flexibility to experimental design and offer various ways to use the ECIS system to monitor different cellular processes. Arrays are available with either one 50nm gold electrode per well or multiple 50nm electrodes per well and are treated with oxygen plasma. Cells are seeded directly onto the wells containing the electrodes. The number of cells that can be observed at one time is limited to the size of the electrode (Xiao and Luong, 2003). As cells grow on the electrode the measurement of impedance or resistance rises as

the current cannot take a path of least resistance between, under or through cells. Once cells become confluent, the impedance measurement plateaus. Once a reproducible and stable plateau is recognized through repeated experimentation, it can be used as a benchmark for further analysis eg. effect of addition of drugs.

1.6.2.2 Using ECIS to investigate and illustrate drug toxicity

Previously published work from our laboratory, measuring total impedance with ECIS technology, has shown a dose-dependant response in HepaRG™cells following exposure to the model hepatotoxin paracetamol (APAP) (Gamal et al., 2017). Within that study HepaRG™ cells were grown on ECIS 8 well 10+ electrode plates and monitored for 8 days. On day 8 APAP was added to the culture and total impedance was monitored. A dose dependant response emerged and further deconvolution of data showed that the parameter of tight junctions/Rb (TJs) was most effected by APAP. This prompted further investigation into the possible mechanisms behind APAP toxicity.

Here, the aim is to use the published HepaRG ™/ECIS model, with a prototype cholestatic drug, chlorpromazine (CPZ). We will use this model to determine if the impedance signature will be the same when cholangiocytes are the main target of toxicity. It is hoped that in modelling two hepatotoxins, each with a distinct mechanism of toxicity, that a pattern may start to emerge between purely hepatic and purely cholestatic toxins.

Chlorpromazine was chosen in the first instance because it is an antipsychotic drug known to cause intrahepatic cholestasis in a short period of time. Cholestasis is a condition characterized by an impaired ability of the bile ducts to secrete bile acids, bilirubin and cholesterol (Antherieu et al., 2013). There is currently a need within the pharmaceutical industry to predict cholestasis *in vitro* before drugs are taken to pre-clinical trials. CPZ has long been used as an *in vitro* model of cholestasis as there is evidence that CPZ causes impaired biliary function, though the mechanisms behind this are not fully understood (Antherieu et al., 2012, Akerboom et al., 1991, Zimmerman and Lewis 1987, Moradpour et al., 1994 and Castell et al., 1996). Using the HepaRG™ cell line with its intrinsic co-culture of hepatocytes and cholangiocytes will offer a unique advantage in elucidating the effect of CPZ on both cell populations (Bachour-El Azziz, P et al., 2015). Understanding the mechanisms behind CPZ toxicity may also provide insight into studies of other xenobiotics that are also known to target the biliary system/cholangiocytes and aid in pre-clinical toxicity studies.

Aims of the thesis

1.7 Aims

1. To compare the human hepatic C3A cell line to the co-culture HepaRG™ cell line in terms of CYP induction and inhibition, capabilities of phase I and II metabolism and integrin expression to determine which cell line is most suitable for use in an *in vitro* drug toxicity testing context.
2. As there has been evidence to show roughness and patterns on cell surface substrate contributes to differentiation and alter cellular behaviour, it was our aim to assess whether seeding HepaRG™-P cells onto NPS accelerates differentiation and maturation into hepatocytes or whether they behave differently compared to those grown on industry standard Corning, tissue culture plastic (TCP).
3. To demonstrate a real-time impedance-based assay using a model cholestatic drug to investigate the usefulness of this technique for potential drug toxicology testing.

Chapter 2 Materials and Methods

This chapter will look at general materials and methods that are used throughout the thesis. Specific materials and methods will be outlined in future chapters.

2.1 Chemicals

Chlorpromazine (CPZ, C8138, Sigma-Aldrich, Dorset, UK) was stored at room temperature. A stock of 100mM in PBS buffer was prepared and stored at -20°C in aliquots. CPZ dilutions were made in HepaRG™ Maintenance and Metabolism Medium (MMM, ADD620, Biopredic International, Rennes, France) according to established dilutions by Antherieu et al., 2013.

Phenacetin (77440, Sigma-Aldrich, Dorset, UK) MW 179.2Da was stored at -20°C. A stock of 1mg/ml was made in methanol (MeOH, 322415, Sigma-Aldrich, Dorset, UK) and this was prepared fresh for every experiment as it was used for LC:MS/MS calibration and degradation could not be risked.

Omeprazole (O104-100mg, Sigma-Aldrich, Dorset, UK) MW 345.32. Dilutions were made in 100% DMSO to concentration of 50mM and aliquots were stored in -20°C. Aliquots were diluted in media to final concentration of 50µM.

Rifampicin >97% HPLC powder (R3501-1g, Sigma-Aldrich, Dorset, UK) MW 822.94 was stored at -20°C in aliquots of 50mM diluted in 100% DMSO. A final stock concentration of 50μM was made in media.

Fluvoxamine maleate (F2802-10mg, Sigma-Aldrich, Dorset, UK) Dilutions were made in 100% DMSO and 25mM aliquots were stored in -20°C. A final stock concentration of 25μM was prepared in media.

Ketoconazole (K1003-100mg, Sigma-Aldrich, Dorset, UK) MW531.43 Dilutions were made to final stock concentration of 25mM in 100% DMSO and aliquots were stored in -20°C. Final concentration of 25μM was prepared in media.

2.2 Cell culture

2.2.1 C3A cells

C3A cells (CRL-10741™, ATCC®, Manassas, USA) derivative of HepG2: were cultured on Corning plates in Minimum Essential Medium Eagle (with Earle's salts and L-glutamine, without sodium bicarbonate, MEME+, MO268, Sigma Aldrich, Dorset, UK – 10x1L) with 10% fetal bovine serum (FBS, Life Technologies, Paisley, UK) and 1% penicillin/streptomycin (pen/strep, 15140122, Life Technologies, UK). The culture was maintained at 37°C in 5% CO_2 until ~80% confluent.

Media was prepared by adding a vial of 1L MEME to sterilized water and adjusting pH by adding 2.2g of Sodium Bicarbonate (S6297, Sigma-Aldrich, Dorset, UK). Media was then sterile filtered under the hood before adding FCS and penicillin/streptomycin.

2.2.1.1 Trypsinisation

C3As were trypsinized for passage and replating weekly. Trypsinisation was performed as below.

Cells were passaged in T75 flasks. Supernatant was removed and cells were washed in 4ml Hanks Balanced Saline Solution (HBSS, 14025092, ThermoFisher, Massachusetts, USA). Trypsin EDTA (25300054, ThermoFisher, Massachusetts, USA) 5ml was added to the flask and cells were incubated in 37°C 5% CO2 for 5 minutes. The reaction was stopped by adding 5ml MEME and cells were transferred to 20ml universal and spun for 3 min on a Sigma 4K15 Laboratory centrifuge at 500 RPM. After centrifugation, supernatant was removed and cells were resuspended in 5ml MEME.

2.2.1.2 Cell counting

15μL of C3A cell suspension was taken and added to 15μl trypan blue 0.4% (T10282, Invitrogen, California, USA). Using an Invitrogen Countess™ automated cell counter, cells were counted twice and an average taken for use in calculating cell seeding density. C3As were seeded at $2.5x10^6$ per T75

and kept at 37C 5% CO2 for duration of culture. Medium was changed every other day.

2.2.2 HepaRG™ Cells

2.2.2.1 HepaRG™ Progenitors (HepaRG™-P)

Progenitors were initially cultured in medium consisting of William's E Medium + GlutaMAX™ (32551-020, Life Technologies, Paisley, UK) and Biopredic's proprietary 711 Medium without Dimethylsulfoxide (DMSO,85190, Pierce™, ThermoFisher, Massachusetts, USA) HepaRG™-Ps were cultured in this medium for 14 days (with media changes on Mondays, Wednesdays and Fridays) before changing to William's E + GlutaMAX™ and Biopredic's proprietary 721 medium with DMSO. It was necessary to culture HepaRG™-Ps in DMSO-free medium for the first two weeks to ensure a healthy culture that proliferated and grew to confluence before switching to a medium containing DMSO which was required for sustaining the differentiation stage of HepaRG™-P development.

2.2.2.2 HepaRG™ fully differentiated cells

HepaRG™ fully differentiated cells were plated in Biopredic's proprietary General Purpose Medium (GPS) without DMSO for up to 2 days. Since traditional HepaRG™s are terminally differentiated it was necessary to provide a medium containing DMSO earlier for this culture than the HepaRG™-Ps. For this reason, on day 3-4 of culture, the medium was

changed to Biopredic's proprietary Metabolism Maintenance Medium (MMM) containing DMSO. Here DMSO continues to support the fully differentiated state of the HepaRG™ cell throughout the life of culture.

2.3 Immunocytostaining

Immunocytostaining was performed identically for all cell cultures and experiments unless otherwise specified in relevant Chapter. Cells were washed with Tris-Buffered Saline (TBS) (TBS; T6664; Sigma-Aldrich, Dorset, UK) for 2 minutes prior to fixation in 4% formaldehyde (28908, Thermo Scientific, Massachusetts, USA) at 4°C for 1 hour. Cells were again washed with TBS and then permeabilized with 0.1% Triton X 100 (85111, ThermoFisher, Massachusetts, USA) for 30 minutes. Following a further TBS wash samples were blocked with 5% goat serum (G6767; Sigma-Aldrich, Dorset, UK) for 1 hour. Primary antibody was then added and incubated at 4°C overnight (**Table 2**), after which, cells were washed on a shaker in TBS for approximately 20 minutes and then washed again briefly before adding secondary antibody, Hoescht and phalloidin. Secondary antibody incubation was at 4°C for 4 to 24 hours depending on antibody.

2.3.1 Primary antibody staining

Primary Antibody	Catalogue Number	Dilution
Z0-1 Santa Cruz Rabbit polyclonal primary antibody	SC 10804	1:50
HNF4α, monoclonal mouse, Abcam Cambridge, UK	Ab41898	1:1000
SOX9 Santa Cruz Rabbit polyclonal antibody	SC20093	1:500
Rabbit-anti-Transferrin FITC –primary antibody, abcam, Cambridge, UK	Ab34670	1:200
CYP3A4 primary antibody, Merck, Millipore Darmstadt, Germany	Ab1254	1:500
Anti- Carbamoyl phosphate synthetase (CPS) monoclonal mouse mAb primary antibody Abnova, Taiwan	H000001373-MO1 (1400-1500)	1:500
Anti-Glutamine synthetase Rabbit primary antibody Sigma Aldrich, St Louis Missouri, USA	G2781	1:1000

Table 2: Dilutions of primary antibodies – Name, product number and manufacturer of primary antibodies used throughout this thesis, alongside optimal dilutions.

2.3.2 Secondary antibody staining

Secondary antibody goat-anti-rabbit Alexa Fluor 488 (11034, Life Technologies, UK 1:1000 dilution) was used for green fluorescent protein (GFP) and Alexa Fluor 555 (A31630, Life Technologies, UK, 1:1000 dilution) was used for red fluorescent protein (RFP) were combined with Hoescht 33342 (HS1492; Life Technologies, UK, 10µg/mL) and Phalloidin-TRITC (R415; Life Technologies, UK, 3 U/mL 1:200 dilution).

2.4 Microscopy

All phase and fluorescent imaging was performed with an EVOS Auto FLO™ imaging platform (Thermo Scientific, Massachusetts, USA). Image magnification is specified on a figure by figure basis.

2.5 General assays

2.5.1 PrestoBlue™- resazurin based assay

PrestoBlue™ 10% (v/v) (A-13262; Life Technologies Paisley, UK) was added to Phosphate Buffered Solution with calcium chloride and magnesium chloride (PBS +)(D8662, Sigma Aldrich, Dorset, UK, 500ml) in a 1:10 solution. Cells were washed with PBS+ prior to addition of 100µl PrestoBlue™ suspension. Cells were then incubated for 30 minutes at room temperature, with the PrestoBlue™ suspension, before reading the

fluorescence signal on a GloMax-Multi™+ Microplate Multimode Reader (Promega, Southampton, UK)(Boncler et al., 2014). (Further optimisation of the PrestoBlue™ assay can be found in Chapter 7 Supplementary data)

2.5.2 Promega CYP450-3A4 assay

CYP3A4 activity was measured using the Promega P450-Glo™ CYP3A4 assay with Luciferin-IPA (V9001; Promega; Southampton, UK).
C3A and HepaRG™ cells were incubated in situ on the plate at 37°C for 24 hours with testosterone and prototypical inducer rifampicin or rifampicin and ketoconazole. Cells were washed twice with HBSS and 50µl 3A4 substrate diluted 1:100 in media. Supernatant was transferred to a white walled/bottom plate and 50µl of 3A4 detection agent added. After a further 10-15 min incubation at room temperature fluorescence was read on the GloMax-Multi™+ Microplate Multimode Reader (Promega, Southampton, UK) using the pre-loaded program designed specifically for this kit.

2.5.3 Luciferin based assays

Luciferin based assays are used routinely to measure specific cytochrome P450 activity and other cellular components such as ATP. Luciferins are luminescent proteins derived from various species. In this case, Promega sources luciferins derived from beetle luciferin. The assay is based on a proluciferin substrate of the specific CYP enzyme which is to be measured. Once the substrate is added to the cell culture, it binds specifically to the enzyme and is converted to D-luciferin which can then be detected by the

addition of Luciferin Detection Agent. This reaction creates a signal that can be read and measured, by a plate reader, where light produced is proportional to CYP activity. Here we use this method to assess CYP1A2, 3A4 and also for quantification of total ATP.

2.5.3.1 Promega CYP450-3A4 assay

CYP3A4 activity was measured using the Promega P450-Glo™ CYP3A4 assay with Luciferin-IPA (V9001; Promega; Southampton, UK).
C3A and HepaRG cells were incubated in situ on the plate at 37°C for 24 hours with testosterone and prototypical inducer rifampicin or rifampicin and ketoconazole. Cells were washed twice with HBSS and 50µl 3A4 substrate diluted 1:100 in media. Supernatant was transferred to a white walled/bottom plate and 50µl of 3A4 detection agent added. After a further 10-15 min incubation at room temperature fluorescence was read on the GloMax-Multi™+ Microplate Multimode Reader (Promega, Southampton, UK) using the pre-loaded program designed specifically for this kit.

2.5.3.2 Promega CYP450-1A2 assay

CYP1A2 was measured with Promega P450-Glo CYP1A2 assay and screening system using Luciferin-ME (V8771; Promega; Southampton, UK)
C3A and HepaRG cells were incubated for 24 hours at 37°C with phenacetin and prototypical inducer omeprazole or omeprazole and inhibitor fluvoxamine. Cells were washed twice using HBSS and 50 µl of Promega1A2

Luciferin detection agent was added to the cells for 20 minutes incubation at room temperature before transferring to a white walled plate for reading using the GloMax-Multi™+ Microplate Multimode Reader.

2.5.3.3 Promega Cell titer glo – total ATP assay

PrestoBlue™ and ATP assays were always carried out on the same culture so data could be directly comparable.

Post PrestoBlue™ experimentation, supernatent was discarded, and cells rinsed with PBS before addition of Promega Cell Titer Glo™ ATP lysis buffer to determine total cellular ATP levels using the CellTiter-Glo™ Luminescent Cell Viability Assay (G7570; Promega, Southampton, UK), as per vendor's instructions. Briefly, incubation in substrate at room temperature for 20 minutes was followed by adding ATP detection solution and bioluminescent signals were detected with the on a GloMax-Multi™+ Microplate Multimode Reader (Promega, Southampton, UK). ATP levels were normalized to no cell control.

2.5.4 Induction assays for C3A and HepaRG™ cells

When comparing CYP activity in HepaRG™ and C3A cells, it was decided that each culture should be induced with drugs known to instigate specific CYP isoform activity. For example, phenacetin is a known substrate of CYP1A2. Therefore, exposing cells to phenacetin should instigate CYP1A2 activity. We chose phenacetin and testosterone to act as substrates to CYP1A2 and 3A4 activity respectively.

C3A cells derivative of HepG2: were cultured on Corning plates in Minimum Essential Medium Eagle (MEME) with 10% FBS and 1% penicillin/streptomycin. The culture was maintained at 37°C 5% CO2 until ~80% confluent. HepaRG™ cells (terminally-differentiated cells, Biopredic International, Rennes, France) were seeded (following the suppliers protocols) on Corning plates and cultured to confluence at 37°C 5% CO2 for 7 days.

Cells were treated for 24h with prototypical inducers 50μM omeprazole (CYP1A2) or rifampicin (CYP3A4), with or without addition of CYP450 isoform-specific specific inhibitors 25μM Fluvoxamine (CYP1A2) or Ketoconazole (CYP3A4), in MEME (C3As) or hepatocyte induction medium (HIM, Biopredic, Rennes, France). Cells were then washed twice with HBSS. Specific CYP450 enzyme activity was subsequently assessed using a non-lytic luminescence assay using specific kits for CYP1A2 and CYP3A4, following the manufacturer's instructions (P450-Glo™, Promega, Southampton, UK). Bioluminescent signals were detected with a GloMax-Multi™+ Microplate Multimode Reader. Individual luminescent assay readings were background-corrected and normalized to cellular ATP content.

2.6 Molecular assessment for genes of interest

2.6.1 RNA extraction

Where stated, RNAlater™ (AM7201, ThermoFisher, Massachusetts, USA) was used to store samples before extraction.

RNA was extracted with Life Technologies RNAqueous™ Total RNA Isolation Kit (AM1912, Life Technologies, UK). Cells were scraped *in situ* in NPS and transferred into Eppendorf tubes where they were spun (3min at 10,000rpm) into a pellet. Supernatant was removed and cells were then lysed in the Eppendorf tube with lysis binding solution (64% ethanol/water) and immediately transferred into provided collection tubes with filter cartridge. Cells were spun as per before. Wash solution 1 was added (700μl) and collection tubes were spun again. A further two wash steps using 500μl Wash Step 2/3 solution were performed before eluting samples. Filter cartridge was transferred into new collection tube for elution step. Elution solution was heated to 75°C and 50μl was added to each filter cartridge and tubes spun as before. This step was repeated. 5μl samples of recovered mRNA were assessed for quantity and quality. The remaining samples were stored at -80°C until reverse transcription was performed.

RNA quality was assessed using A Grant NanoDrop™ ND-1000 Spectrophotometer which measures absorbance at 260 and 280nm. A ratio of 2 is considered to be uncontaminated with genomic DNA and of good quality/purity. Our total RNA samples showed high quality on nanodrop technologies i.e. (260/280 ratios: 1.8-2.0). However, for cells grown on NPS, the quantity of mRNA was relatively low. For this reason, when considering reverse transcription into cDNA, mRNA was kept at as high concentration as possible.

2.6.2 Reverse transcription (cDNA synthesis)

Reverse transcription for both NPS experiments and CPZ experiments was carried out using Primer Design Precision nanoScript^{TM} 2 Reverse Transcription (Primer Design, Cambridge, UK) kit following manufacturers instructions. The following reagents were added to a 0.2ml DNAse and RNAse free PCR tube; Reverse transcription oglio-DT primer (1μl), RNA template (varied from 2-9μl due to concentration of RNA), and water (as needed to make final volume of 10μl). Samples were heated to 65°C for 5 minutes. In all cases RNA was kept as concentrated as possible to ensure optimal reverse transcription. Tubes were then transferred to ice for addition of extension master mix which comprised 5μl nanoscript 2 buffer, 1μl dNTP mix 10mM, 3μl RNAse free water and 1μl nanoscript 2 enzyme. Tubes were incubated at 42°C for 20 minutes before a 10 minute heat inactivation at 75°C. Samples were stored at -20°C.

2.6.3 Quantitative Polymerase Chain Reaction (qRT-PCR)

cDNA samples throughout were diluted to 5ng/μl, for normalisation, and qRT-PCR was performed using Primer Designs Precision® PLUS Master Mix (Primer Design, Cambridge, UK) for real-time PCR. Each sample comprised 5ng/μl cDNA template (5μl), Precision® PLUS Master Mix (10μl),

Primer/Probe mix (1μl) and RNAse/DNAse free water (4μl). Samples were run in 96 well format using a Roche Light Cycler 96. As we used a SYBR® Green detection our qRTPCR steps were as follows; enzyme activation 2 mins/95°C, denaturation 10s/95°C, data collection 60s/60°C. Data was analyzed using qBase+ (Biogazelle geNorm software Ghent, Belgium).

2.7 Statistical Analysis

Data evaluation and graphical illustration were performed with GraphPad Prism™ 5.0 and 7.0 (GraphPad Software, Inc., San Diego, CA, USA). Three technical replicates were assessed for each experimental condition across three separate experiments, unless stated otherwise, and results are presented as mean ± SD. Appropriate statistical analysis was performed for each experiment including one way ANOVA, t-test, multiple ANOVA and post hoc Tukey test, each detailed in individual chapters. Results were considered significant at $p<0.05$.

Chapter 3 Human hepatic HepaRG™ cells maintain an organotypic phenotype with high intrinsic CYP450 activity/metabolism and significantly outperform standard HepG2/C3A cells for pharmaceutical and therapeutic applications

3.1 Introduction

As mentioned previously, PHHs have been regarded as the gold standard in *in vitro* models. However, they represent an isolated cell (hepatocytes only), are difficult to obtain, usually come from an already damaged liver, and introduce variability in experimental testing due to phenotypic differences between donors. PHHs are also limiting in that they only survive in a fully differentiated state for a few days in culture.

One of the most frequently used cell lines are the HepG2 derived C3A cells. This cell line contains only isolated hepatocytes. It has been shown in previous studies, that when compared to PHHs, C3A cells show low CYP enzyme activity (Castell et al., 1996). For this reason, C3As often need to be manipulated to produce adequate CYP450 enzymes. (Filippi et al., 2004, Elkayam et al., 2006, Prot et al., 2011, Lu and Cederbaum, 2008)

In contrast, the HepaRG™ cell line has been shown to express significant basal levels of CYP activity compared to C3A and PHHs (Grime, Ferguson and Riley, 2010, Antherieu et al., 2012).

This co-culture, with cholangiocyte-like cells and bile duct formation alongside fully mature and functional hepatocytes offers a unique opportunity to assess the interaction of two key liver cell types at a time providing a model more comparable to *in vivo* studies (Antherieu et al., 2012, Gripon, et al., 2002, Gunness et al., 2013). *In vitro* human models of hepatic/cholestatic

DILI could aid pharmaceutical companies in initially identifying compounds less likely to fail in moving from *in vitro* to *in vivo* animal and human pre-clinical models. Such a model could also improve/inform pre-clinical trials while reducing the need for animal testing in line with government regulations. A hepatic cell line, such as the HepaRG™, comprising more than one liver cell type, that expresses CYP enzymes at levels comparable to PHHs, if proven, has the potential to provide a valuable platform for *in vitro* pharmacological testing. There is currently limited information directly comparing these cell lines. For this reason, we compare the CYP450 activity, induction and inhibition and metabolic competency of HepaRG™ and C3A cell lines.

3.1.1 Aims

To compare the metabolic strengths and weaknesses of both the HepaRG™ and the C3A cell line by evaluating their ability to

1. Metabolise phenacetin and testosterone and analyse which cell line is most competent in elimination of compounds.
2. To compare CYP450 activity between the two cell lines and in parallel, CYP450 inhibition in response to phenacetin and testosterone.
3. To assess and compare levels of integrin expression in C3A, HepaRG™ progenitors (HepaRG™P) and fully differentiated

HepaRG™ cells as a marker in defining maturity and polarity of cells in culture.

Rationale: To make a direct comparison between C3A and HepaRG™ cells to determine which cell line would be most appropriate as a model in future DILI studies.

3.2 Materials and Methods

The inducibility of CYP activity in C3A and HepaRG™ cells alongside inhibition of the same pathways were assessed to highlight functionality of each cell line. Cells were challenged with testosterone and phenacetin, known to be metabolized by CYP3A4 and CYP1A2 respectively, to assess metabolic competency. Primary and secondary steroid and drug metabolites were identified using liquid chromatography and tandem mass spectrometry (LC:MS/MS) and high performance liquid chromatography (HPLC). Further inhibition with ketoconazole and fluvoxamine was used to confirm specificity of induction and analyse how each cell type would respond to treatment. Finally, flow cytometry was used to compare integrin expression between C3A and HepaRG™ cell lines to determine maturity of the hepatic phenotype. Here, HepaRG™-P cells were also used for comparison as they represent an immature phenotype.

In order to assess the CYP1A2 or CYP3A4-specific metabolic activity HepaRG and C3A cells were exposed to 50μM phenacetin (CYP1A2) or testosterone (CYP3A4) for 24 hours at 37°C. Reactions were stopped on ice, and supernatant of samples stored at -80°C and transferred for assessment via HPLC (testosterone) or LC-MS/MS (phenacetin).

3.2.1 Induction/Inhibition of CYP enzymes

Both C3A and HepaRG™ cells were treated for 24 hr with prototypical inducers 50μM omeprazole (OMP) (CYP1A2) or rifampicin (RIF) (CYP3A4), with or without the addition of CYP450 isoform-specific inhibitors 25μM fluvoxamine (FLUVOX) (CYP1A2) or ketoconazole (KETO) (CYP3A4) Compounds were added to media for the duration of incubation (in MEME for C3As or hepatocyte induction medium for HepaRG™s)
The cells were then washed twice with HBSS. Specific CYP450 enzyme activity was subsequently assessed using a non-lytic luminescence assay using specific kits for CYP1A2 and CYP3A4, following the manufacturer's instructions (P450-Glo, Promega, Southampton, UK). Bioluminescent signals were detected with a GloMax-Multi+ Microplate Multimode Reader (Promega).

3.2.2 Liquid chromatography with tandem mass spectrometry

Phenacetin metabolism was assessed using an ABI Applied Biosystems 5500 QTrap Mass spectrometer and AB Sciex software, Analyst 1.5.1; and LightSight software to identify metabolites.

This instrument was chosen as it is a triple quadrupole mass spectrometer which includes an ion trap. This allows for a qualitative measurement/identification of metabolites. Metabolites can also be quantified as a percentage of the parent molecule, but as the metabolic fate of phenacetin was unknown in context of hepatocyte cell line metabolism, we focused on the specific capability of the instrument to identify metabolites via MS/MS.

Initially samples were fractionated within the HPLC column before identification and quantification by the mass spectrometer (MS) which separates ions on the basis of their mass to charge ratio (m/z). This happens within the Q1 chamber of the mass spectrometer. Ions are then moved into the Q2 chamber where collision energy is applied and the ions are further disassociated. Ions then move into the final Q3 chamber where they are separated a second time on the basis of their mass to charge ratio. The identification of ions at Q1 and Q3 based on their m/z ratio incorporates tandem mass spectrometry readings or MS/MS. This technique is well suited to the aims of this project because the ions that we are setting out to identify and quantify have a known molecular weight,

Initially, we looked for phenacetin with a known molecular weight of 179.2 Daltons (Da). The LC-MS/MS was tuned using a standard solution of the parent ion phenacetin as this has a known, and unique, m/z ratio. The phenacetin standard was made up to 1mg/ml in MeOH. (0.0057g phenacetin in 5700µl of MeOH). The 1mg/ml stock solution was then serially diluted 1 in 10 in methanol to a final dilution of 1:1000. Methanol is easily removed from the solution by evaporation during flight through the MS-MS, increasing the ratio of analyte to solvent, meaning the analyte should ionize more readily Samples were directly injected into the instrument in Electrospray ionization (ESI) mode. The machine was calibrated to identify molecular ions in the 50-200 Da range as the phenacetin ion has an m/z of 180.1 and was detectable either as a singly or doubly charged species.

A base line for paracetamol and its metabolites was generated using a 10µg paracetamol control and, as a source of paracetamol metabolites, a sample of urine (10µl) collected from a patient administered paracetamol. Acuity HPLC system and Light Sight software was used to collect and interpret the data.

Experimental samples analysed included 7 Controls; untreated C3A or HepaRG™, 3 samples in duplicate of phenacetin treated HepaRG™ cells and 3 samples in duplicate of phenacetin treated C3A cells. Using data generated from the phenacetin standard and the baseline of human urine for metabolites of paracetamol, it was possible to identify primary Phase I and

Phase ll metabolites of phenacetin. Control data was used to exclude background noise from untreated cells and media from experimental results. Samples were stored at -20ºC until use, when they were defrosted at room temperature for one hour. They were prepared for liquid chromatography by pipetting 200µl into an eppendorf tube and adding 200µl of acetyl nitrile to precipitate proteins, which were removed by centrifugation at 6000rpm for 5 minutes.100µl of supernatant was transferred to LC vials for analysis. Samples ran on 10 minute cycles, and a Carbon 18 solid phase column was specifically used for its ability to separate metabolites into separate peaks. Results were evaluated using Light sight metabolite I.D. software. HPLC excluded material outside the chosen molecular weight (MW) boundaries, and molecules of MW 50-200kDa passed into the MS-MS.
An AB SCIEX Q Trap 5500 LC-MS/MS was used to process the samples. The machine was calibrated and prepared for use by flushing tubes and syringes with a weak H_2O solvent. The temperature was set at 20°C and a mobile phase solvent was prepared using 65% H_2O and 35% MeOH.

3.2.3 HPLC

Samples for HPLC were mixed with the internal standard (20 µg/ml 11 α-hydroxyprogesterone in methanol) and extracted with dichloromethane before they were resuspended in 30% MeOH and analysed by Dr Philipp Treskes and Dr Helen Grant with an Eclipse XD8-C18 3 µm 3 x 100mm column (Agilent, Cheadle, UK).

3.2.4 Polymerase chain reaction

C3A and HepaRG ™ cells from one well of a 6 well plate were scraped in cold PBS and aliquoted in RNAlater for further RNA extraction. Aliquots were then stored in -80°C. RNA extraction was performed as per section 2.6.1 in Chapter 2.

The concentration of RNA obtained from both fresh and stored cells was nearly 100ng/μl, with a 260/280 ratio 2.03 for a total of 3μg. Concentration of DNA was 50ng/μl, 260/280 ratio was 1.82 for a total of 1.5μg.

Samples collected from above were electrophoresed on a 1.5% agarose gel and run for up to 30 minutes. Gel was exposed to UV light and picture was taken with gel documentation system.

3.2.5 Flow Cytometry

Integrin expression was compared in C3A, HepaRG™ P and fully differentiated HepaRG™ cell lines. This allowed assessment of integrin expression in C3A cells, known to express foetal markers (eg alpha-fetoprotein), with both the HepaRG™ P (hepatoblast-like) progenitors, and their derivatives (HepaRG™), as comparators. To assess expression of integrins, single cell suspensions were enzymatically recovered using xeno-free Tryple (Life Technologies) – which protects cellular surface proteins, washed and resuspended in FACS-PBS (PBS containing 0.1% Bovine serum

albumin (BSA) and 0.1% sodium azide), for simultaneous staining with a panel of fluorochrome-labeled integrin antibodies: CD29-BV510, CD49f-BV451, CD49d-FITC, CD49c-PE, CD49a-APC-Vio770, CD49b-PE-Vio770, CD49e-APC, (all Miltenyi Biotec, Bergisch Gladbach, Germany). Cells were incubated with antibodies at 4ºC for 20min, washed twice and re-suspended in FACS-PBS. Unstained cells were included as controls, whilst dead cells and debris were excluded from the analysis based on scatter characteristics. Data for at least 10,000 live events per sample were acquired using a MACSQuant Analyzer (Miltenyi Biotec) and was analyzed using FlowJo version 9.6.7 software (FlowJo LLC). Data is presented as percentage positive staining.

3.2.6 Statistical analysis

Differences between the different culture conditions (with or without treatment) were detected applying a one way Anova. Results were considered significant at $p<0.05$

3.3 Results

3.3.1 Presence of CYP enzymes confirmed by immunocytostaining and PCR

Phase microscopy showed that both HepaRG™ and C3A cultures were healthy and had grown to desired threshold of confluency before experimentation.

HepaRG™ cells formed terminally-differentiated *in vivo*-like hepatic cords and cholangiocyte-like cells (**Figure 3.1 A**). C3A cells were grown to 80% confluence as per manufacturers instruction (**Figure 3.1 B**) Functional polarity can be seen in the HepaRG™ culture as evidenced by punctate staining of F-actin bands indicative of bile-canalicular structures [phalloidin-staining] and showcased a level of CYP3A4 indicated in GFP staining (**Figure 3.1 C**). C3A cells were also stained with F actin and CYP3A4 antibody. However, this culture lacks the cholangiocytes seen in HepaRG™s and shows little to no presence of CYP3A4. (**Figure 3.1 D**) In contrast, high CYP3A4 activity with strong expression of CYP2E1, CYP1A2, and CYP3A4 genes, was evident only in HepaRG™; indicative of high metabolic competence for drug metabolism of these cells (**Figure. 3.1 E**).

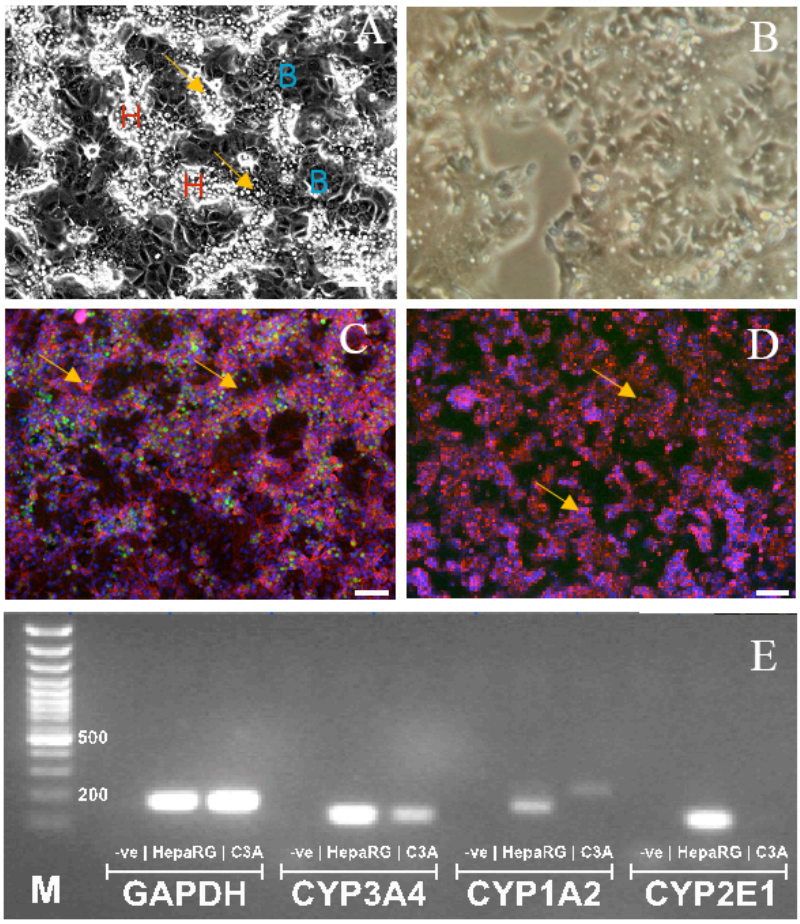

Figure 3.1 Morphological and phenotypic assessment of HepaRG™ vs C3A cells A) Phase contrast microscopy of HepaRG™ cells showing bile canaliculi indicated by yellow arrows and hepatocyte islands indicated by H. Population of biliary cells with endothelial morphology indicated with B. **B**) Phase contrast microscopy of C3A cells showing a near confluent culture of purely hepatic cells. Immunostaining of F-actin cytoskeleton (Red), nuclei (blue) and CYP3A4 (green) for HepaRG™ and C3A **C**) & **D**) cells. Immunocytostaining materials and methods undertaken as detailed in Chapter 2 section 2.3 **E**) End point PCR produced by Dr. Mai Abd El-Aziz showing positive expression of GAPDH for HepaRG ™ and C3A cells for use as positive control. Presence of CYP3A4, 1A2 AND 2E1 can be seen in HepaRG™ cells indicated through the white bands. C3A cells show presence of CYP3A4, but no presence of CYP1A2 or 2E1 indicating lower overall CYP activity in C3A cells compared to HepaRG™s.

3.3.2 Induction/inhibition of CYP activity

Assessing induction of CYP activity using the Promega assays (Chapter 2, 2.5.2 and 2.5.3), prior to using model inhibitors, demonstrated that HepaRG™ cells respond specifically to induction and inhibition while C3As do not.

Induction of CYP1A2 by OMP in HepaRG™ was significantly higher ($p<0.00001$) than that seen in C3A, which was negligible (**Figure 3.2 A**). Addition of the inducer (OMP) with its inhibitor fluvoxamine significantly reduced ($p=<0.00001$) the level of CYP1A2 in HepaRG™, but was unchanged in C3A, suggesting that CYP1A2 was not induced in C3A cells by treatment with OMP and the level measured was background.

RIF induced a high level of CYP3A4 activity in HepaRG™ cells, which was significantly inhibited ($p<0.0001$) by addition of its inhibitor ketoconazole. CYP3A4 was not detected in C3A cells treated with RIF, suggesting that no induction of CYP3A4 took place within this culture (**Figure 3.2 B**).

The total concentration of CYPs was higher in both induced and inhibited HepaRG™ cells compared to C3As. There were significant differences when comparing induction and inhibition of HepaRG™ cells for CYP3A4 to C3As.

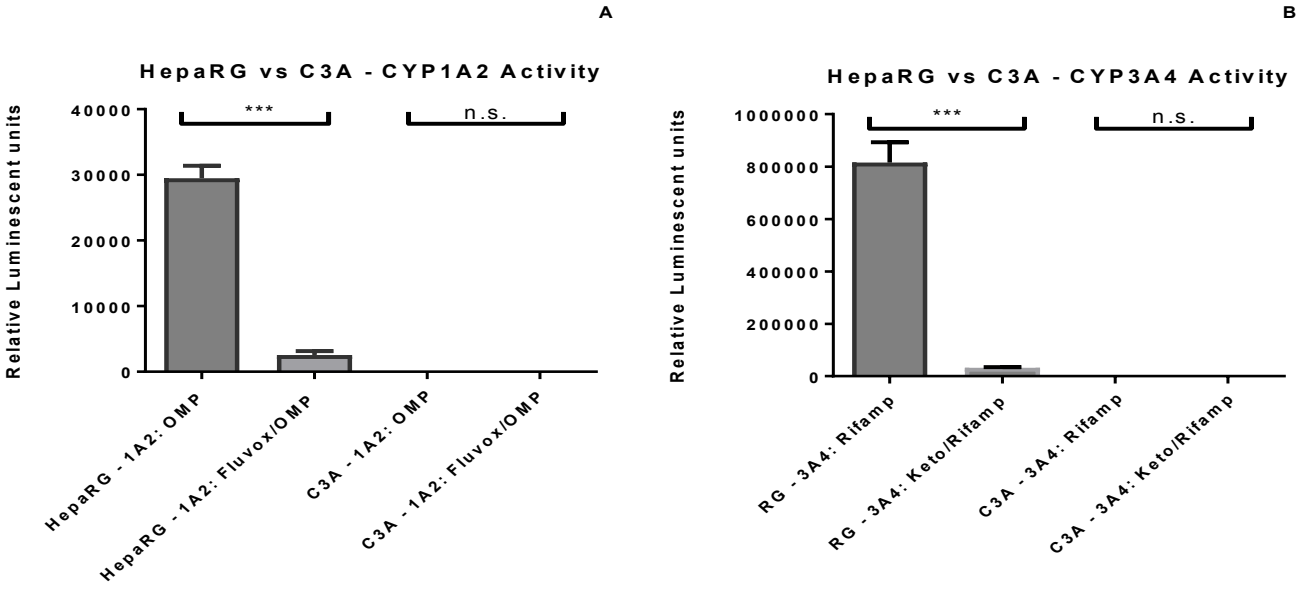

Figure 3.2 Induction and Inhibition of CYP3A4 and 1A2 in HepaRG™ and C3A cells. **A)** Comparison between HepaRG™ and C3A cells cultured with CYP1A2 inducer Ompeprazole (OMP), and compared to HepaRG™ and C3A cells cultured with OMP and inhibitor fluvoxamine (Fluvox) (n=3)($p<0.00001$) or **B)** with CYP3A4 inducer Rifampicin (Rifamp), as well as with rifampicin and CYP3A4 inhibitor ketoconazole(Keto). After normalisation to the untreated control, whereby the relative value of the control was subtracted from treated samples, HepaRG™ cells show high induction and significant inhibition for both CYP3A4 and CYP1A2. Whereas, little to no fluorescence within the C3A culture was observed for either induced or inhibited cultures. All data is displayed as the mean of 3 experimental replicates, with eight technical replicates each experiment. Materials and methods are detailed in section 3.2.1.

3.3.3 Metabolism of parent compounds

Compounds phenacetin and testosterone were chosen as model compounds to assess metabolic competency of C3A and HepaRGs™ as they are known to be metabolized by CYP3A4 and CYP1A2 respectively. Their turnover and ratio of analyte to metabolite were assessed using HPLC and LC:MS/MS.

3.3.3.1 Phenacetin

LC:MS/MS showed HepaRG™ cells yielded a higher turnover of phenacetin and gave a clear yield ratio of analyte to metabolite via end-point analysis (**Figure 3.3**) compared to C3As. HepaRG™ cells metabolized approximately 30% of the parent compound phenacetin compared to less than 20% in C3A cells. Likewise, HepaRG™ cells metabolized almost 60% of testosterone compared to 0% turnover in C3As.

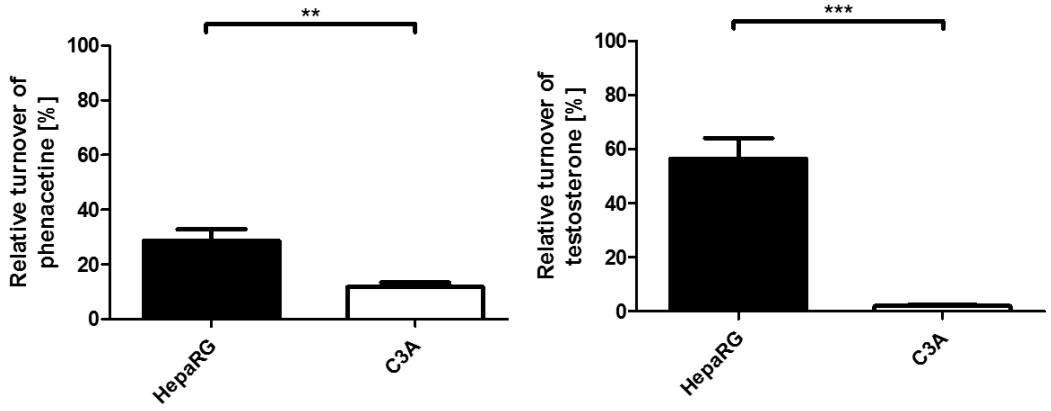

Figure 3.3: Relative turnover of parent compounds phenacetin and testosterone Liquid Chromatography alongside tandem mass spectrometry (LC:MS/MS) shows the relative turnover of parent compounds based on initial quantity vs quantity after 24 hours exposure. This allows for a percentage of turnover to be calculated giving the overall amount of parent compound metabolised. HepaRG™ and C3A cells were treated with phenacetin and testosterone and total percentage turnover was calculated based on LC:MS/MS using 3 experimental replicates with 3 technical replicates each experiment (n=3). HepaRG™ cells show a significant increase in turnover of both phenacetin ($p=0.0024$) and testosterone ($p<0.0001$) compared to C3A cells. Materials and methods listed in section 3.2.2. (Figures adapted from Morgan, K., 2014)

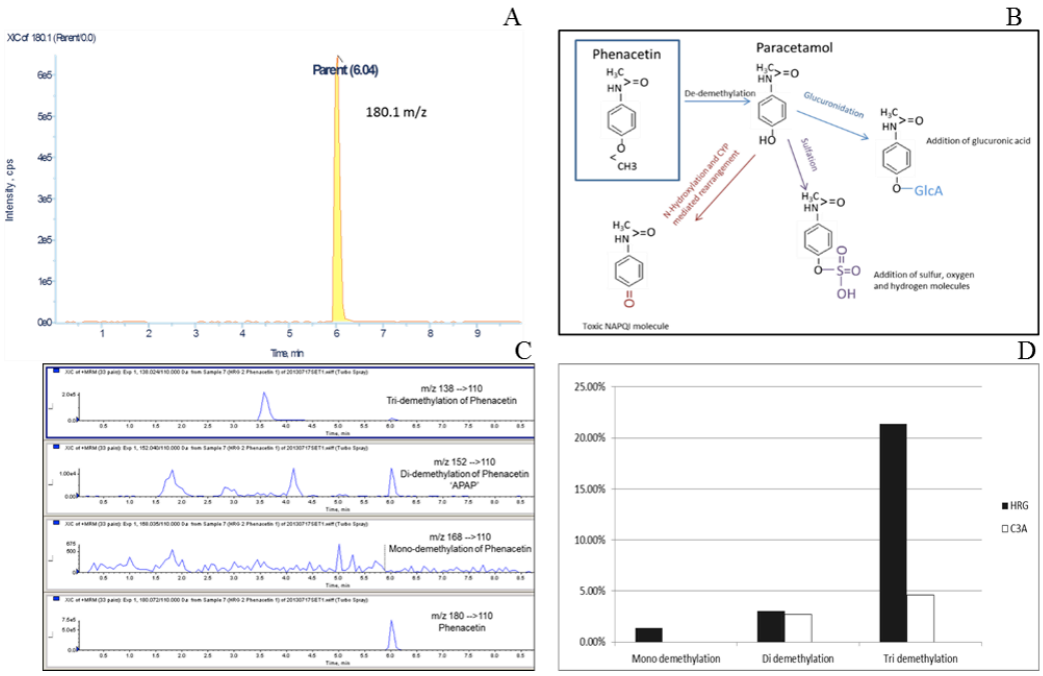

Figure 3.4 Phenacetin metabolites as seen on Light Cycler alongside diagram of phase I and II metabolites and graphical representation of methylation detected using LC:MS/MS: **A**) Representative chromatograph extracted from Light Sight software showing peak of parent compound phenacetin at its unique m/z ration 180.0. **B**) Schematic diagram showing Phase I and Phase II metabolism of phenacetin. **C**) Representative chromatograms of mono-, di- and tri- demethylation. **D**) Comparison of mean % turnover of mono-, di- and tri- demethylation between HepaRG™ and C3A cells (HepaRG™ represented in black and C3A represented in white).(Figure adapted from Morgan, K., 2014)

The data gathered from Light Sight software allowed us to identify the unique m/z ratio of phenacetin (**Figure 3.4 A)** Phenacetin is metabolised to paracetamol and its tertiary metabolites (**Figure 3.4 B**) through demethylation. It was also possible to characterize demethylation of our substrate, phenacetin, by observing separate signatures for demethylation, di demethylation and tri demethylation of the parent metabolite into paracetamol (**Figure 3.4 C**) and to quantify and compare the overall demethylation between C3As and HepaRG™s **(Figure 3.4 D)**.

3.3.3.2 Testosterone

HPLC was used to analyse the relative turnover of testosterone substrate by hydroxylation (**Figure 3.5**). Comparing C3A cells to HepaRG™s shows pronounced presence of 6 Beta hydroxytestosterone, the main metabolite of testosterone, in HepaRG™ cells, while no trace of this metabolite can be seen in C3A cells.

Analysis showed HepaRG™ cells metabolised more than 50% of testosterone and demonstrated evidence of major metabolite 6 Beta hydroxyl testosterone as well as a panel of other secondary metabolites, whilst C3A cells only showed presence of the minor metabolites 16 alpha and androstenedione, and relatively small turnover of the parent compound **(Figures 3.3 and 3.5).**

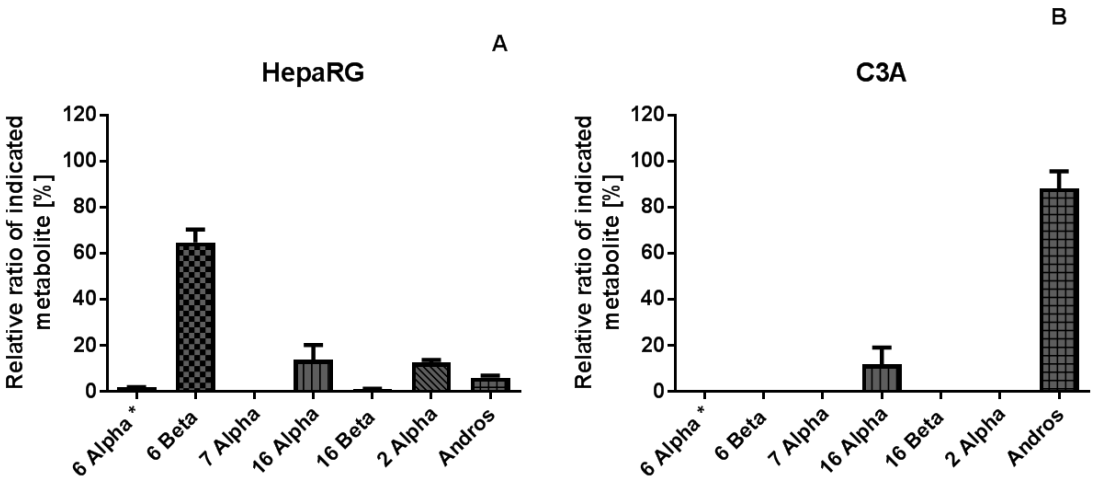

Figure 3.5 Metabolites of testosterone: Drug metabolite profiling of testosterone (CYP3A4) using HPLC. Metabolism of testosterone in **A**) HepaRG™ or **B**) C3A cells. on culture day 8. HepaRG cells showed a significant level of the major secondary metabolite 6-beta-hydroxytestosterone and a wider range of secondary metabolites. Data presented from 2 experiments with 6 technical replicates. Work carried out by Dr Phillip Treskes and Dr Helen Grant.

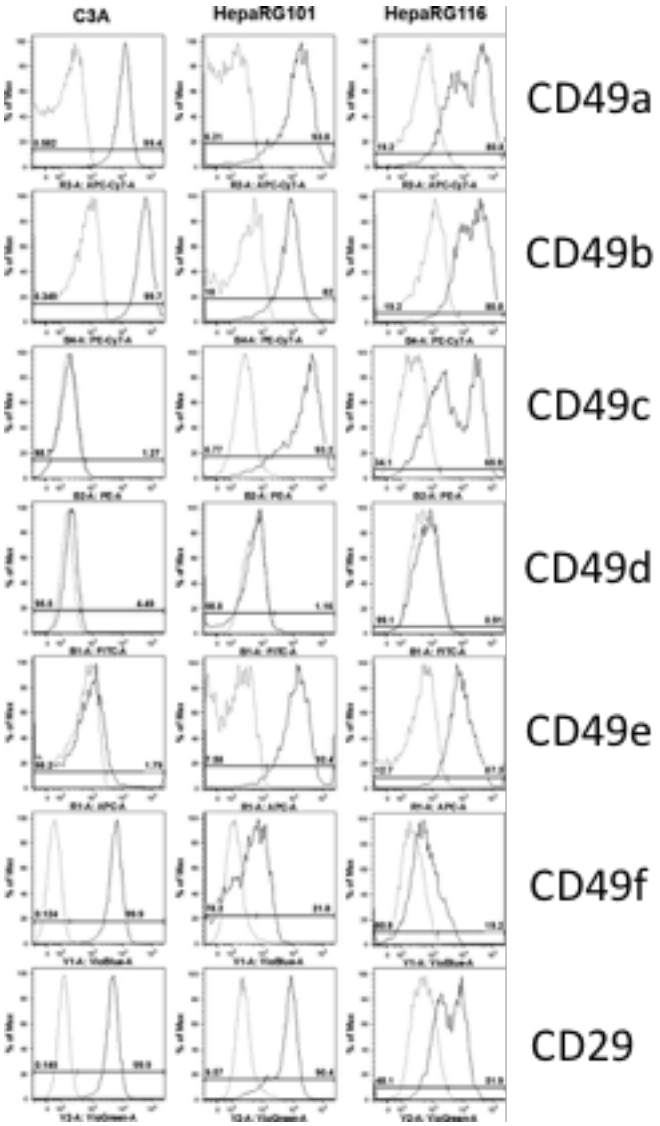

Figure 3.6 Flow cytometry profiling of integrin expression in C3A, HepaRG™P and fully differentiated HepaRG™ cells. Flow cytometry histograms comparing integrin expression (CD49a-f: α1–α6) and CD29 (integrin β1) between C3A, HepaRG™ P and HepaRG™ fully differentiated cell lines (dark lines), and isotype controls (grey lines). CD49d was not expressed by any line. Expression of CD49a, CD49b and CD29 was comparable between all 3 cell lines, though downregulated on a proportion of HepaRG™ fully differentiated cells. Expression of CD49e absent from C3A cells was detected on HepaRG™ P cells and maintained on HepaRG fully differentiated cells. This was also true for the expression of CD49c, except that there was some down-regulation of expression by HepaRG™ fully differentiated cells. Conversely, C3A expressed CD49f, whilst it was absent or low on HepaRG™ P and fully differentiated cells.

3.3.4 Flow cytometry

There is very little information associating cell type with specific integrin expression. Expression of integrins CD49a-f (α sub-units 1-6) and CD29 (β1 sub-unit) by C3A, HepaRG™ P and HepaRG™ cells is shown in Figure. 3.6. C3A cells expressed CD49a, CD49b, CD49f and CD29 but showed no staining for CD49c-e. The immature/undifferentiated hepatoblast-like cell line HepaRG™ P, showed a comparable phenotype, expressing CD49a, CD49b, CD49f, although the frequency and level of expression of CD49f was lower than seen for C3A. In addition HepaRG™ P cells expressed CD49e, which was absent from C3A cells. HepaRG™ differentiated cells show hepatocyte, biliary and epithelial morphologically (**Figure. 3.6).** Looking at cellular morphology there is a clear difference between C3A and HepaRG™ cell cultures. It is clear that the HepaRG™ cell culture comprises two different cell types. Using integrin expression to see if there was a difference between the two cell types we start to see the differences described above. There is a difference in modulation of integrin expression between C3A and HepaRG™ cells where there are clearly two different cell populations in the fully differentiated HepaRG™ cells as shown in CD49a, b and c and CD29 (Figure 3.6). This is possibly due to the differentiation process and time in media containing DMSO

However, more work is needed to demonstrate integrin modulation is an indicator of differentiation and a key to defining the two cell types seen in HepaRG culture.

3.4 Discussion

Appropriate *in vitro* human models are urgently required to help reduce high drug attrition rates in clinical trials by detecting toxicity at earlier stages and improving predictive outcomes. This may also reduce the reliance on subsequent animal testing in drug development. Here the human hepatic cell lines C3A and HepaRG™ were assessed in terms of intrinsic CYP enzyme activity, metabolic competency, and integrin expression to determine which cell line is best suited in pharmaceutical applications.

Compared with C3As, HepaRG™ co-cultures, exhibit a more organotypic phenotype, including evidence of hepatic polarity with strong expression of CYP3A4 (**Figure. 3.1**), the major isoform involved in the metabolism of over 60% of marketed drugs (Newsome et al., 2000, Tsiaoussis et al., 2001). Using immunocytostaining, cytochrome P450 assays, LC:MS/MS and flow cytometry we show HepaRG™ cells to be a superior model to C3A cells for *in vitro* applications and pre-clinical toxicity testing.

Major CYP enzymes CYP3A4, 1A2 and 2E1 are more abundant in HepaRG™ cells compared to C3A (**Figures 3.1 & 3.2**) This shows a more sophisticated metabolic machinery that is comparable to newly isolated

PHHs. Furthermore, HepaRG™ cells show a specificity of CYP activity induction and inhibition, not seen in C3A cells. (**Figure 3.2**). This could, in part, be due to the phenotype of the HepaRG™s. HepaRG™s were isolated from a mature female in her 30's while C3A cells were isolated from a teen. It is speculated that HepaRG™s mature differentiated function and phenotype is due to the donors exposure to compounds such as ethanol, paracetamol, ibuprophen and other over the counter or prescribed meds that a younger donor would not have necessarily been exposed to.

HepaRG™s mature function can also be seen in the turnover of phenacetin and testosterone. LC:MS/MS is used for a variety of applications to identify and quantify compounds and metabolites. Here it is employed to analyse the turnover of phenacetin and testosterone and to discover if the cell lines are metabolizing the parent compound into secondary or even tertiary metabolites.

The results of LC:MS/MS within this study supports preferential usage of HepaRG™ cells over C3A in terms of metabolic proficiency of phase I metabolites. Adding to this the HepaRG™ cells reproducibility and stability in culture for >28 days, make it an attractive model which would give a more detailed analysis of drug metabolism and exhibit CYP activity comparable to PHH. This level of CYP activity would normally have to be engineered into other cell lines. Metabolism and turnover of phenacetin and testosterone showed HepaRG™ cells turned over significantly more of the parent

compound than C3As (**Figures 3.3, 3.4 and 3.5**). While we show no presence of CYP1A2 in C3A cells using end point PCR (Figure 3.1) we also show that there is roughly a 20% turnover of phenacetin using LC:MS/MS (Figure 3.3). While this project was focusing on one of the major enzymes, CYP1A2, involved in the metabolism of phenacetin, there are other CYP enzymes which are also responsible for metabolism (CYP2E1 and CYP3A4) of this compound which may explain turnover of phenacetin in LC:MS/MS (Kobayashi et al., 1999). The major metabolite of testosterone, 6 Beta hydroxytestosterone, is only seen in HepaRG™ cells. Given that hepatic clearance of drugs depends on the activity of transport proteins located on the bile canalicular membranes, the unique property of bipotency in HepaRG cells, which gives rise to a representative split of hepatocytes and biliary cells, may permit focused approaches for cholestatic DILI studies.

This is in agreement with other reports which show HepaRG™ cells to exhibit superior Phase I-III metabolism when compared to C3A and PHHs (Gerets et al., 2012). Using real time impedence biosensing with various CYP450 assays containing prototypical inducers, Gerets et al., (2012) found HepaRG™ cells to be the most inducible model, and metabolically more closely related to PHHs than HepG2. When comparing gene expression of Phase I, II and III mRNA between HepG2, HepaRG™ and PHHs cells, they also found that HepG2 cells expressed the lowest mRNA values for almost every gene tested (Yu et al., 2012).

Flow cytometric analysis was also performed to compare the expression profile of cell surface integrin receptors. Integrin-mediated cell adhesion sites link the actin cytoskeleton with the extracellular matrix, and are important modulators of cell behaviour including growth and survival, differentiation, and polarity (Giancotti and Ruoslahti, 1999). Several integrins were assessed to determine if we would see two separate populations of cells in the HepaRG™ fully differentiated cell culture. While these integrins are not definitive of cell type, understanding how they respond to their environment can be informative. Integrins are best known to be involved in migration and homing with the best example being the hematopoetic system (Magnon and Frenette, 2008, Yu,et al., 2002) Expression profiling reveals that differentiated HepaRG™ cells have markers associated with hepatocyte, biliary and epithelial morphology and modulate integrin expression as compared to progenitors (**Figure 3.6**). Expression of CD49a, CD49b, CD49c and CD29 was comparable between all 3 cell lines, though downregulated on a proportion of HepaRG™ fully differentiated cells. This may indicate two distinct populations within the HepaRG™ fully differentiated culture. In contrast, the C3As, notably express the most abundant hepatocyte integrin a5 (the fibronectin receptor, a5b1), important in development and cell differentiation processes. Therefore, HepaRG™ cells may represent a valuable model in which to study hepatic cell-cell and cell-matrix interactions. Further flow cytometry may identify and specify integrins that may ultimately

delineate the HepaRG™ co-culture into its two separate populations. This could have a significant impact on future experimentation and the ability to identify damage and characterise toxicology profiles by cell type.

C3A cells have been utilized in tissue engineering and cell therapeutic applications, such as the extracorporeal liver assist device (ELAD) system, which failed to meet expectations in clinical trials (Ellis et al., 1996). It is well known that detoxification capacity and mixed function oxidase activity is very poor (Yu et al., 2012) in C3A cells, that require various manipulations, including transfection, to stimulate CYP450 activity (Vermier et al., 2005) and functional suitability for BALs, drug safety or pharmacological experiments. The present study shows C3As exhibit a lack of specific liver function (CYP450 activity/ metabolism) and potentially miss significant toxic effects (secondary metabolites) of candidate compounds under investigation, while HepaRG™ cells basal level of CYP expression, Phase I, II and III metabolism and longevity in culture show differentiation and function comparable to PHH.

3.5 Conclusion

In conclusion, comparison of C3A and HepaRG™ cell lines supports human HepaRG™ cells as a more relevant organotypic *in vitro* human model, which may permit more predictive pre-clinical screening of drugs and could potentially reduce drug attrition, DILI and animal testing, leading to lower drug development costs.

Chapter 4 Optimisation and assessment of HepaRG™-P cells grown on nanopatterned substrates

4.1 Introduction

It has been shown that tissue culture substrates play an important role in the development and maturity of a cell culture, especially those which retain some form of plasticity. Traditional culturing methods to differentiate the HepaRG™ –P cell line involve a 4 week protocol of proliferation and differentiation that uses a variety of media including DMSO in the later 2 week phase of differentiation. Alternative substrates that have been shown to promote differentiation in stem-like cell cultures have been proposed. However, there is currently no data on the ability of NPS to promote proliferation and differentiation in hepatic cell lines, therefore this will be investigated in detail in this chapter.

4.1.1 Cell differentiation and use of DMSO in hepatic cell culture

HepaRG™ cells are a surrogate of PHHs for use in pharmacological applications. Maintaining phase I and II metabolism and superior CYP activity to C3A cells makes the HepaRG™-P cell line attractive and more physiologically relevant for evaluating the toxicity of compounds. NPS have increasingly been used in tissue engineering because they do seem to promote differentiation of stem/progenitor cells (Dalby et al., 2007, Curtis et

al., 2004). For this reason, HepaRG™-P cells, known to retain some stem-like properties are an attractive cell line for assessing whether differentiation and enhanced function can be achieved using NPS.

HepaRG™-P cells are a bipotent progenitor culture consisting of fibroblastic cholangiocyte-like cells which normally mature into a co-culture of hepatocyte and cholangiocyte-like cells 14 days after addition of DMSO to culture medium (**Figure 4.1**). DMSO is traditionally used in many cell cultures to promote differentiation by pushing cells already committed to a specific lineage and to maintain and stabilise a differentiated phenotype (Pal et al., 2012, Czysz, Minger and Thomas, 2015)

While the effect of DMSO creates a stable co-culture of hepatocytes and cholangiocyte-like cells within the HepaRG™-P cell line, in toxicity assays DMSO's induction of CYP pathways could mask specific drug-induced CYP activity or cause other unintended inductions or inhibitions (Park, 1988). Therefore, it has been suggested in toxicology studies, testing for the presence of phase I metabolism, that DMSO be kept below 0.5% to allow the detection of toxic effects of the tested drug (Schevchenko, 2014). Whereas, it is recommended to increase the concentration of DMSO when looking for toxic secondary metabolites, as DMSO induces pathways which increase production of secondary metabolites (Schevchenko, 2014). At low DMSO concentration direct effects of the drug are seen, and at high concentration, increased production of secondary metabolites can be seen. Finding a platform whereby HepaRG™ cells could form characteristic hepatocyte

chords and maintain a stable ratio between hepatocytes and cholangiocytes, without the need for DMSO-induced differentiation, in drug toxicity studies would eliminate its secondary concentration dependent effect on either phase 1 or phase 2 metabolism.

Timing of the addition of DMSO is also important. Added too early, DMSO can cause a decrease in cell mass as some non-committed cells die off. However, induction of CYP activity by DMSO in cells committing to hepatocyte lineage appears to enable detoxification pathways allowing survival of committed cells. It is speculated that this promoted differentiation is due to a 'survival' mechanism within the cells (Guguen Guiliozo, 2014) and cues undifferentiated cells to become hepatocytes to further 'filter' their environment of toxins.

DMSO is also reported to induce several CYP pathways including CYP3A4 which is key in removing toxic substances. A study carried out by Kanebratt and Andersson (2008) showed a correlation between DMSO and the induction of CYP enzymes 2C9, 3A4, and 7A1. It also showed an increase in phase II enzymes and efflux transporters further supporting the theory that DMSO induces a detoxifying mechanism of survival. While HepaRG™-P cells do not need DMSO to initiate the differentiation process, it is required to sustain this process and to produce a confluent culture comprised of hepatocyte and cholangiocyte-like cells which is maintained for 4 weeks + in culture.(**Figure 4.1**)

Finding a NPS that would advance the timing of differentiation of HepaRG™-Ps without the need for DMSO would be more cost effective, and eliminate the variable, or bias, that DMSO lends to experimentation with potential pharmaceuticals or compounds.

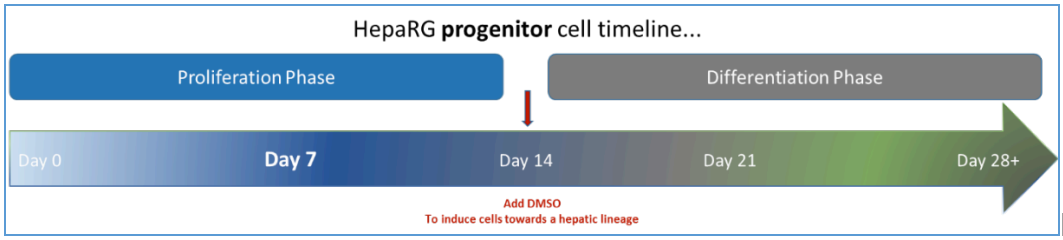

Figure 4.1: HepaRG™ progenitor timeline: Timeline of HepaRG™ –P cells showing a distinct proliferation and differentiation phase, separated by a media change at day 14 with media containing DMSO supplementation required for induction and sustained commitment of hepatocytes.

4.1.2 Outline of experimental work

This chapter will examine the HepaRG™-P cell line on NPS developed by the UoG to assess if there was a change in growth, viability or function. Culturing multipotent cells on NPS is a trial and error process. Initially, it was unknown whether HepaRG™-P cells would adhere to the NPS and grow into a viable culture. The first stages of this study assessed HepaRG™-P cells by studying morphology when grown on NPS vs those grown on TCP to assess adherence to NPS. Secondly, it was important to assess cell viability and to identify a NPS that may give rise to earlier hepatic differentiation without the addition of DMSO. After identification of a NPS, which showed promise of

inducing earlier the hepatic morphology as assessed by microscopy, we studied a number of genes of interest (GOI) to assess in depth differentiation. In order to adhere to the minimum information for publication of quantitative real-time PCR experiments (MIQE) guidelines we assessed a panel of stable reference genes (RGs) for use in normalisation of GOI for molecular analysis of this study, that would be used to assess phenotype. Where cells go through a maturation process with changes in the cytoskeleton and gene profile, it may be difficult to determine a panel of appropriate RGs as these may change as culture conditions and cell maturity are altered. This also raises questions as to whether traditional RGs may become GOI. For instance, traditional RGs such as the cytoskeleton protein B-actin may be a GOI under tissue engineering experimental conditions (where cell morphology is expected to be modified). For this reason, MIQE guidelines established strict criteria for assessing GOI by ensuring that the RGs used to normalise data are appropriate across all experimental conditions (Bustin et al., 2009). This is particularly relevant to HepaRG™-P cell line which retains a stem-like plasticity.

The next step evaluated the phenotype of cells grown on specific NPS vs unpatterned control (UP) and TCP using immunocytostaining and qRT-PCR.

4.1.3 Aims

The specific aims of this chapter are

1. To evaluate HepaRG™-P cell adhesion and proliferation on NPS
2. To investigate whether or not cell viability on NPS is stable compared to internal unpatterned control (UP) and standard tissue culture plastic (TCP) routinely used in HepaRG™ differentiation process.
3. To evaluate a number of RGs against all of our experimental conditions to acquire an appropriate set of RGs for use in normalising GOI in accordance with MIQE guidelines.
4. To identify a promising specific nanopattern likely to promote earlier hepatic morphology in HepaRG-P cells without using DMSO which is known to promote and sustain differentiation of HepaRG cells in culture. To use biochemical, molecular and immunostaining techniques to assess in depth maturation and function to ascertain if differentiation can occur on NPS via only biomechanical cues that NPS provides.

Rationale: Having shown that HepaRG cells are a surrogate to PHH in DILI studies (Chapter 3), here we assess the effect of surface pattern and treatment on proliferation and differentiation of HepaRG-P cells. Finding an NPS which would differentiate HepaRG-P cells without the use of media containing DMSO would save time and money in the process of growing

these cells for use in DILI studies and also exclude any toxic or metabolic effects of DMSO which may confound other studies.

4.2 Materials and methods

4.2.1 Nanopattern plates

NPS for this study were produced by UoG Bioengineering Department, based on the nano-architecture used by Dalby et al. (2007) using EBL a patterned silicon chip was manufactured in the UoG clean room. A nickel shim was created based on this chip and used at high pressure to print the various nanopatterns onto a molten polymer (**Figure 4.2**). Once hardened this polymer was fixed within a plate framework and treated with oxygen plasma before arriving at UoE. Twenty-four wells accommodated 21 different patterns with replicates of DSQ50 and Near 50 making up the 3 final wells. The names given to the patterns were based on how far apart the pits were in relation to one another. For example, on the DSQ10 pattern nanopits were 10nm apart, pits on DSQ20 were 20nm apart, DSQ30's nanopits were 30nm apart, and so on. It is important to mention that the polymer used as support medium for nanopatterning was also included as an internal planar control or unpatterned (UP): the wells on the UP control were of the same size and dimensions and received the same surface treatment, however, there was no nanopattern. Very few published papers on NPS consider a planar control. Here we will use the UP to normalize for the surface chemistry treatment where necessary, but also as a comparison of non-patterned oxygen plasma treatment vs NPS and TCP.

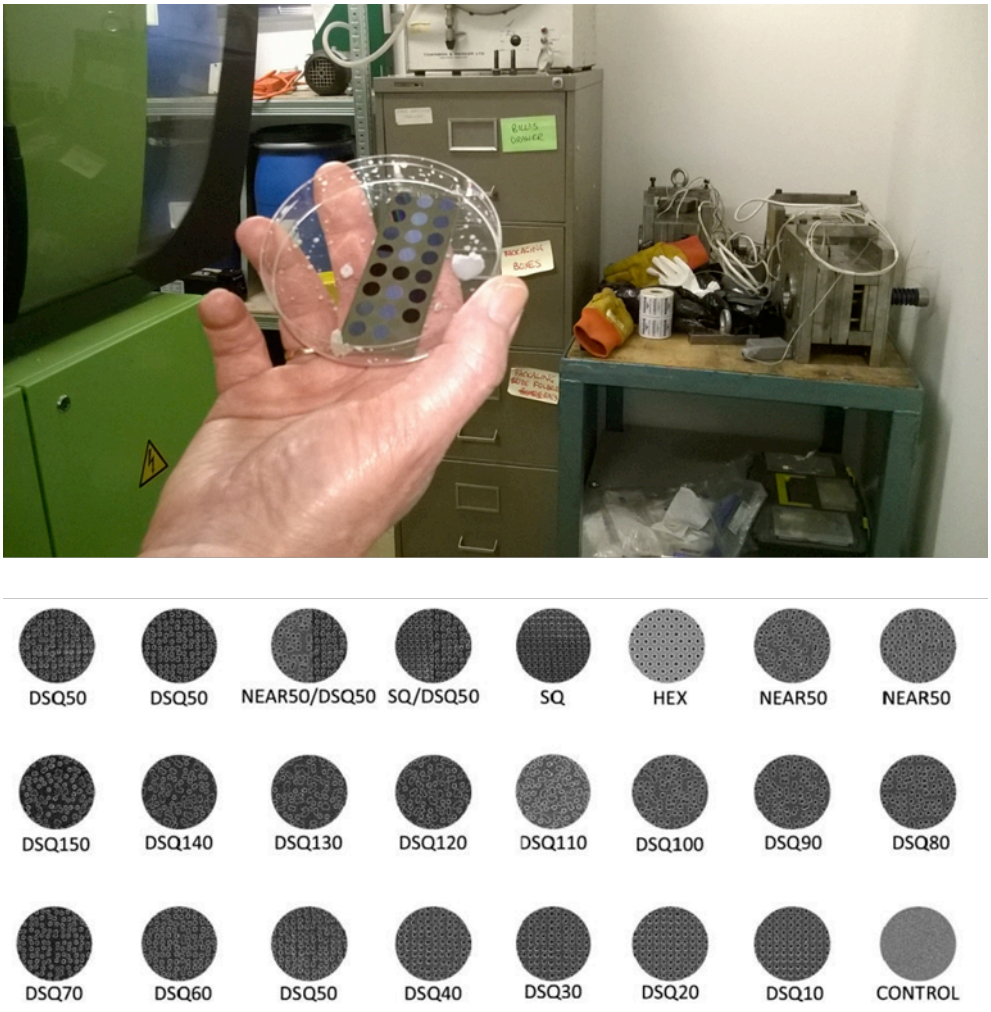

Figure 4.2 Nanopattern nickel shim and graphical illustration of all 24 patterns **A**) Nickel shim designed in Glasgow and produced in Germany showing the ¾ 96 well format of the various 24 well patterns.
B) Visual representation of 24 well nanopattern array DSQ signifies disordered square patterns and corresponding number indicates the distance in nanometers between each pit. Hex stands for hexagonal pattern while SQ stands for ordered square array. Control well was oxygen plasma coated alongside wells containing nanopits, but does not have any pattern or roughness.

4.2.2 Coating of nanopattern substrates

There are various surface treatments available to create an adhesive hydrophilic surface. The two main types of treatment are oxygen plasma and corona treatments, both discussed in Chapter 1, section 1.2.2.5. In this study, oxygen plasma treatment was the treatment of choice because it was done under controlled conditions with high reproducibility. Corona treatment of plates was also possible. However, this is currently done manually using a hand held device resulting in variability between plate treatments. We also trialled non-coated plates to see if nanopatterns had an effect on adhesion without surface chemistry treatment.

4.2.3 Seeding HepaRG™-P cells on nanopattern substrates

Prior to seeding the HepaRG™-P, the NPS were wetted with 100μl of media at room temperature for 1 hour. This ensured better adherence of cells to the surface substrate, and also confirmed that there was no leakage on the plate.

Cells were seeded, as described in Chapter 2, 2.2.2.1. The first batch of plates was used to identify nanopattern wells that supported normal growth and adherence of HepaRG™-P cells. Once this had been established cells were seeded on NPS from batches 2 and 3 alongside TCP 96 well plate.

Cells were kept in 711 growth media (DMSO negative) for the duration, and media was changed every other day. Phase microscopy on the EVOS Flo Auto was used to assess cultures on a daily basis and pictures were taken across a variety of time points.

4.2.4 Surface treatment

4.2.4.1 Quality control of C3A cells grown on oxygen plasma treated plates

Initially C3A cells were used to test various surface treatments as they were a more cost effective way to investigate adhesion. Two batches of nanopatterned plates were used for assessment in comparison to TCP. Batch 1 was untreated and batch 2 was treated with oxygen plasma. C3A cells were seeded at 25k cells per well on NPS batch 1, batch 2 and TCP 96 well plates.

4.2.4.2 Assessment of cell viability, confluency and morphology using EVOS Auto flo microscopy

The EVOS flo auto™ has the ability to set a ‘beacon’, a customized focal point that can be saved as a routine so the microscope can return to the same spot to take consecutive pictures over time. The routine is saved and can be run automatically or manually. Two beacons were set per well, at random, on the EVOS flo auto to observe morphology and adhesion.

C3A cells were cultured in MEME+ for 5 days with media changes on Day 1, Day 2 and Day 4. PrestoBlue™ was used on day 4 to assess cell viability.

4.2.4.3 Testing oxygen plasma surface treatment with HepaRG™- P cells

Each NPS required oxygen plasma treatment to create a hydrophilic substrate that would allow cells to adhere to the surface. This treatment was applied across the whole plate (21 different patterns, repeated patterns and UP control).

As no standard oxygen plasma treatment had previously been used, it was decided that various wattages over time should be assessed to determine the best treatment for use with HepaRG™-P cells. Plates were treated with oxygen plasma at UoG before being sent to UoE for use. The wattages and times chosen were; 40W oxygen plasma 30s, 40W oxygen plasma 60s, 40W oxygen plasma 120s, Corona treatment, 80W oxygen plasma 30s, 80W oxygen plasma 60s, 80W oxygen plasma 120s. Two plates were used per treatment.

Once the plates arrived in Edinburgh they were gamma sterilized using a CIS bio international IBL 637 gamma steriliser for 5 minutes on the bottom shelf, which equates to 10 greys of gamma irradiation.

For this experiment, HepaRG™-P cells were seeded at 20k cells per well on plates receiving oxygen plasma and corona treatment and viability assessed at days 3 and 7. Phase contrast pictures taken on day 6.

4.2.5 Viability assays

PrestoBlue™ and total ATP assays were carried out in accordance to the materials and methods described in Chapter 2, 2.5.1 & 2.5.3.

4.2.6 Pierce BCA total protein analysis

Pierce™ BCA protein assay kit (ThermoFisher catalogue number 23225) was used to measure total proteins of HepaRG-P™ day 7 cells grown on TCP, UP and DSQ120 cell culture substrates. This kit uses a detergent reagent which quantitates a total protein concentration when compared to a protein standard. Standards were made according to manufacturers specifications using an albumin standard (BSA). Cells were washed once with PBS+ before addition of lysis buffer (100μl per well). After addition of lysis buffer, cells were put onto a cell shaker for 30 minutes. After 30 minutes in lysis buffer, 25μl of each sample was added to a clear 96 well plate, 200μl of working reagent was added to wells before incubation at 37°C for 30 minutes. This reaction measures proteins through the colorimetric detection of copper by bicinchoninic acid. Known as the 'biuret reaction', amino acids form a blue coloured complex when they react with cupric ions. Bicinchoninic acid (BCA) is then added to develop the colour further so it can be read at 562nm. Binding of 2 BCA to 1 cuprous ion intensifies the colour from a light blue to an intense purple which is more readily detected. Absorbance was measured at 562nm on Promega GloMax multi-well plate reader.

4.2.7 Materials and methods of molecular analysis

In accordance with MIQE guidelines a record of RNA integrity and quantity was stored. (Further evidence can be found in Chapter 7 Supplementary data), RNA samples were stored in -80°C and cDNA samples were stored at -20°C until processed.

RGs are crucial as a control in interpreting fold changes and analysing GOI. Appropriate RGs are especially important in tissue engineering applications where a cell line retains progenitor or stem cell-like properties and moves through various stages of development.

Within this tissue engineering experiment, the RG analysis was repeated independently three times using HepaRG™-P cells synchronized at a specific passage. Thawed cells were plated separately in order to create 3 independent technical replicates (n=3, technical variability: the results from one separately set-up plate are independent). As this experiment was carried out 3 times, the total independent replicates were 9.

Based on current literature (Celeen et al., 2001, Hart et al., 2010) and personal preference 12 RGs were selected, for use in normalising GOI for experiments using HepaRG™-P grown on NPS. All samples were run against 12 RGs; UBC, YWHA, SDHA GAPDH EIF4A1, B2M, TOP1, RPL13A, ATP5B, CYC1, 18s and ACTB.

Table 3: Tested reference genes with names and functions

Abbreviation	Name	Function
18S	18S ribosomal RNA subunit	Component of eukaryotic ribosomal subunit 40S
ATP5b	ATP synthase subunit 5b	Encodes a subunit of mitochondrial ATP synthase
β-Actin	Beta-actin	Isoform of actin proteins – part of cytoskeleton
B2M	Beta-2microglobulin	Encodes a protein found in major histocompatibility protein (MHC) 1
CYC1	Cyclin D1	Encodes a subunit of the mitochondrial transport chain
EIFa2	Eukaryotic initiation factor 4a2	A component of a complex which facilitates recruitment of mRNA to ribosome

GAPDH	Glyceraldehyde-3-phosphate dehydrogenase	Important enzyme for ATP production
RPL13a	Ribosomal protein L13a	Ribosomal subunit
SDHA	Succinate dehydrogenase complex, subunit A	Subunit of succinate dehydrogenase that plays a role in energy conversion within mitochondria
TOP1	Topoisomerase 1	Encodes an enzyme responsible for the breaking and subsequent joining of DNA during transcription
UBC	Ubiquitin C	Encodes a polyubiquitin precursor which helps regulate and modify various effects within the cell
YHWAZ	Phospholipase A2	Adapter protein which binds other protein complexes in many

		signalling pathways

The geNorm output ranked the candidate reference gene according to their expression stability (M).

All primers were obtained from, and validated by, Primer Design.

Biogazelle geNorm software was used to analyse M and V values which are an indicator of RG stability.

4.2.7.1 Experimental design for reference gene validation

HepaRG™-Ps were seeded on NPS as outlined in chapter 5. Cells were collected on day 7 for RNA extraction.

4.2.7.2 Total RNA preparation and reference gene selection

In brief, RNA extraction was undertaken using Life Technologies RNAqueous™ kit and RNA purity/quantity was measured using Thermo Fisher nanodrop and Agilent chip technology. Every sample was assessed on nanodrop and a selection of samples at random were assessed on the Agilent chip (Further information can be found in Chapter 7 Supplementary data).

4.2.7.3 cDNA synthesis and qRT-PCR analysis

cDNA was prepared using PrimerDesign nanoScript to RT kit and qRT-PCR was performed using PrimerDesign-validated primers and master mix on a Roche light cycler 96 system. As previously mentioned, 12 candidate genes were analysed and results were assessed using Biogazelle geNorm software

which uses raw Ct values taken from the Light Cycler 96 to rank RGs in order of stability by assigning an M value to represent stable expression and V values to suggest how many RGs should be used to create a geometric mean that gives the best stability throughout all experimental conditions. Graphpad Prism software was used for performing statistical analysis. A one way Anova and Tukey test were used to assess statistical significance between genes of interest.

4.3 Results

4.3.1 NPS surface treatment

Initially untreated and treated surface were compared. Significant discrepancies between batch 1 (untreated) and batch 2 (oxygen plasma treated) were observed. When grown on untreated NPS, C3A cells exhibited a different morphology than those seen on treated or TCP (**Figure 4.3**). Cells grown on the TCP grew to confluency and started differentiation around the same time as those grown on the treated NPS. These cells formed a typical polygonal morphology reproducibly seen in C3A cultures. The TCP resembled a normal culture and no abnormalities could be seen. However, cells grown on untreated NPS did not grow to confluency. These cells struggled to adhere to the NPS in the first 48h of culture and then started moving towards other cells in the area via elongated filopodia-like structures. Confluency was never reached on untreated plates and large

gaps could be seen across the culture wells. Cells aggregated into spheroid like balls with ragged edges. Around day 7 these aggregated structures disappeared and cells that were congregated together started growing upward through the z plane. Cellular debris was observed on the NPS and remaining cells had a ragged and unhealthy appearance. Cells grown on oxygen plasma treated substrate grew to confluency and exhibited typical C3A morphology. Further confirmation of this assessment of cell viability was carried out using the PrestoBlue™ assay (**Figure 4.4**). Cells grown on untreated plates showed a negative viability due to subtraction of no cell control. Cells grown on treated plates showed viability, though it was variable by pattern.

When surface treatment was assessed the UP well on untreated and treated plates, UP well was observed first to remove the variable of patterning from the experiment. However, all wells were viewed and taken into consideration when assessing viability.

Day 1 Untreated Treated

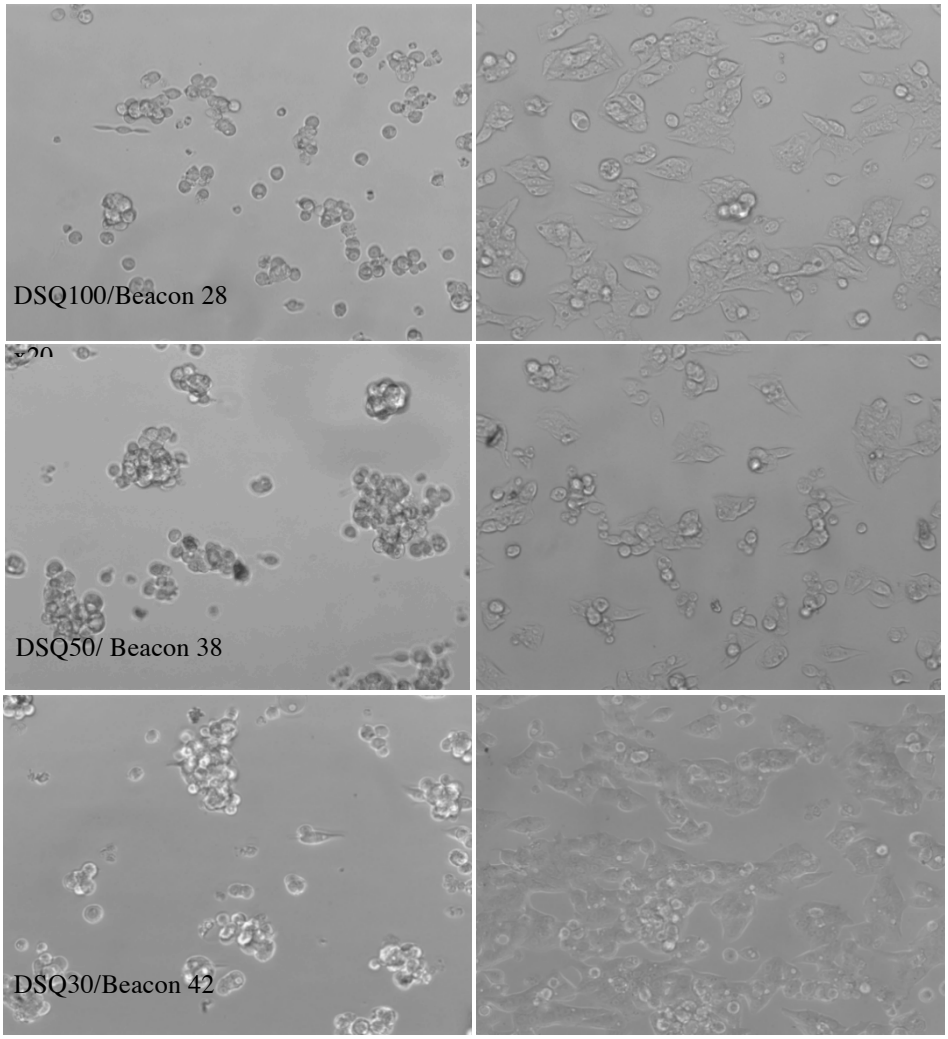

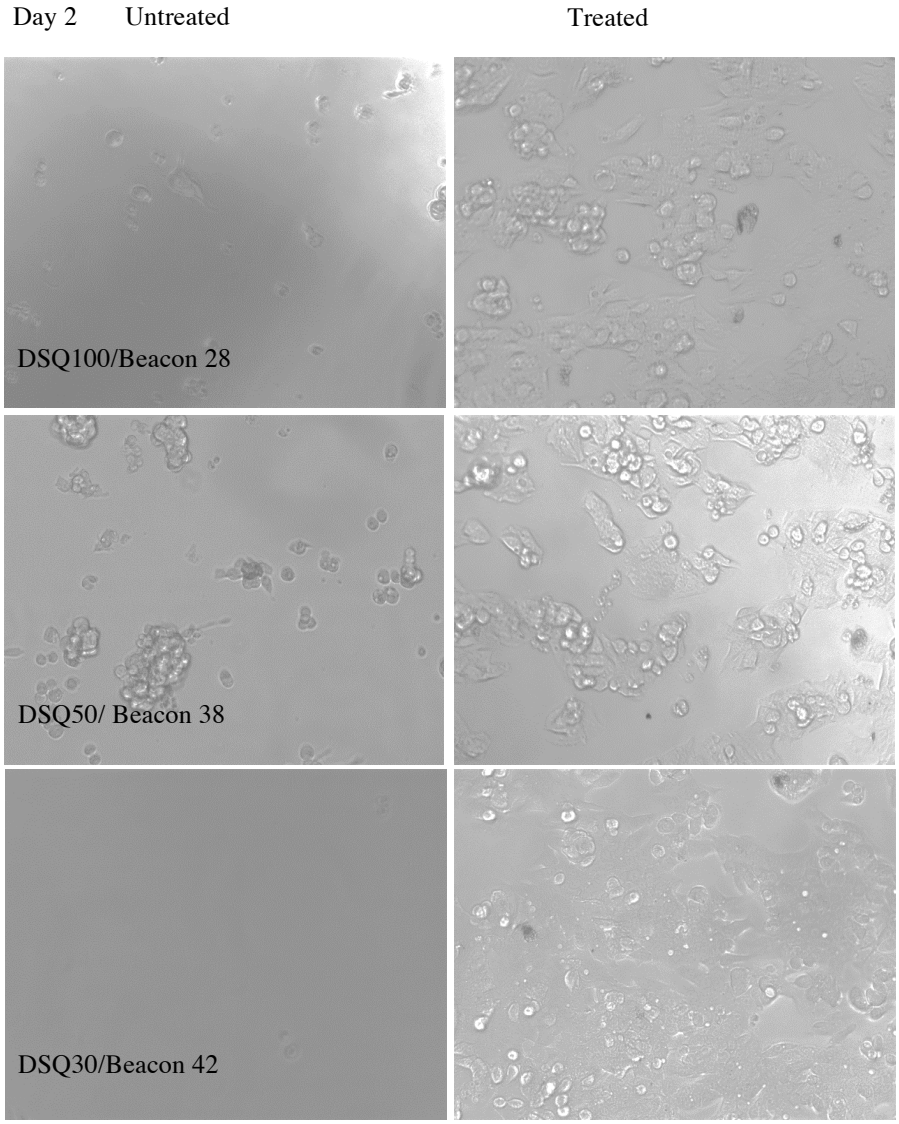

Figure 4.3 Comparing untreated and treated NPS plates on day 1 and day 2: A&B Batch variation of nanopattern plates: C3A cells grown on untreated and treated NPS plates (unpatterned well), show significant morphological changes between batches. Pictures were taken at days 1(a) and 2(b) at x20 on an EVOS autoflo microscope. Beacons were picked at random, but once picked, were used consistently for assessment across days 1 and 2. (not all data shown) Major discrepancies were seen between untreated and treated plates. Cells grown on untreated plates were not confluent, were ragged in appearance and culture contained excessive debris compared to treated. C3A cells grown on treated plates grew to confluency and showed clearly defined cells.

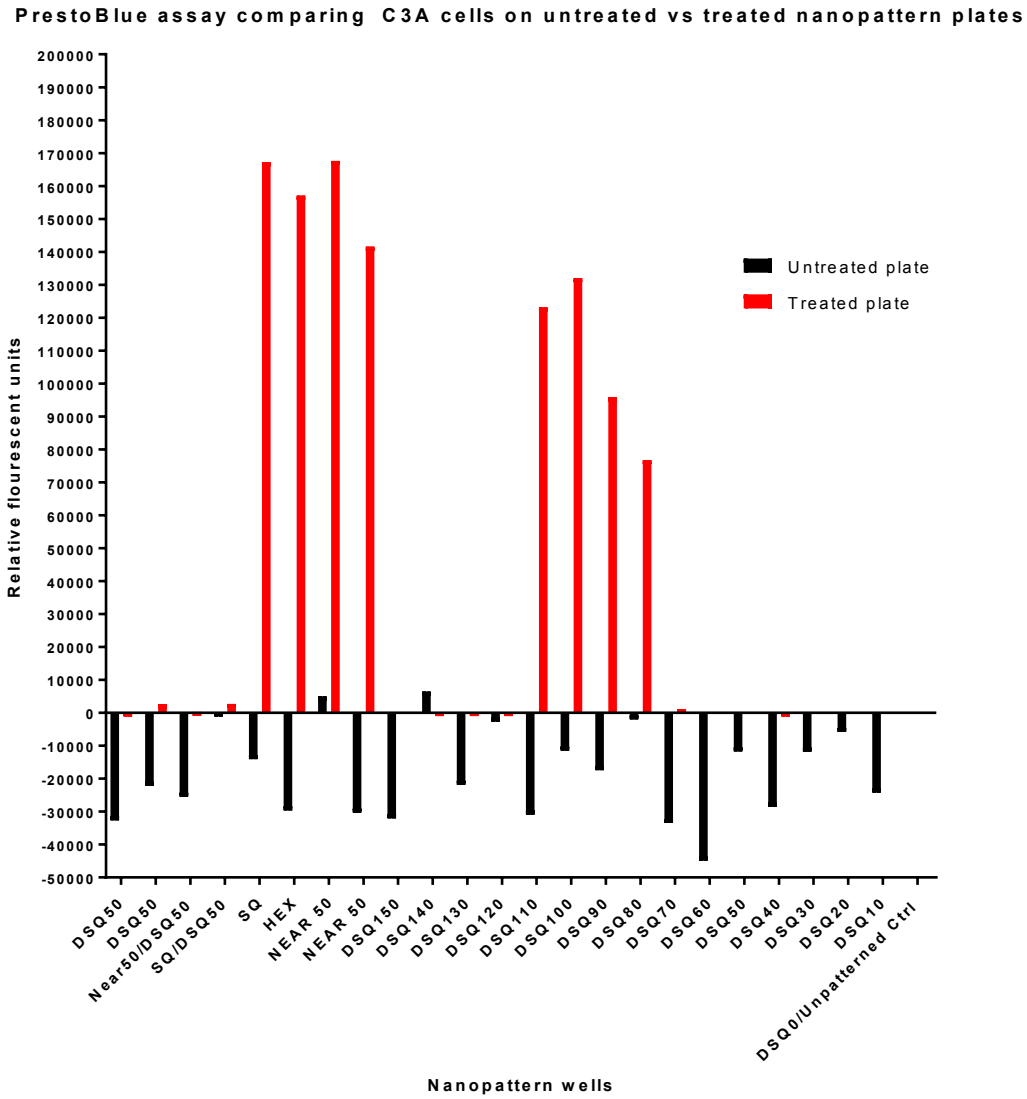

Figure 4.4: Viability of C3A cells grown on untreated and treated NPS plates Quantitative fluorescent measurement of cell viability using PrestoBlue™ resazurin based assay comparing C3A cells plated on untreated and treated nanopattern plates. Data normalized to unpatterned control on each plate. Data shows cell viability at Day 4 (n=1 One experimental replicate with one sample each condition).

4.3.2 Surface chemistry treatments

Basic cell morphology highlighted the importance of surface chemistry in preparing NPS for cell culture, as major discrepancies could be seen between untreated and treated NPS. Once it was confirmed that cells could not remain viable on untreated NPS, various types of oxygen plasma were trialled to determine the best surface chemistry for the duration of the project. For this stage of the project HepaRG™-P cells were used to assess morphology and adhesion.

As oxygen plasma treatment is a combination of wattage for a set time, seven different concentrations of oxygen plasma were trialled (**Figure 4.5**). Corona treatment was also included for comparison. Microscopy showed that cells grown on low wattage treatments for a short time displayed a morphology of healthy, well defined cells which grew to confluency within a traditional time frame.

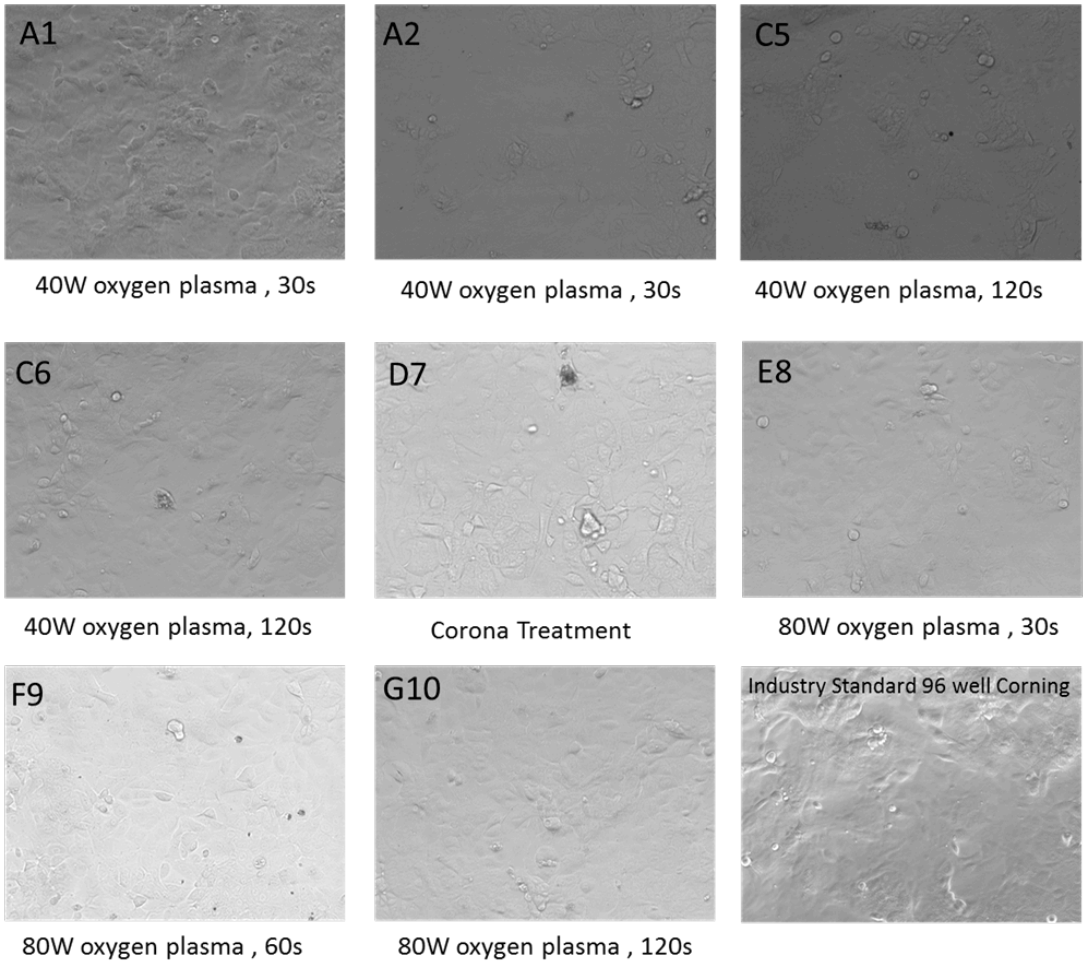

Figure 4.5: Comparing HepaRG™ progenitor cells grown on various oxygen plasma and corona surface treatments Day 6 of HepaRG™-P cells grown on a variety of oxygen plasma and corona treated plates and compared to industry standard 96 well Corning. Only the planar control of the nanopatterned plate was used in this experiment as we wished to compare like for like between the various treatments. Oxygen plasma treatments of 40W 30s, 40W 60s and 40W 120s (A1, A2, C5 and C6) were trialled alongside manual corona treatment (D7) and higher wattage oxygen plasma of 80W 30s, 80W 60s, and 80W 120s (E8, F9, G10) and a 96 well industry standard control.

4.3.3 Morphology on NPS

While assessing HepaRG-P™ cells on each pattern of the NPS, it was noted that cells grown on DSQ120 regularly formed a more cuboidal and bi-nucleated morphology around day 7 compared to other patterns or TCP. The ratio of hepatocytes to flat cholangiocyte-like cells was above average. It was estimated that on DSQ120 there was an 80:20 split of hepatocytes to cholangiocyte-like cells. As hepatocytes make up around 80% of the human liver with the remaining 20% made up of cholangiocytes, stellate cells, Kupffer cells and other, it was thought that this pattern could be a more clinically relevant model (Wisniewski et al., 2016)

Repeated observation of HepaRG™-P cells grown on DSQ120, UP and TCP also showed confluency alongside the emergence of cuboidal, hepatocyte like cells ~ days 6 and 7 (**Figure 4.6**) Cells grown on TCP were not confluent at day , and still showed only fibroblastic morphology, and did not show any cuboidal hepatocyte-like cells. Cells grown on the UP substrate were confluent and showed signs of committing to hepatocyte lineage, acquiring a cuboidal shape.

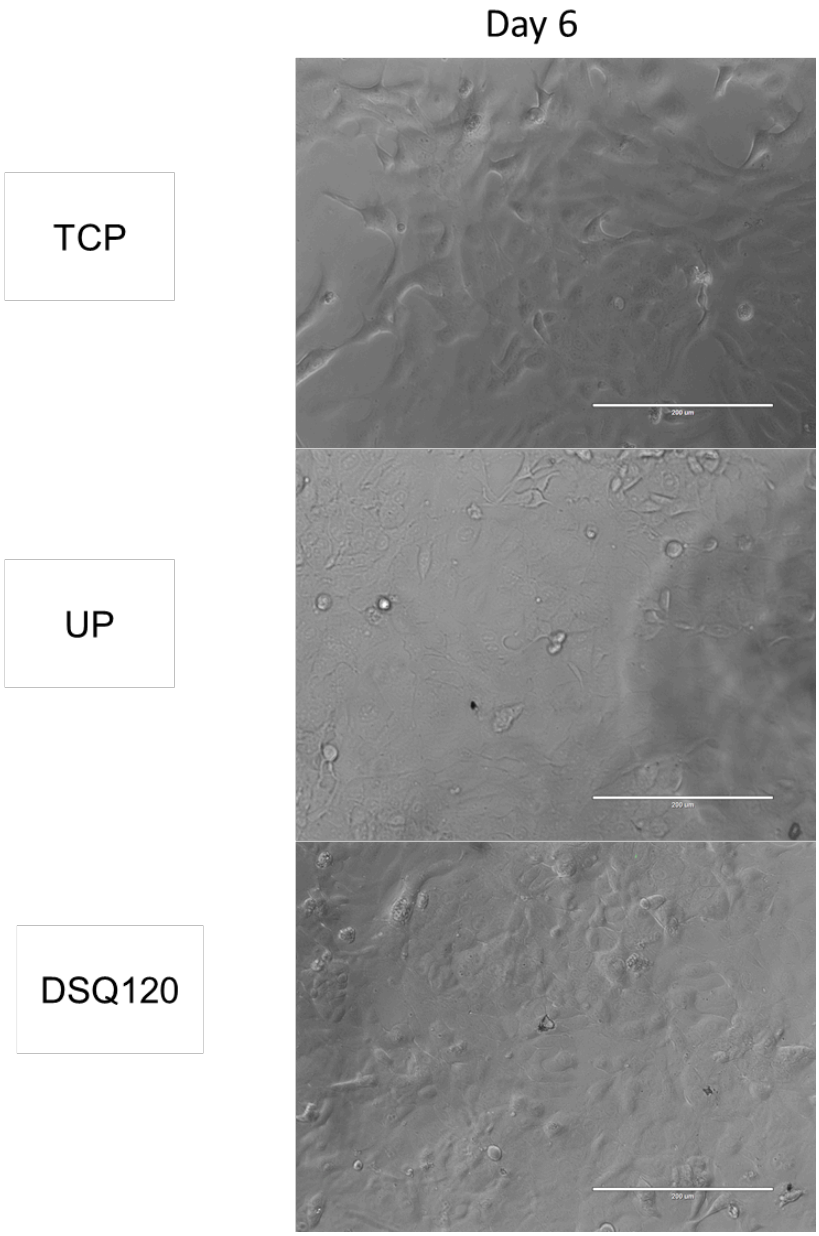

Figure 4.6 Morphological assessment of HepaRG™-P cells on TCP, UP and DSQ120 at day 6. Phase contrast microscopy from EVOS Flo Auto (x20, line measures 200µm) showing HepaRG™-P cells at day 6. Cells grown on TCP (96w Corning) UP (unpatterned control on nanopattern slide) and DSQ120 (nanopattern substrate).Cells grown on TCP are not confluent. Cells grown on UP are smaller and more confluent than TCP, while cells grown on DSQ120 are confluent and signs of a cuboidal morphology indicative of hepatocytes can be seen.

4.3.3.1 Selection of reference genes

As sections 4.3.5 and 4.3.6 show results of molecular investigations of GOI, the process whereby a set of RGs was established is described below.

4.3.3.2 RNA preparation and quality

Nanodrop 260/280 was used to assess RNA purity. A nanodrop 260/280 ratio of 2 is considered to be uncontaminated with genomic DNA and of good quality (260/280 ratios: 1.8-2.0) and RNA integrity. Further materials and methods are in Chapter 2, section 2.6.1 (**Figure 4.7**)

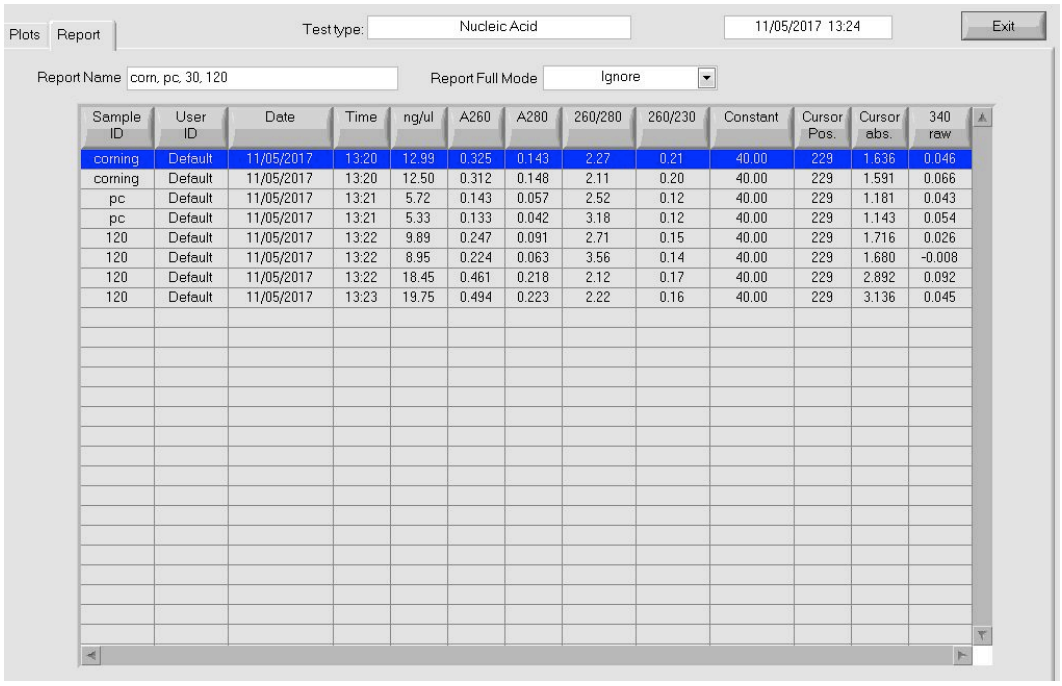

Sample ID	User ID	Date	Time	ng/ul	A260	A280	260/280	260/230	Constant	Cursor Pos.	Cursor abs.	340 raw
corning	Default	11/05/2017	13:20	12.99	0.325	0.143	2.27	0.21	40.00	229	1.636	0.046
corning	Default	11/05/2017	13:20	12.50	0.312	0.148	2.11	0.20	40.00	229	1.591	0.066
pc	Default	11/05/2017	13:21	5.72	0.143	0.057	2.52	0.12	40.00	229	1.181	0.043
pc	Default	11/05/2017	13:21	5.33	0.133	0.042	3.18	0.12	40.00	229	1.143	0.054
120	Default	11/05/2017	13:22	9.89	0.247	0.091	2.71	0.15	40.00	229	1.716	0.026
120	Default	11/05/2017	13:22	8.95	0.224	0.063	3.56	0.14	40.00	229	1.680	-0.008
120	Default	11/05/2017	13:22	18.45	0.461	0.218	2.12	0.17	40.00	229	2.892	0.092
120	Default	11/05/2017	13:23	19.75	0.494	0.223	2.22	0.16	40.00	229	3.136	0.045

Figure 4.7: Selection of nanodrop analysis of mRNA. Screen shot of mRNA analysis by nanodrop spectrophotometer across all cell culture substrates (corning (TCP), planar or untreated control (UP) and DSQ120. Nanodrop records ng/ul and assesses purity of sample. A 260/280 ratio of sample purity ranged from 2.1-3.6 where 1.8 and above is considered ‘pure’.

4.3.3.3 Standard deviation, M and V values in reference gene selection

Standard deviation (SD) has traditionally been used to assess stability between Ct values for individual sample assessment (Figure 4.8). Here we calculate SD alongside analysis performed using geNorm software to gauge robustness of individual gene expression (SD) and how stable each gene is across all experimental conditions. geNorm software calculates the gene expression stability (M value) for a reference gene by using the average pairwise variation (V value) for that gene against other tested reference genes across all experimental conditions (Vandesompele et. al, 2002). Low SD and M values suggests high stability.

Within the tissue engineering experiment, mean SD was 0.3 with a range from 0 to 0.5 in individual samples showing high stability. However, tissue engineering M values show low stability when individual samples are assessed across all experimental conditions (**Table 2**). V values assess the optimum number of RGs needed for normalization of data. Within the NPS study the V values indicating variability between sequential normalization factors is relatively high (geNorm V > 0.15) and at least 7-8 RGs were recommended to normalize GOI **(Figure.9).**

It is advised that genes with an M value higher than 1 are not stable enough for use as RG. Within the NPS experiment, CYC1 was the only gene with an

M value ranking less than 1, SDHA and 18S M values ranked between 1 and 1.2, and UBC, EIF4A1, GAPDH and ATP5B ranked between 1.2 and 2.5. This confirms that the selection of the set of 7 reference genes should be considered for HepaRG™-P transcriptional profiling across all conditions as confirmed in the V values generated from geNorm software.

Though due to the cost of running 7 genes alongside each GOI, it was decided that the geometric mean of the top three genes would be used as the minimum requirement specified in MIQE guidelines (Bustin et al., 2009)

Most stable

Least stable

Reference genes for nanopattern project ranked from most to least stable		
Tissue Engineering		
Ct value	M value	Reference Gene
30.7	<1.0	CYC1
34.5	1	SDHA
24.3	1.2	18s
32.7	>1.4	ATP5B
30.8	1.8	GAPDH
38.9	2.2	EIF4A1
35.9	2.5	UBC

Table 2: Reference gene ranking for nanopattern project Ct and M Values generated by geNorm software Reference genes for tissue engineering/nanopattern project using HepaRG™-P cells ranked in order of most to least stable in accordance to their M value

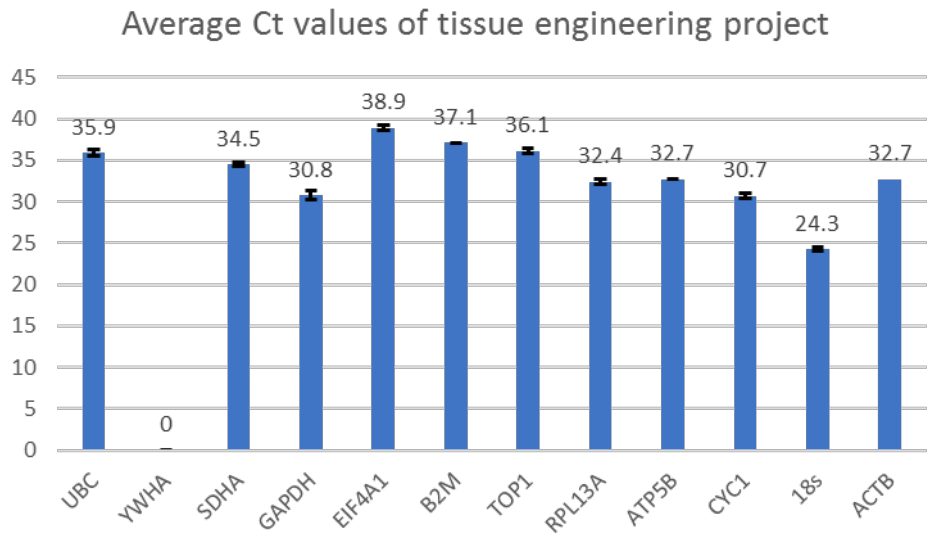

Figure 4.8: Average Ct values for tissue engineering/Nanopattern substrate reference gene selection: Graphical representation of average Ct values are shown for all 12 genes used in validating optimal reference genes. SD shown in error bars of SEM.

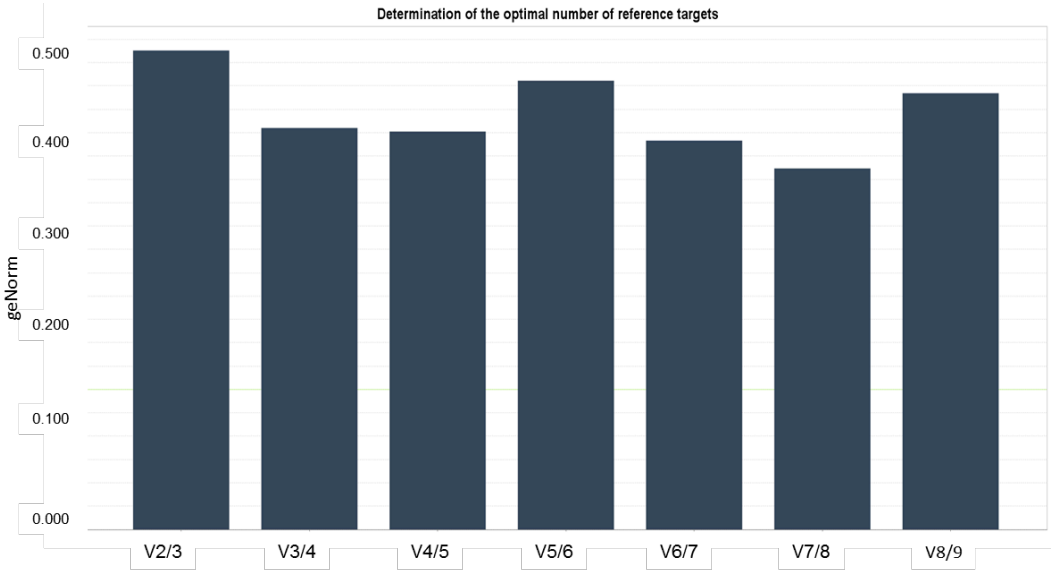

Figure 4.9 V values generated by geNorm software for Nanopattern project: The optimal number of reference genes is determined by pairwise variation known as a V value. The lower the V value the more optimal the number of reference genes for use in nomalisation. In this study a combination of 7/8 reference genes is suggested for use in normalising genes of interest

4.3.4 Phenotype

4.3.4.1 Zonula occludens 1 as a marker of polarity

One of the basic indications that a cell is a mature hepatocyte is the exhibition of polarity. ZO-1 is a membrane bound protein that stabilizes tight junctions by interacting with the F-actin portion of the cytoskeleton. As hepatic epithelial cells establish bile canaliculi (BC) at sites of intercellular contact separated by tight junctions from basolateral domains, the presence of ZO-1 localized within the membrane at cell-cell junctions would represent polarity.

Here we see distinct membrane bound positive staining for ZO-1 on UP and DSQ120 at day 7 (**Figure 4.10**). Because of the known bipotent nature of this cell line a positive ZO-1 staining localised to the cellular membrane indicates that this population of cells has reached maturity. Therefore, it is most likely that these cells are differentiating towards a hepatocyte lineage.

Staining is backed up by qRT-PCR for expression of TJP1 a gene encoding for ZO-1. Significant fold increases can be seen on DSQ120 and UP on day 7 compared to TCP, with UP having the highest fold change (**Figure 4.11**).

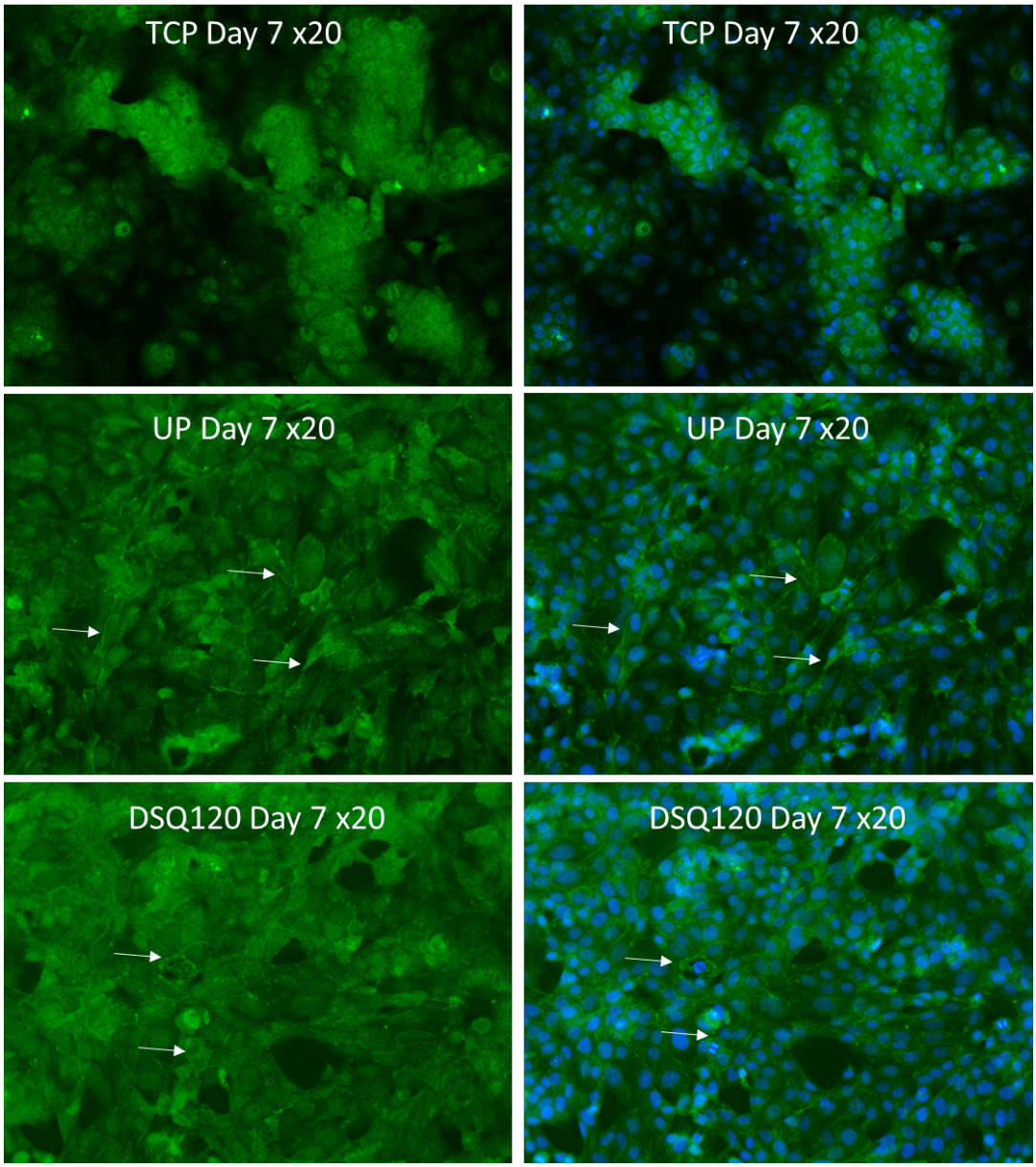

Figure 4.10 Primary staining of Zonula Occludens 1, a marker of cellular polarity: HepaRG™-P cells were grown for 7 days on UP, DSQ120 and TCP. Cells were fixed and stained on day 7 with primary antibody of Hepatic polarity marker Zonula Occludens 1 (ZO-1) (See materials and methods chapter 2). ZO-1is shown in green alongside blue Hoescht nuclei staining. Images were taken on an EVOS Flo Auto at x20 magnification. Day 7 TCP immunocytochemistry shows ZO-1 un-localized in the cytoplasm of cell, while UP and DSQ120 shows localized membrane bound ZO-1 ('chicken wire' appearance) and formation of bile canaliculi typically seen in a mature HepaRG™ culture.

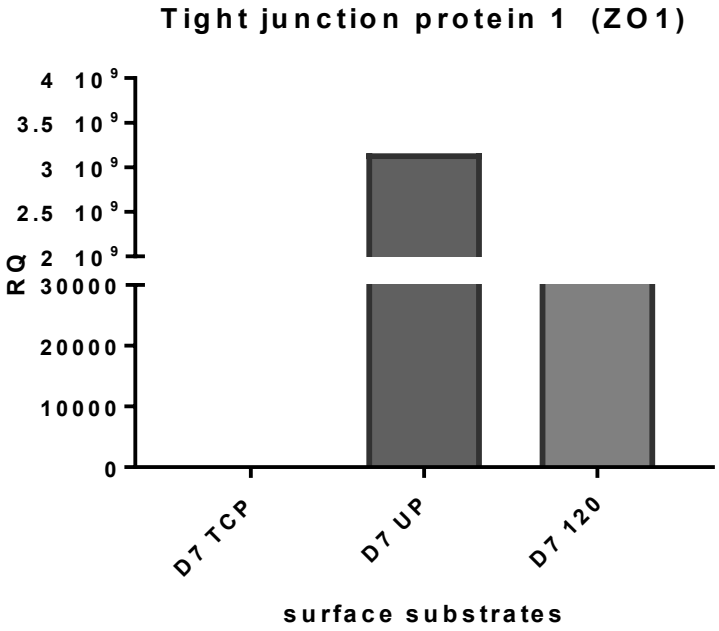

Figure 4.11 qRTPCR of TJP1 (ZO-1) Fold change (±SD) in mRNA expression of tight junction protein 1. Quantitative Real Time PCR showing presence of Tight Junction Protein 1, the gene encoding for ZO-1, on day 7 of HepaRG™-P culture. qRT-PCR correlates little TJP1 at Day 7 on TCP with previous and significant fold increases of TJP1 Day 7 on UP and 120. Results are presented as fold-changes in gene expression relative to untreated control calculated with the ΔΔCq method. (n=3, representing 3 independent experiments with 3 technical replicates each experiment).

4.3.4.2 SOX9/HNF4α reciprocal expression

SOX9 is found in various tissues. However, it is a known marker of a cell committing to the cholangiocyte lineage. Mature hepatocytes should stain negative for SOX9. Therefore, within this bipotent culture, the presence of SOX9 shows a population of cholangiocyte-like cells.

Although hepatocyte nuclear factor 4 α (HNF4α) is found in tissue other than the liver, within this bipotent culture it is used as a marker of a mature hepatocyte. Positive staining of HNF4α is indicative of a mature hepatocyte culture. Here we show reciprocal staining of SOX9 and HNF4α.

When cultured on UP substrate, expression of SOX9 is bright and well defined by day 6, becomes diffuse by day 14 and increases again by day 28. On the DSQ120 substrate SOX9 expression follows that seen on UP up to day 14, but is much lower by day 28 and is also lower than that seen in TCP (**Figure 4.12**).

Low levels of HNF4α are expressed by day 14 on TCP and maintained to day 28. Expression is localized to areas of culture which have committed to hepatocyte lineage. This was also seen when cells were grown on the UP

substrate. Using DSQ120, diffuse staining is seen at day 6, becoming more localized by day 14 and is maintained at day 28.

SOX9 expression is present and clearly detectable until around day 14 where it becomes diffuse. HNF4α is either absent or un-localised until ~ day 7 where some emergence is seen on UP and DSQ120. High levels of HNF4α are detected from day 14 onwards on all substrates/treatments.

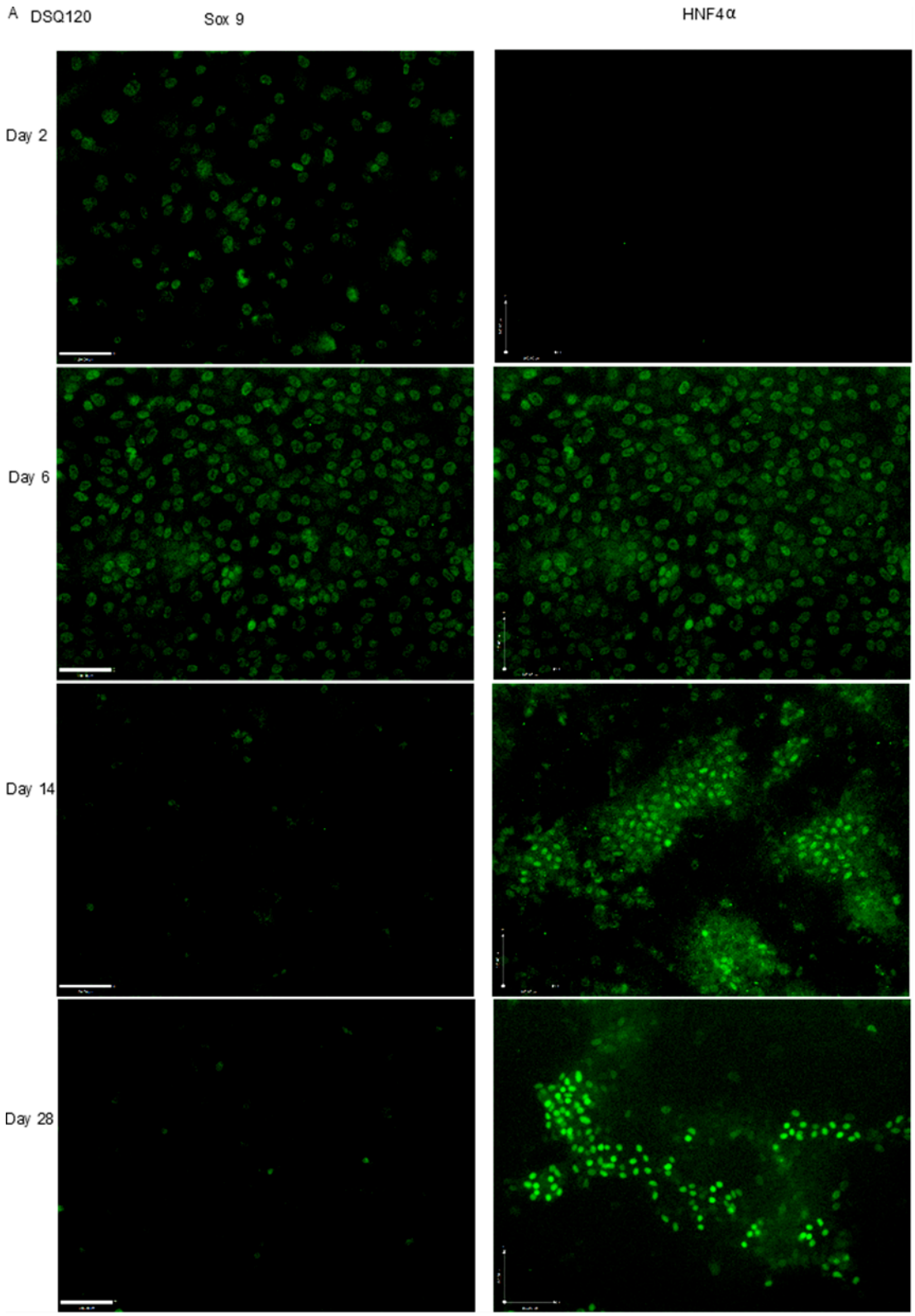
A DSQ120
Sox 9
HNF4α
Day 2
Day 6
Day 14
Day 28

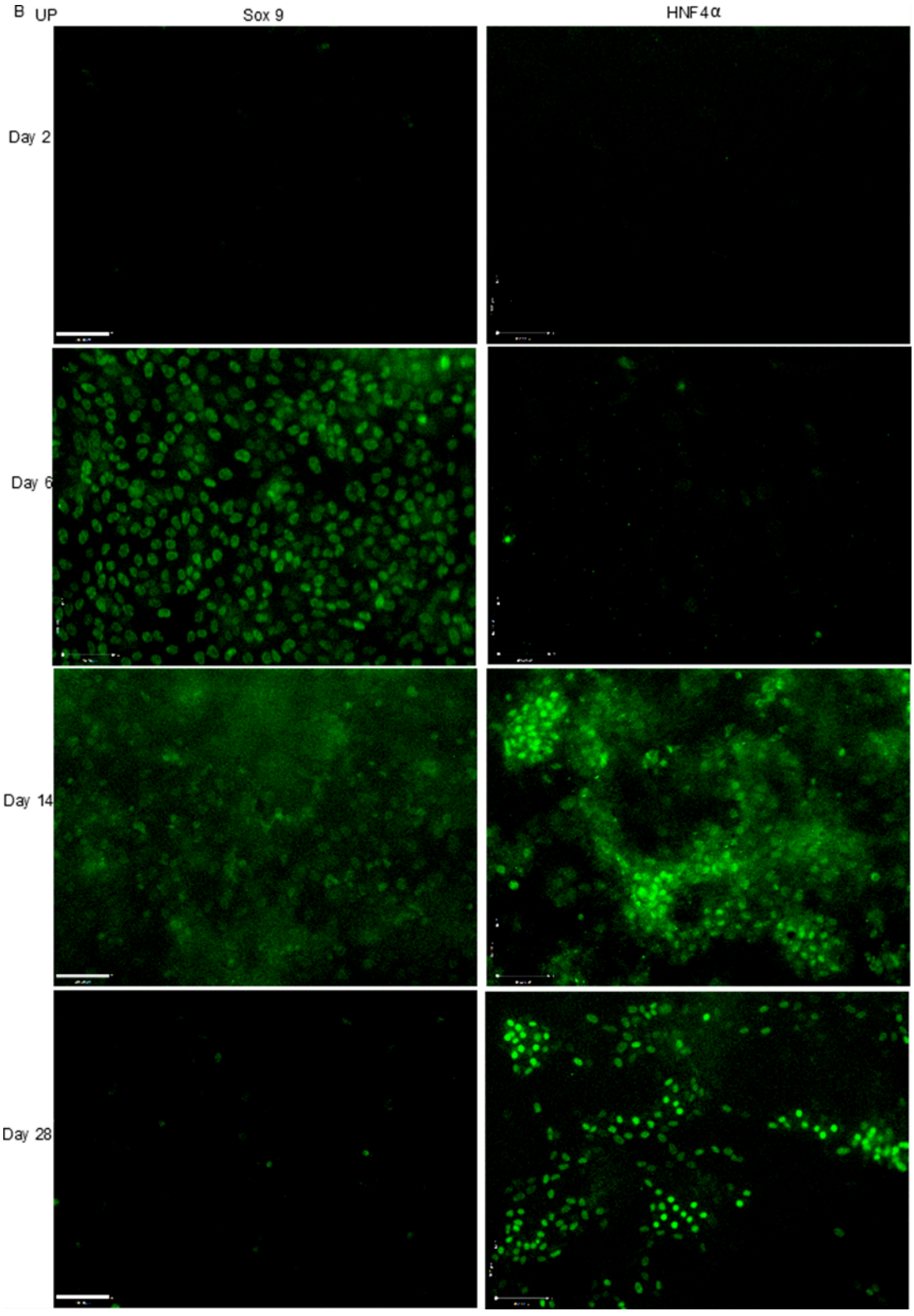
B UP
Sox 9
HNF4α
Day 2
Day 6
Day 14
Day 28

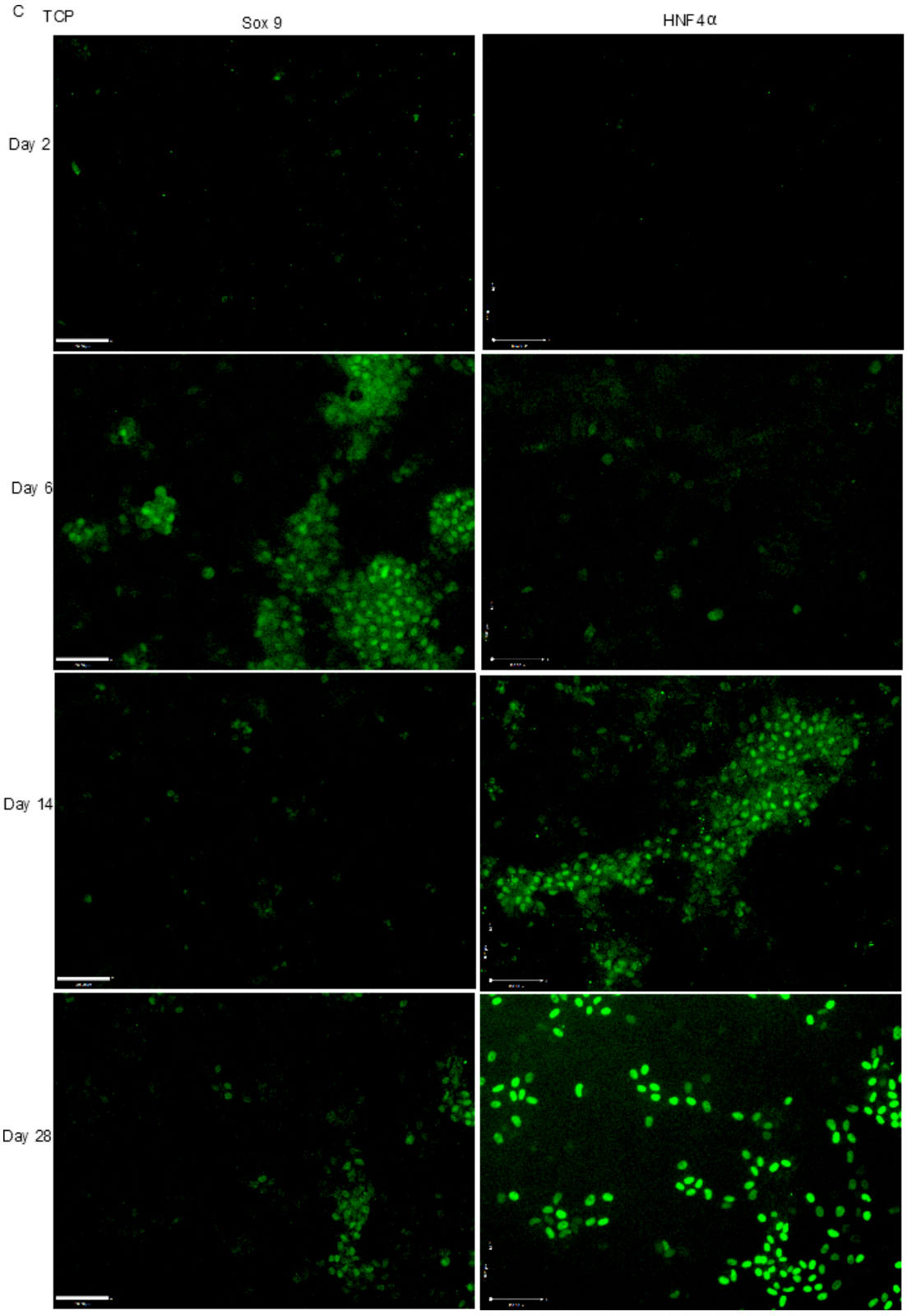
C
TCP
Sox 9
HNF4α
Day 2
Day 6
Day 14
Day 28

Figure 4.12 Phenotypic staining of progenitor protein SOX9 and mature hepatic marker HNF4α: All conditions showed reciprocal staining of SOX9 and HNF4α throughout a 28 day culture period.Sox9 can be seen at days 2 and 6 on all substrates as localised green staining within the cytoplasm. HNF4α is also a cytoplasmic stain which becomes more localised as cells mature, between day 6 and 14. Pictures taken on EVOS fl Auto at x20 A) Reciprocal staining of SOX9/hnf4a on DSQ120 B) Reciprocal staining of SOX9/hnf4a on UP control C) Reciprocal staining of SOX9/HNF4α on TCP. Scale bars representative of 160μM. Background fluorescence subtracted across all images equally using Volocity image analysis software (Perkin Elmer).

qRT-PCR analysis of SOX9 showed no presence at any time under any condition. This analysis was repeated 3 times with 3-4 technical replicates each time. HNF4α is present in all conditions on day 7 and 14 (**Figure 4.13**). High expression of HNF4α mRNA is seen when proteins are starting to be detected through immunostaining. HNF4α gene expression is lower at day 14 when there is protein expression across all conditions is high.

A)No expression of Sox 9

B

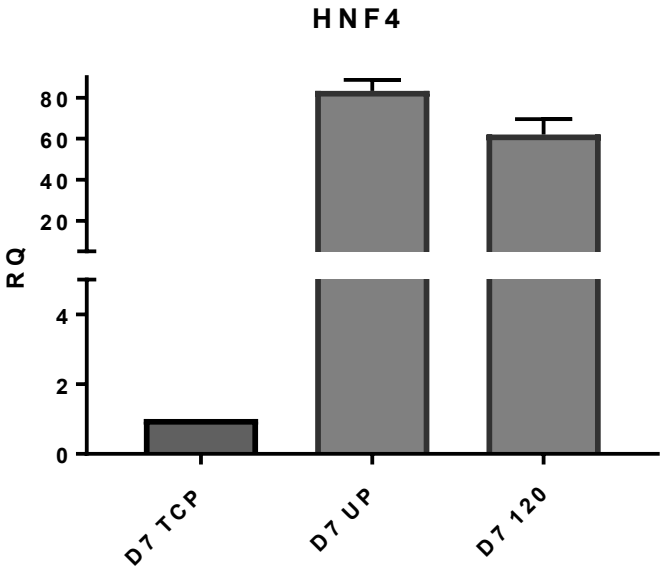

Figure 4.13 qRTPCR data for HNF4α day 7: A) There was no expression of SOX9 under any condition (n=6). **B)** mRNA expression of HNF4α. qRTPCR data shows mRNA expression of HNF4α on day 7 for TCP, UP control and DSQ120. Both UP and DSQ120 showed higher levels of mRNA expression on day 7 than TCP. Results are presented as fold-changes in gene expression relative to untreated control calculated with the ΔΔCq method. (n=3, representing 3 independent experiments with 3 technical replicates each experiment).

4.3.5 Function

4.3.5.1 Viability assays

Total ATP and metabolic competence was measured at day 7. Total ATP data shows a significant difference between DSQ120 and UP compared to TCP. However, no difference was seen at day 7 in the PrestoBlue™ assay which measures metabolic competence (**Figures 4.14 & 4.15**).

A comparison was then made between DSQ120 and UP day 7 and TCP day 14. No statistical significance was seen suggesting that by day 7 total ATP and metabolic competence of cells grown on DSQ120 and UP are comparable to TCP at day 14 (**Figures 4.17 & 4.18**).

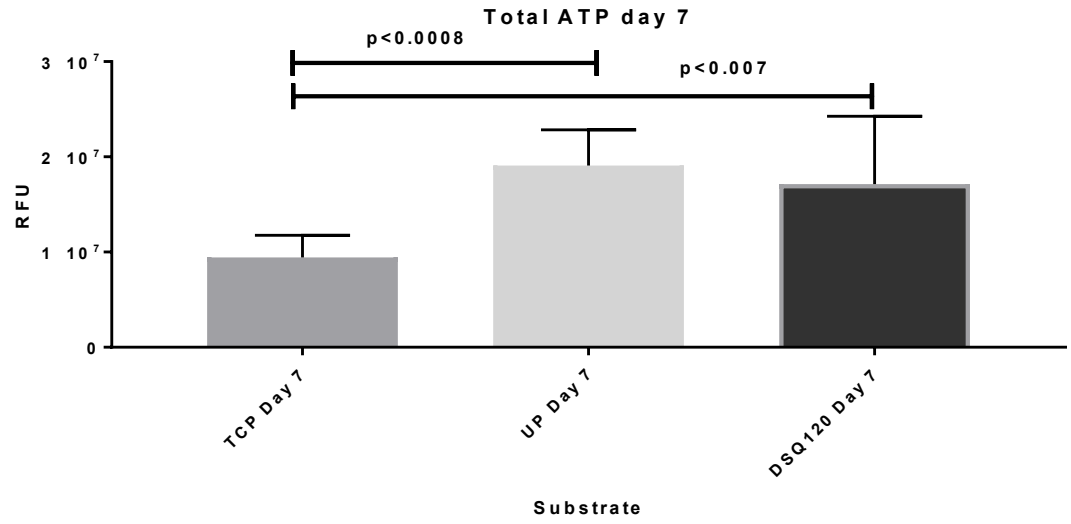

Figure 4.14 Measuring total ATP in HepaRG™-P cells at day 7 across cell culture substrates: Measurement of total ATP in relative fluorescent units on day 7 showed a statistically significant difference between HepaRG™-P cells grown on TCP and HepaRG™-P cells grown on both unpatterned ($p<0.0008$) and nanopatterned ($p<0.007$) substrates. There was no statistically significant difference in total ATP when comparing cells grown on unpatterned control and DSQ120 patterned oxygen plasma treated surfaces (n=3, representing 3 independent experiments with 3 technical replicates each experiment).

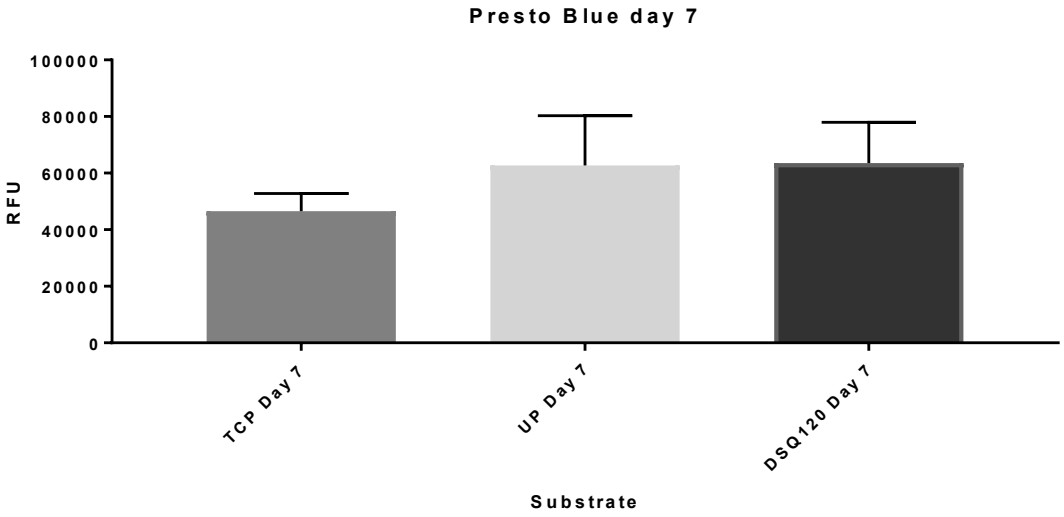

Figure 4.15 Measuring metabolic competency in HepaRG™-P cells at day 7 across cell culture substrates: Results of PrestoBlue™, resazurin based assay, in relative fluorescent units on day 7 showing no difference of metabolic proficiency between TCP and cells grown on both unpatterned (UP) and nanopatterned substrate DSQ120. (n=3, representing 3 independent experiments with 3 technical replicates each experiment)

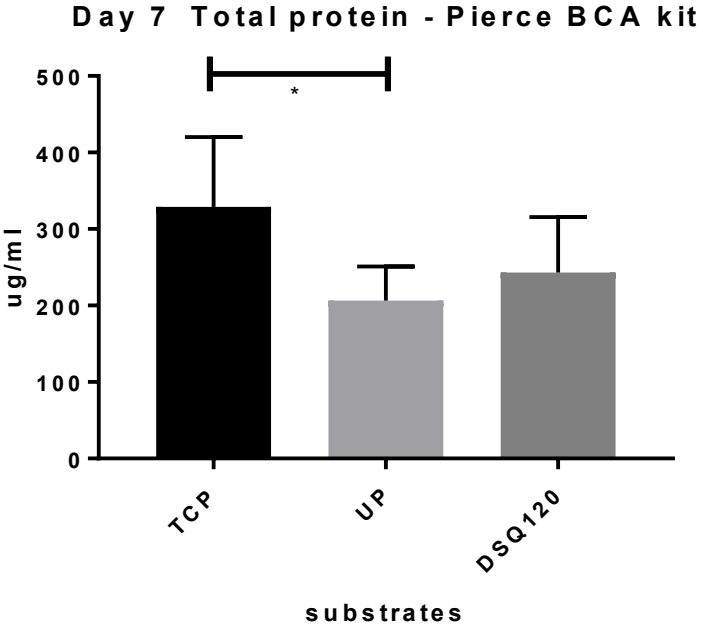

Figure 4.16 Pierce BCA total protein analysis of HepaRG™-P cells at day 7 across all cell culture substrates: Results of Pierce total protein assay was performed on HepaRG™-P cells across TCP, UP and DSQ120 cell culture substrates on day 7 to quantify the levels of protein in cells grown on each substrate. There was no statistical difference in the amount of protein between UP and DSQ120 or TCP and DSQ120. There was some significance between TCP and UP, with TCP expressing the highest levels of protein ($p=0.25$). Data comprises 3 experiments with 2 technical replicates each experiment. Technical replicates were pooled from 5 wells for each condition.

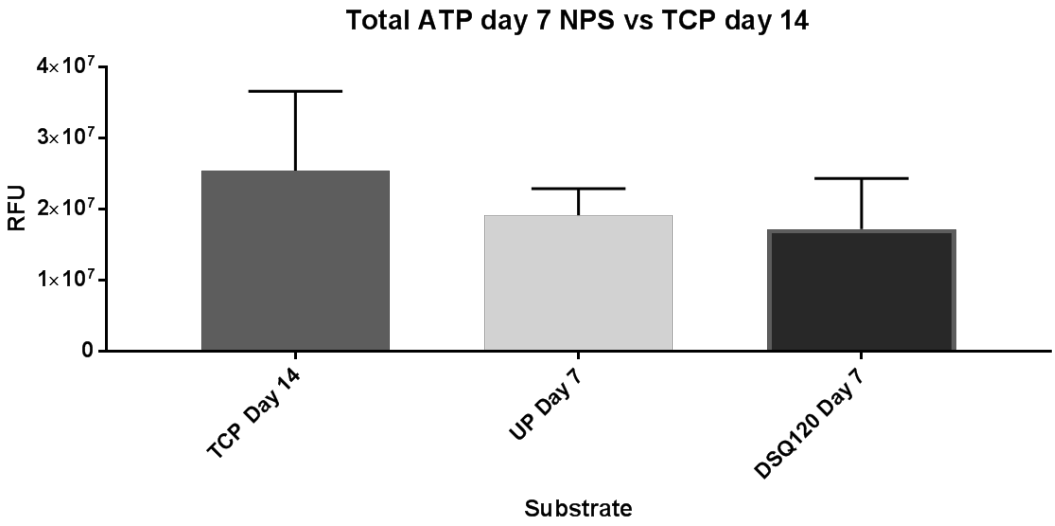

Figure 4.17: **Comparing total ATP of HepaRG™ cells at day 14 on TCP to day 7 on UP and DSQ120** Measurement of total ATP in relative fluorescent units comparing HepaRG™-P cells grown on oxygen plasma treated substrates UP and DSQ120 at day 7 to HepaRG™-P cells grown on TCP at day 14. There is no significant statistical difference between HepaRG™-P cells grown on oxygen plasma treated substrates at day 7 vs HepaRG™-P cells grown on TCP at day 14 (n=3, representing 3 independent experiments with 3 technical replicates each experiment).

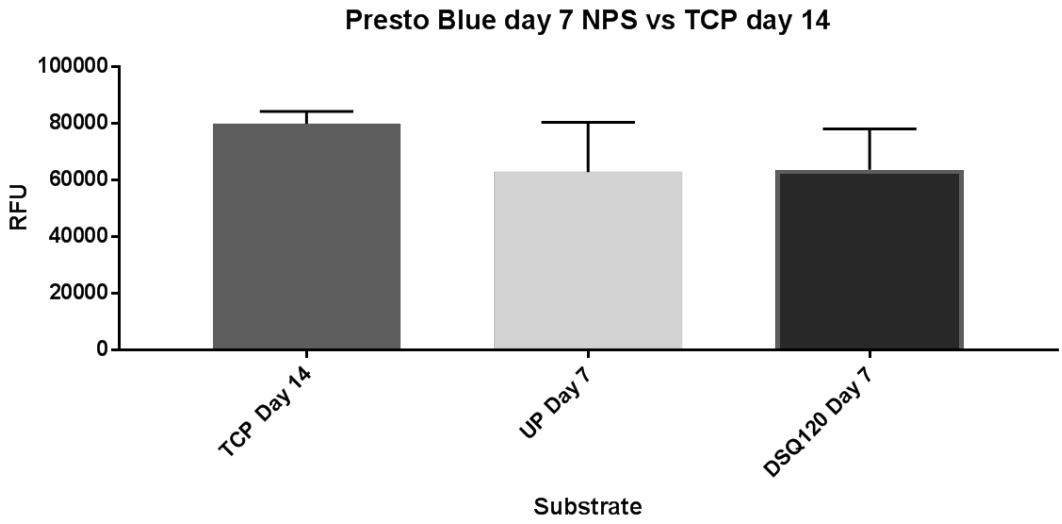

Figure 4.18 : **Comparing metabolic proficiency of HepaRG™ cells at day 14 on TCP to day 7 on UP and DSQ120:** Measurement of metabolic proficiency in relative fluorescent units comparing HepaRG™-P cells grown on oxygen plasma treated substrates UP and DSQ120 at day 7 to HepaRG™-P cells grown on TCP at day 14. There is no significant statistical difference between HepaRG™-P cells grown on oxygen plasma treated substrates at day 7 vs HepaRG™-P cells grown on TCP at day 14 (n=3, representing 3 independent experiments with 3 technical replicates each experiment)

4.3.5.2 Transferrin

Transferrin is required for transport of iron into hepatocytes and is therefore a marker of a functional hepatocyte (Hine and Martin, 2016). At day 7 localized transferrin expression is seen most abundantly on cells grown on UP, and there is also expression on cells cultured on DSQ120. On TCP, cells show some diffuse and un-localised transferrin staining suggesting the protein is not yet functional (**Figure 4.19**)

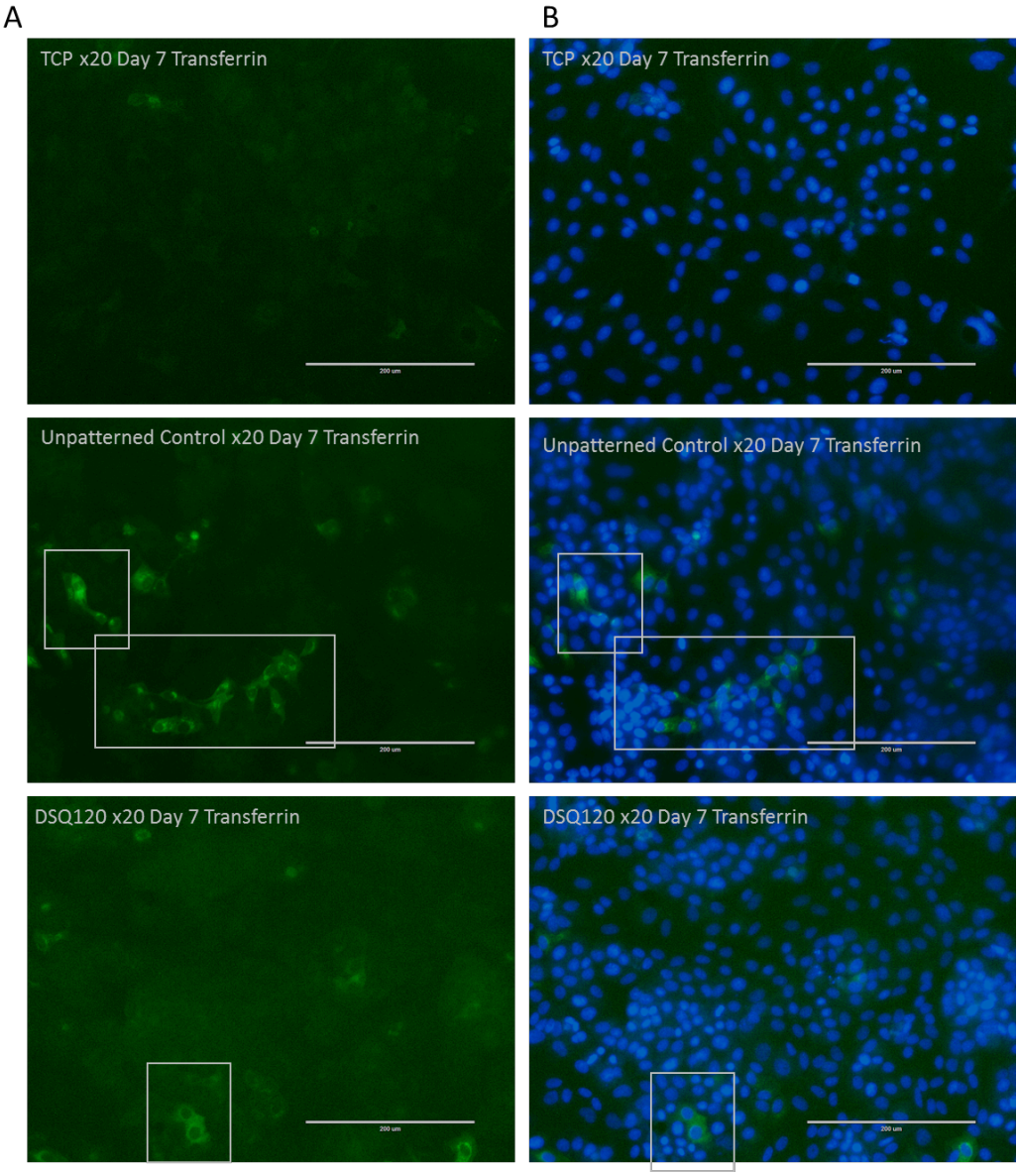

Figure 4.19 Transferrin primary antibody staining: **A**)Primary antibody staining of HepaRG-P™ cells with transferrin (green) shows localized staining on UP at day 7. TCP and DSQ120 showed diffuse staining throughout with little to no localised staining. **B**) Same images as panel A showing Hoescht nuclear staining overlay (X20 magnification on EVOS Auto-fl microscope. Images acquired in GFP and DAPI channels channels (scale 160μm). Images representative of n=2 biological with 3 technical replicates. Background fluorescence subtracted across all images equally using Volocity image analysis software (Perkin Elmer).

4.3.5.3 CYP3A4 activity

Mature cytochrome P450 enzymes also show functionality of hepatocytes. On day 7 CYP3A4, one of the major CYP enzymes in the metabolism of xenobiotics, is detected on all three substrates. However, UP and DSQ120 shows an abundance of CYP3A4 not normally seen without the addition of DMSO. (**Figure 4.20**) qRT-PCR showed a 70 fold increase of CYP3A4 mRNA expression between UP and TCP. DSQ120 had a high fold increase ~60, but this was not significantly different to UP. (**Figure 4.21**)

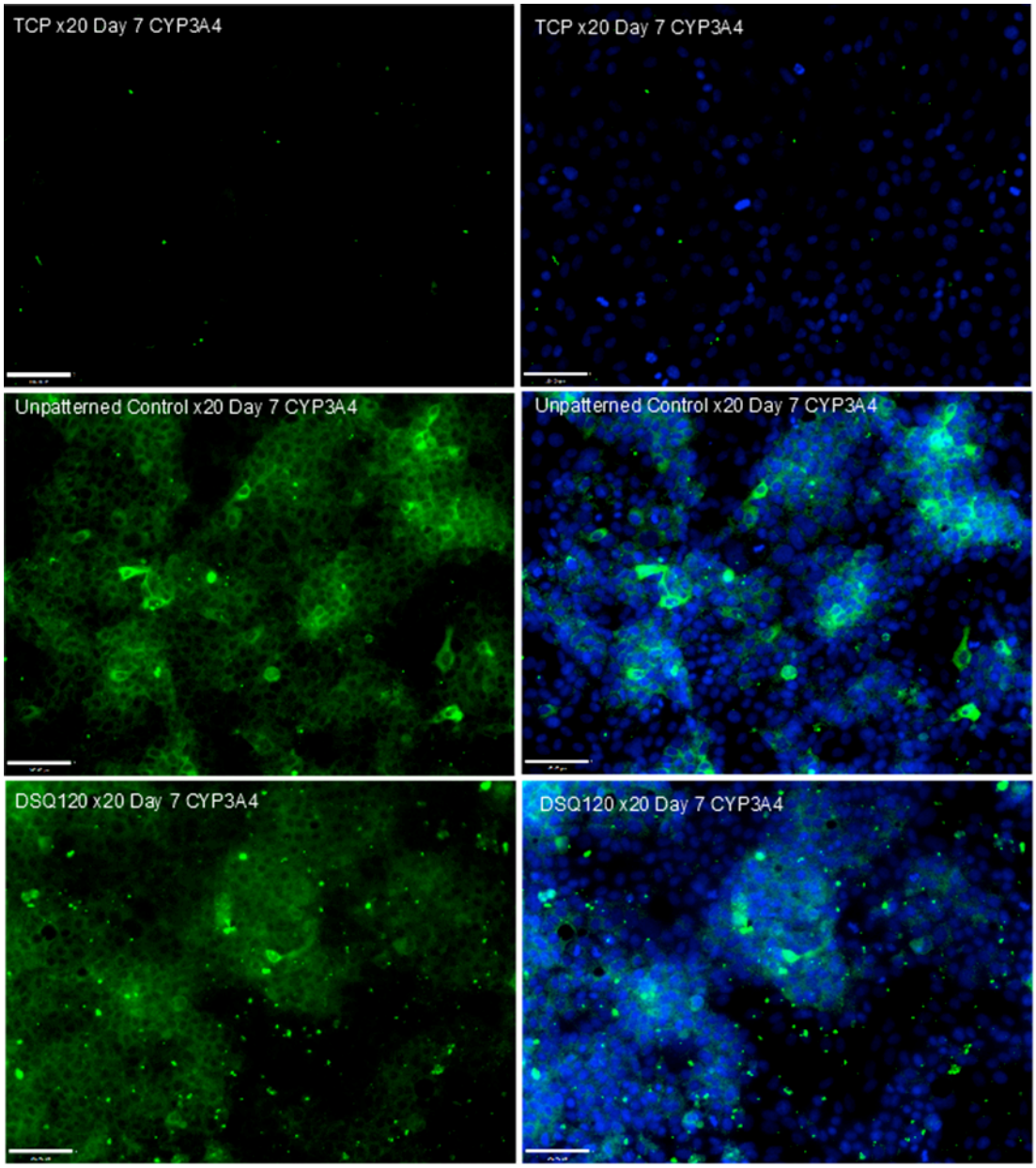

Figure 4.20 Assessing functionality of CYP3A4 through immunocytostaining: HepaRG™-P cells were grown on various substrates and stained for CYP3A4 (green) on day 7 A) Primary antibody staining of HepaRG™-P cells show little to no localized staining on TCP,and clear and abundant staining localised to cytoplasm in UP and DSQ120. **B**) Same images as panel A showing Hoescht nuclear staining overlay (X20 magnification on EVOS Auto-fl microscope. Images acquired in the GFP channel (scale 160μm). Data representative of n=2 biological and 2 technical replicates. Background fluorescence subtracted across all images equally using Volocity image analysis software (Perkin Elmer).

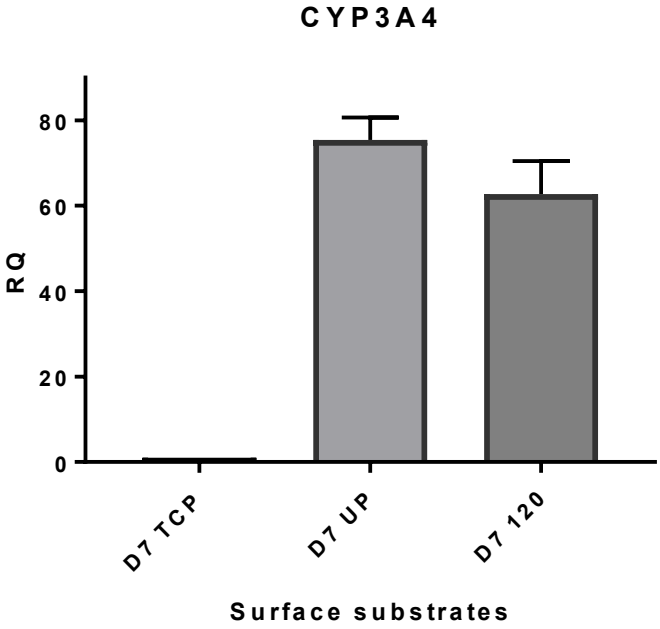

Figure 4.21 Fold changes of CYP3A4 on various substrates using qRT-PCR: mRNA expression of CYP3A4 in the HepaRG™ cells comparing Day 7 TCP, UP and DSQ120 substrates. There is significant upregulation of CYP3A4 on UP and DSQ120 compared to TCP. Results are presented as fold-changes in gene expression relative to untreated control calculated with the ΔΔCq method. (n=3, representing 3 independent experiments with 3 technical replicates each experiment).

4.3.5.4 Glutamine synthetase/Carbomyl Phosphate Synthetase

Glutamine synthetase (GS) and Carbomyl phosphate synthetase (CPS) were investigated to assess the cells ability to regulate and detoxify ammonia. Using immunocytochemistry, HepaRG™-P cells were observed on all three substrates (DSQ120, UP and TCP). There was no expression of CPS in any sample **(Figure 4.22)**. GS was visible in all samples, however, it was more localised in DSQ120 and UP. GS appeared diffuse in TCP (**Figure 4.23**).

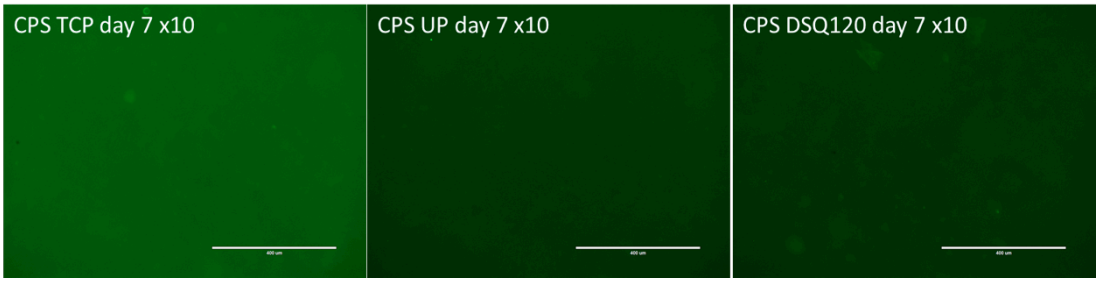

Figure 4.22 Carbomyl phosphate synthetase antibody staining.
Immunocytochemistry showing negative staining for carbomyl phosphate synthetase across all substrates on day 7. X10 magnification on EVOS Auto-flo microscope. Image acquired in the GFP channel (scale 400μm) However, the experimental results of CPS need to be interpreted with caution in the absence of a positive control and low n number. Data representative of n=1 with 2 technical replicates.

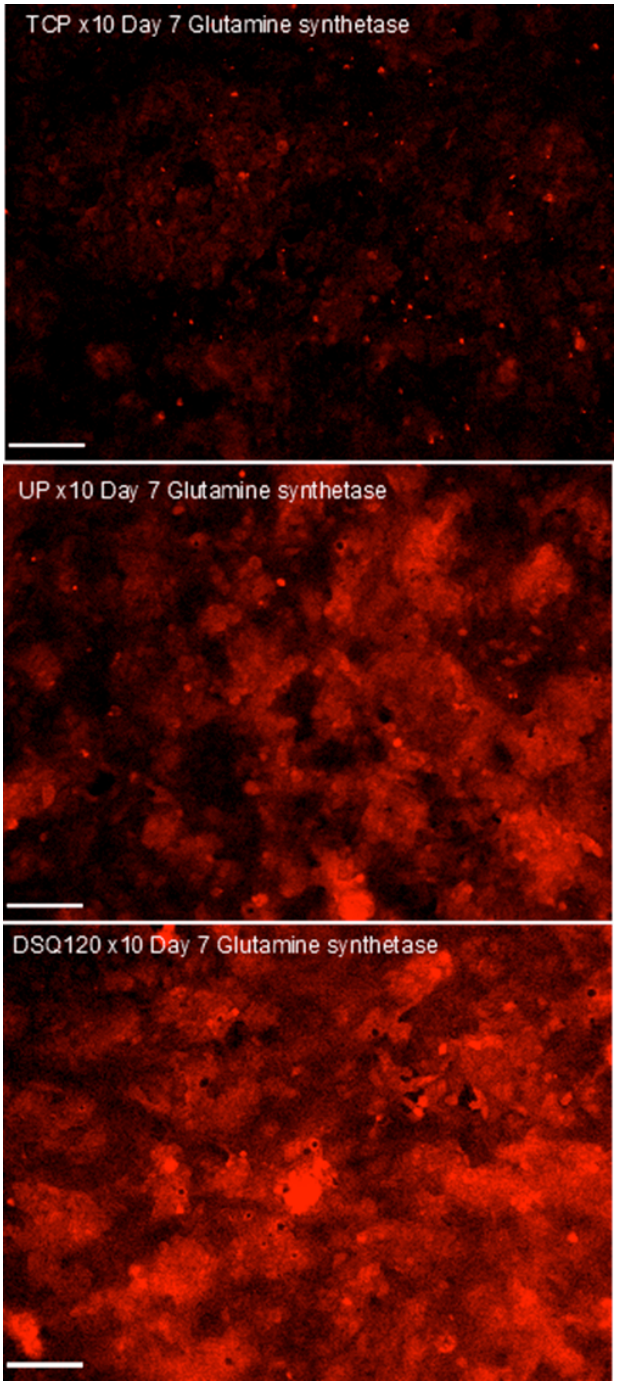

Figure 4.23 Presence of glutamine synthetase at day 7: HepaRG™-P cells were grown on TCP,UP and DSQ120 substrates for 7 days before fixing and staining with glutamine synthetase (GS) (shown in red, RFP channel) Detection of GS on TCP is present, but diffuse. Presence of GS on UP and DSQ120 is more localized, clustered and more abundant that TCP. Images taken on the EVOS fl Auto x10 Images acquired in the RFP channel (scale 160μm). Data representative of n=1 with 2 technical replicates. Background fluorescence subtracted across all images equally using Volocity image analysis software (Perkin Elmer).

4.4 Discussion

4.4.1 Types of patterns used

Previously, mesenchymal stem cells grown on nanopattern topography at UoG differentiated into bone fragment without the use of additional chemicals or nutrients in the cell media (Dalby et al., 2007). The conclusion from this study suggested that stem/progenitor-like cells grown on certain patterns may be directed into specific lineages without the need of supplements to stimulate differentiation. Schernthaner (2012) also showed evidence that the orientation of patterned surfaces resulted in morphological changes and directional cell alignment along wall like structures. Other studies used nanopatterns to direct cell migration by altering the likelihood of cell adhesion by modifying the form of nanopattern (Qian and Wang, 2010). For this reason, we grew HepaRG™-P cells on 21 different nanopattern topographies and UP control to determine if lineage specific commitment could be directed by the pattern alone.

4.4.2 Surface treatment

C3A cells grown on untreated nanopattern plates exhibited very different morphology to those grown on oxygen plasma treated plates (**Figure 4.3**) or TCP. C3A cells grown on untreated plates were ragged, congregated into spheroid like balls and were not sustainable for more than a week. The PrestoBlue™ assay (**Figure 4.4)** showed a significant difference in cell viability between untreated and treated NPS. Once data was normalized to

no cell/prestoblue only control, it was clear that untreated performed less well than treated. Untreated plates showed relative fluorescent units in the negative due to subtraction of background fluorescence and normalisation to the no cell control.

After confirming the need for a surface treatment we set out to determine the parameters causing variation in adhesion and morphology and to understand the technical mechanisms used in coating plates so that we could ensure quality control and reproducibility between experiments. To choose the surface treatment most suited to the HepaRG™-P cells, we tried various concentrations of oxygen plasma treatment and compared this to TCP control (**Figure 4.5**).

Further to the descriptions of oxygen plasma treatment and corona treatment described above in Results section 4.3.2, several oxygen plasma treatments and one corona treated plate were trialled and compared to TCP. Only growth on the UP well of these oxygen plasma treated plates was compared to TCP. This allowed us to remove the variable of the pattern surfaces so that only the effect of oxygen plasma or corona treatment was observed. Higher wattage and long exposure time of oxygen plasma may cause damage to nanopatterned substrates which would not be visible using light microscopy, and would be difficult to quantify. It was therefore decided to exclude treatments above 40W. As time of exposure can also be damaging,

we narrowed our choice of parameters further to plates treated with 40W oxygen plasma for no more than 30s.

Cell morphology was also a factor, and cells grew similar to TCP plates on A1 and A2 configuration of 40W 30s (**Figure 4.5)** confirming further that the lowest wattage and shortest duration of oxygen plasma treatment was ideal. There was also a corona treated plate used for comparison. This treatment is similar to current industry standard TCP, but corona treatment can only be applied at the UoG by hand. Hand coating plates introduces high variability, and it was decided that the corona treatment would not be reproducible until an automated machine is built that can evenly coat plates, and so this treatment had to be discarded from the experiment, again, due to issues with reproducibility.

This left us with A1 and A2 configuration which were treated with 40W oxygen plasma over 30s. While this method was used throughout the rest of the study, a lower wattage time could be trialled in future to further optimise this process.

From assessing growth and viability of HepaRG™-P cells cultured on a variety of surface chemistry treated patterned and unpatterned wells, it became clear that surface chemistry has as much effect on morphology as does growth on nanopatterned substrates. Therefore, instead of using UP as an internal control for experiments, it was used as a test of surface chemistry vs NPS and all results were then compared and normalised to TCP data.

4.4.3 Reference gene selection for normalising genes of interest

After selection of surface chemistry a protocol was established for analysing the molecular profile of HepaRG™-P cells grown on the NPS. The practice of using one untested RG can lead to inaccurate findings (Marx, 2013, Bustin et al., 2009). This is especially applicable within tissue engineering applications where use of one RG or an untested set of RGs can cause wildly varying results. This is because genes typically stable in a normal 2D culture can be up or down regulated by the very act of tissue engineering. This can make traditional structural RGs such as β-actin, a GOI in tissue engineering applications. For this reason, it is essential to validate a wide panel of RGs that consider proteins involved in many different basic cellular processes. High reference target stability (average geNorm M ≤ 0.5) is typically seen when evaluating candidate RGs on a homogeneous set of samples (e.g. untreated cultured cells, or treated cultured cells upon one type of condition)(Bustin et al., 2009). While SD was low between our individual sample sets, the overall stability (M value) of RGs across all experimental conditions was high (**Table 4**). This demonstrates the importance of evaluating samples across all conditions before deciding on the set of RGs which should be used within a given experiment.

While there were benefits to using the HepaRG™-P cells within the tissue engineering experiment, there were also disadvantages. Due to the

progenitor state of these cells it was difficult to extract adequate quantities of RNA. While RNA of 5 individual experiments was pooled for analysis, the quantity of RNA was still quite low. However, RNA integrity, or quality, was high.

GeNorm software advised the use of 7/8 RGs to normalise GOI within the TE experiment. Due to the costs involved in running 7/8 RGs and the limited quantity of RNA, it was decided that the minimum requirement within MIQE guidelines of 3 RGs would be adhered to.

4.4.4 Using nanopatterned substrates to alter HepaRG™-P form, phenotype and function

After a blinded assessment of morphology, DSQ120 was identified as a NPS on which HepaRG™-Ps grew to confluency and acquired a morphological hepatic phenotype by day 7 without the addition of DMSO (**Figure 4.6**). However, biochemical and molecular assessments were carried out to ensure viability and function.

Assessment of the effect of DSQ120 vs UP/TCP was carried out across three parameters using specific markers. Form (Morphology and tight junction assessment of polarity), phenotype (immature cholangiocyte marker SOX9 and mature hepatocyte marker HNF4α), and function (Transferrin and CYP3A4).

4.4.4.1 Form

4.4.4.1.1 Morphology

First, it was important to distinguish the morphology of both cell types within a normal culture. Normally, cholangiocytes are elongated, thin cells, with singular nuclei compared to hepatocytes where form is more cuboidal, bi-nucleation is seen, and cells take on a more granular appearance. Since it was hypothesized that an early change in morphology would be directed by a NPS, particular interest was paid to the first week of culture where mature hepatocytes seemed to be forming in DMSO negative media on several patterns. However, morphology was assessed by phase microscopy between day 1 and 14 to identify any effects NPS may have on the cells in week 2 of culture.

On 2 separate occasions, a blind test was carried out to assess the top 3 patterns for establishing an early hepatocyte culture, without the addition of DMSO. Day 7 was chosen as the time point for this investigation as it indicated the earliest day where we would see a culture resembling hepatocytes. Unanimously, 3 separate scientists concluded that cells grown on DSQ120 were the most confluent, mature and looked the healthiest of cultures across all patterns.

4.4.4.1.2 Immunocytochemistry of Zonula Occludens 1

Once ideal parameters of time and pattern were identified we began immunostaining and molecular assessment. First we assessed zonula

occludens 1 (ZO-1) as a marker of polarity. ZO-1 is part of a membrane bound complex which regulates signal cascades of the tight junctions. Tight Junction Protein 1 (TJP1) is the gene encoding for ZO-1. Tight junctions are important cellular constructs that regulate passage of molecules from the apical to the basal membrane. **Figure 4.10** shows presence of ZO-1 under all conditions. However, it is important to note where this protein is congregated within the cell to assess it as a marker of polarity. In TCP, ZO-1 is clearly present, but remains mostly cytoplasmic and irregular in expression. This is typical of a protein undergoing translation as it migrates to its point of function. In both DSQ120 and UP, ZO-1 can be seen clearly within the membrane where ZO-1 is functional. qRT-PCR supports this pattern showing significantly higher expression of TJP1 in UP and DSQ120 than TCP (**Figure 4.11**). As polarity is a sign of a mature cell, this marker was used to satisfy the criteria that we had the morphology of a mature hepatic culture containing polarised cells and the beginnings of formation of bile canaliculi.

4.4.4.2 Phenotype

4.4.4.2.1 SOX9

SOX9 is an ubiquitous protein found in a variety of cell types and is known by several different names (CMD1; SRA1; CMPD1; SRXX2; SRXY10; SRYBOX9) (National Center for Biotechnology Information) For the purposes of this study, we evaluate SOX9 in its role as an early marker of a cholangiocyte lineage (Poncy et al., 2015)(Antoniou et al., 2009). Therefore,

the knowledge that the HepaRG™-P cell line will only differentiate into a cholangiocyte or hepatocyte gives confidence that SOX9 will be associated with an early stage cholangiocyte while HNF4α will only be seen in hepatic cells. For this reason, SOX9 was used as a marker of cholangiocytes to investigate reciprocal expression of early markers within the HepaRG™ P cell culture. Sox9 was seen early in culture across all conditions. However, it reappears between day 21 and 28 across all conditions. Personal communication with Christophe Chesne (2017) confirms that this has also been seen at Biopredic International where the cells have been fully characterised. While SOX9 is known to be a marker of an early cholangiocyte lineage, it is possible that this gene has many other functions. It is believed that many genes have a degree of pleiotropy, or the ability to multitask (Guillaume and Otto, 2012). It is possible that while SOX9 is a marker of early phenotype, it may also have other functions at a later stage of cellular development especially since it is so well conserved across a variety of tissues.

4.4.4.2.2 HNF4α

HNF4α is part of a nuclear receptor family of transcription factors found in digestive tissue such as gut (Ahn et al., 2008, Babeu et al., 2014) and liver (Bonzo et al., 2012). It is responsible for downstream regulation of many metabolic processes such as bile acid synthesis, lipid and glucose metabolism and the uptake of iron through transferrin (Bonzo et al., 2012,

Matsuo et al., 2015). Loss of function studies using HNF4α knock out mice results in mortality (Bonzo et al., 2012). Furthermore, acute disruption results in hepatosteatosis, and impacts apoptosis, cell cycle and growth factors downstream (Bonzo et al., 2012). Therefore, we use HNF4α as a marker of hepatocytes when assessing the HepaRG™ and distinguishing between hepatocytes and cholangiocytes.

4.4.4.2.3 SOX9/HNF4α reciprocal expression

As previously stated, although SOX 9 and HNF4α are found in a variety of tissues within the body, they were chosen for phenotypic characterization due to the fact that the HepaRG™-P cell line is bipotent and can only differentiate into a cholangiocyte-like cell or a hepatocyte. Therefore, phenotype and maturity of hepatocytes within this culture can be determined by the presence of HNF4α and the absence of SOX9. However, where SOX9 is present and HNF4α absent, it can be assumed that a population of early cholangiocytes are present.

To establish reciprocal expression, one would expect to see clear indication of SOX9 early in the culture (week 1-2) and no, or diffuse expression in later weeks. Whereas, HNF4α should not be present early in the culture or should not be well established until the cells following the hepatocyte lineage become committed. At this stage it would be expected that HNF4α would become localized and clear.

Under all conditions (DSQ120, UP and TCP), SOX 9 is present and localized in cytoplasm with a sharp and clear appearance on days 2 and 6. This would be expected in support of the hypothesis of reciprocal expression. Around day 14 staining for SOX9 becomes more diffuse. More interestingly, qRT-PCR data suggests that there is no SOX9 expression at any time point on any condition. This experiment was performed on 3 separate experimental samples with 3-4 technical replicates for each experiment. As qRT-PCR data gives quantity of total mRNA of specific genes, in this case SOX9, we could speculate that the gene has already been transcribed into the protein seen in immunocytochemistry. However, to add credence to this analysis we would need to validate our primer for SOX9 against a cell line or tissue known to express high levels of SOX9. This analysis would show us that the SOX9 primer is working and that there was no expression within our experimental parameters. As we show SOX9 staining clearly in all samples, this would indicate that further work needs to be done to validate our SOX9 primer before further experimentation takes place.

HNF4α is either not present or extremely diffuse on day 2, suggesting the protein is absent or not completely translated. At day 6 HNF4α starts to emerge on DSQ120 with clear cytoplasmic staining on a representative group of cells (**Figure 4.12**). This emergence is not seen to the same extent on TCP or UP, though some expression of HNF4α is present on these conditions. In relation to qRT-PCR data, where TCP was used as a control, we see that day 7 UP has higher HNF4α mRNA expression than DSQ120,

however both contain significantly higher expression than TCP (**Figure 4.13**). On day 14 HNF4α staining emerges as clear and localized expression of the protein, however, qRTPCR data shows a decline in expression. Considering qRTPCR gives a quantitative expression of mRNA and Immunocytochemistry shows downstream translation of the protein, it is understandable that mRNA expression for HNF4α would be high on day 7 when the protein is starting to emerge and would be lower on day 14 when the protein has been further translated.

4.4.4.3 Function

We have established that HepaRG™-Ps grown on DSQ120 show morphology and phenotype around Day 7 that would suggest commitment to a hepatocyte lineage without the use of media containing DMSO. After establishing form and phenotype of cells grown on this condition, we further investigated whether there is cell functionality as a mature hepatocyte and compared this to UP and TCP controls. From here, we focus on day 7 for comparison as this is the earliest day at which hepatocyte morphology can be seen and HNF4α is detected suggesting a hepatic lineage is present. Metabolic assays PrestoBlue™ and ATP were used to compare day 7 conditions and also to compare DSQ120 and UP day 7 with day 14 TCP to ascertain what the correlation of metabolism and total ATP between cells grown on the nanopattern and UP and those at a further stage of development on TCP.

4.4.4.3.1 Total ATP and metabolic function

There are many ways to assess the health and viability of a cell culture. Some of the most widely available are live/dead staining, resazurin based assays such as MTT, or Alamar Blue and through the quantitation of ATP. Within this study it was decided that two biochemical assays would be employed to assess cell health and viability. The PrestoBlue™ assay was used to assess metabolic function of the cells alongside an assay to measure total ATP.

Within the PrestoBlue™ assay resazurin is reduced to resarufin which emits fluorescence and can be measured quantitatively. As PrestoBlue™ is not an end point assay, the Promega cell titer glo assay was used directly after PrestoBlue™ on the same population of cells to measure total ATP.

The Pierce BCA total protein kit was also used to quantify total protein which would correlate cell number between conditions. This would allow us to see if there was a statistical difference between total protein and if one condition prompted more proliferation than the others. It also allowed for a direct comparison of metabolic proficiency assuming there was not statistical difference.

Total ATP was measured on day 7 and day 14 across all conditions. On day 7 there is a significant increase of fluorescence related to total ATP on DSQ120 and UP compared to TCP suggesting the cells grown on DSQ120

and UP are more viable. However, there was no statistical difference on day 7 measurement of metabolic proficiency (**Figures 4.14 & 4.15**). Here we can postulate that cells are viable and equally metabolically active across all conditions, but cells grown on DSQ120 and UP contain significantly higher ATP. This is especially significant when we consider the Pierce total protein assay which shows a significant difference in the level of protein on day 7 between TCP and UP. This shows that more proteins are present in TCP, but metabolic proficiency is higher in UP and DSQ120 suggesting that there may be fewer cells on UP and DSQ120, but they are more metabolically active especially in production of ATP.

Comparing day 7 total ATP and PrestoBlue™ on DSQ120 and UP against day 14 TCP we see there is no statistical difference. This comparison was done using day 7 data of UP and DSQ120 vs day 14 TCP. Showing no statistically significant difference between day 7 DSQ120/ UP to day 14 TCP shows that at day 7 HepaRG™-Ps grown on the NPS and UP well show metabolic proficiency and total ATP comparable to day 14 TCP without the addition of DMSO (**Figures 4.17 & 4.18**). Unfortunately, there was not a total protein assay carried out at day 14. While we can speculate that there is no metabolic differences between day 14 TCP and day 7 UP and DSQ120, further experiments measuring total protein or cell counting using flow cytometry would lend more information to this model, normalise the data and make the data more comparable between timepoints.

4.4.4.3.2 Transferrin

Transferrin plays an important role within the liver where it is needed for the metabolism and uptake of iron from red blood cells (RBCs). Iron is needed for many processes in the body and the absence of iron can cause anemia. Anemia is a disease state where the body lacks healthy RBC. As hemoglobin in RBCs binds oxygen, if healthy RBCs are diminished, hemoglobin will be insufficient and the binding of oxygen will be insufficient. Therefore, a functional hepatocyte should show presence of transferrin.

On day 7 diffuse transferrin is shown by immunocytostaining on TCP and within clusters of cells on DSQ120 and UP, however, DSQ and UP are the only two conditions where localized and clear staining was observed on this early time point (**Figure 4.19**).

4.4.4.3.3 CYP3A4

Within the liver over 50 different isoforms of cytochrome P450 enzymes responsible for metabolism, can be found. Of these, CYP3A4 is responsible for the metabolism of most xenobiotics. Normally for the HepaRG™ culture to produce a high level of CYP3A4, it must be induced with DMSO (Guguen-Gouillozo, Corlu, and Gouillozo, 2010). As such, HepaRG™ cells staining positive for CYP3A4 within a system where DMSO is not used, would be indicative of a functional cell capable of metabolic enzymatic activity not usually seen in traditional cultures.

Here we show high CYP3A4 expression and activity through immunocytostaining and qRT-PCR on day 7 in DSQ120/UP compared to TCP (**Figures 4.20 & 4.21**). Diffuse staining is seen on TCP at day 7 indicating that CYP3A4 is not as abundant on TCP as DSQ120/UP. Abundant localized staining can be seen on DSQ120 at day 7. However, highly localized staining is seen on UP on day 7 compared to both DSQ120 and UP. This suggests that, in terms of CYP3A4 activity, UP outperforms both DSQ120 and TCP.

4.4.4.3.4 Urea cycle: Glutamine synthetase/Carbomyl Phosphate Synthetase

Carbamoyl phosphate synthetase (CPS) and glutamine synthetase (GS) are enzymes used in the regulation and detoxification of ammonia. GS is regulated by the amount of ammonia within the body and plays a role in converting nitrogen to ammonia. CPS is one of the main metabolic enzymes responsible for the conversion of ammonia into urea. These enzymes are found in specific zones of the liver.

The liver is made up of functional units called liver lobules. Each lobule consists of acini which run from the portal triad (periportal) to the central vein (pericentral). The portal triad consists of a bile ductile, portal vein and hepatic artery. The pericentral end of this structure is where blood leaving the liver enters the central vein. The acinus is split into 3 zones correlated to the distance from the arterial blood supply to the pericentral end of the acinus (**Figure 4.24**).

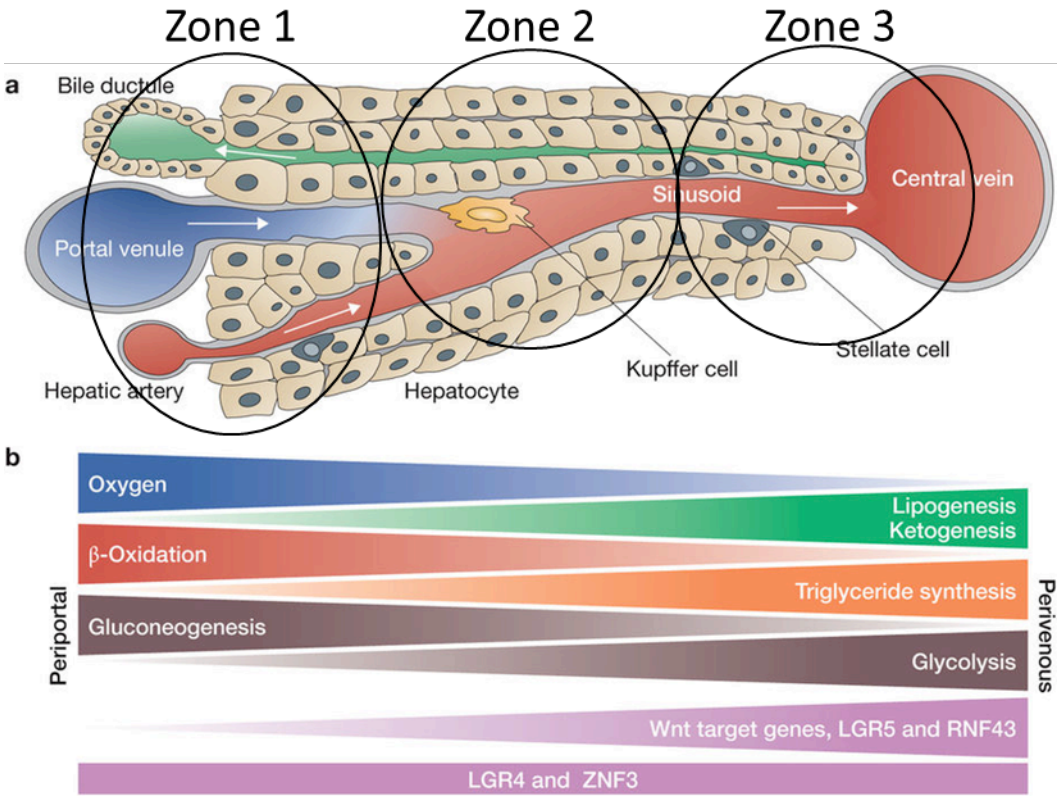

Figure 4.24 Representation of liver zonation Figure adapted from Birchmeier,W. 2016 Schematic representing the functional gradient of the liver acinus showing representation of both parenchymal and non-parenchymal cells between the portal triad and central vein.

The zones have been described as both having a gradation and being compartmentalized (Christoffels et al., 1999). Within the gradient of the acini, each cell can express the same genes, but the expression level of these genes is determined by the position of the hepatocyte along the gradient. As zones follow a gradient there can be overlap between enzymes found within the acini. This gradient is structural and functional for liver microcirculation and plays a key role in liver homeostasis including processes such as β oxidation, gluconeogenesis and glycolysis which are specific to a zone within the acinus.

Markers such as CPS and GS may overlap in one zone, but are also restricted to, or absent from, other zones (Christoffels et al., 1999). For example, CPS is found mainly in zones 1 and 2 and GS is found in zones 2 and 3 specifically. Therefore, these markers can be used to determine a zone 1 vs zone 3 hepatocyte by the presence or absence of either marker (Christoffels et al., 1999). A further analysis of these two markers can be made by describing them as either dynamic or stable. A dynamic marker would be categorized by adaptive changes in response to a metabolic or hormonal state that then has a direct impact on gene expression. CPS is one such gene. A stable marker would be characterized by the total absence of the gene in certain zones despite metabolic or hormonal changes. This applies to GS. Therefore, using this definition, we can categorize CPS and

GS as compartmentalized markers of liver zonation with CPS being a dynamic marker and GS being a stable marker. Using the combination of these markers, knowing their characteristics and where they are found along the acini, we can build a picture of the type of cell (zone 1, 2 or 3) through protein analysis.

Within this study HepaRG™-P cells were stained with CPS and GS on day 7, across all substrates. There was negative staining of CPS and positive staining for GS (**Figures 4.22 & 4.23**). Cells which stain positively for GS and negatively for CPS suggest a zone 3 phenotype. Another criteria for zone 3 is high CYP3A4 activity which we have also shown on day 7, especially in those cells grown on DSQ120 and UP. Taking this alongside the functional capabilities and other mature markers of the cells (presence of transferrin and HNF4α) it can be theorized that HepaRG™-P cells grown on DSQ120 and UP show a mature phenotype, functionality and characteristics of zone 3 hepatocytes.

While this creates a hypothesis for the zonation of HepaRG™-P cells grown on certain substrates, this study of zonation is limited to immunocytostaining of proteins. While immunostaining of CPS appeared to be negative, a positive control should be used to ensure that the antibody is indeed staining for CPS. Once it is proven that the antibody is staining specifically for CPS, then we can say that staining was negative and further assessment through biochemical assays and mRNA expression of CPS and GS should be undertaken to further establish the model. This could be done by assessing

upstream nuclear regulators, such as the 469 base pair upstream regulatory fragment for CPS (Christoffels et al., 2000) and precursors of GS, should be considered to ultimately classify the zonation of HepaRG™-P cells when grown on specific substrates.

4.5 Conclusion

Within this study, HepaRG™-P cells were plated on DSQ120 and UP and assessed by various experimental techniques to characterize their form, phenotype and function vs TCP at day 7. The following conclusions were formed:

1. Morphology on DSQ120 and UP consistently showed a culture of cells committed to a hepatic lineage which is supported by morphological observations and reciprocal expression of SOX9 and HNF4α, with HNF4α emerging as early as day 6. While there was some reciprocal expression of SOX9/HNF4α on TCP, there was little evidence of morphological criteria of hepatocytes at day 7 when compared to DSQ120 and UP.
2. Immunocytochemistry and qRT-PCR showed presence of polarity marker ZO1 on DSQ120 and UP at day 7.
3. Viability assays assessing total ATP and metabolic proficiency show significant differences in cells grown on DSQ120 and UP compared to TCP at day 7. Further investigation showed no significant difference between day 7 DSQ120/UP viability to day 14 TCP. This suggests that at day 7, DSQ120 and UP are as metabolically viable as day 14 on standard TCP.

4. Both DSQ120 and UP stained positive for functional markers transferrin and CYP3A4, on day 7. Here UP control showed significant increases in functionality compared to DSQ120 and TCP.
5. Cells stained with CPS and GS showed negative CPS and positive GS staining on all surfaces. This alone would not constitute a characterization of liver zonation, but taken alongside CYP3A4 data for DSQ120 and UP, could show a propensity of zone 3 phenotype.

In summary, UP is a superior substrate to either DSQ120 or TCP and should be considered for further investigation, alongside other oxygen plasma treatments, especially in relation to procuring a zonation model of the liver *in vitro.*

Chapter 5 Chlorpromazine disrupts structural integrity of cell membranes in HepaRG™ cells and initiates a pro-inflammatory response

5.1 Introduction

ECIS technology provides a unique opportunity to explore how a cell culture responds, in real time, to a challenge of model compounds. By measuring impedance and using the innate mathematical modelling built into the ECIS Zθ software, it is possible to ascertain if there are any changes in impedance to specific parameters i.e. TJs, basolateral adhesion or cell membrane integrity (Cm).

As previously discussed, the fully differentiated HepaRG™ cell line is a bipotent co-culture of hepatocytes and cholangiocytes exhibiting differentiated functions including CYP activity comparable to PHHs and phase I and II metabolism. The fully differentiated HepaRG™s maintain stability for up to 4 weeks in culture and beyond, so have become a cell line of choice for studies in drug development.

Chlorpromazine (CPZ) has long been used as an *in vitro* model of intrahepatic cholestasis (IHC) as there is evidence that CPZ causes impaired biliary function, though the mechanisms behind this are not fully understood and side effects are usually idiosyncratic (Antherieu et al., 2013, Akerboom et al., 1991, Zimmerman et al., 1987, Moradpour et al., 1994 and Castell et al., 2005). Cholestasis is a condition characterized by an impaired ability of the bile ducts to secrete bile acids, bilirubin and cholesterol (Antherieu et al., 2012). There is currently a need within the pharmaceutical industry to predict

cholestasis *in vitro* before drugs are submitted for pre-clinical trials.

Investigating the mechanisms behind CPZ toxicity may be informative for studies of other xenobiotics known to target the biliary system/cholangiocytes and aid in pre-clinical toxicity studies.

Here we examine the effect of a model cholestatic drug on differentiated HepaRG™ cells and investigate the changes in impedance as detected by ECIS technology.

Alongside impedance-based monitoring qRT-PCR will also be used to quantify fold changes in GOI that pertain to adhesion, tight junctions, inflammatory, adaptive and apoptotic pathways.

This combined assessment could provide vital clues to the mechanistic action of CPZ and produce a model that could be used for high throughput assessment of other drugs and compounds.

5.1.1 Aims

1. This study aimed to establish a cholestatic model using CPZ on terminally differentiated HepaRG™ cells using the ECIS Zθ impedance system.
2. To gain further insight into the mechanism of action of CPZ in IHC in particular in relation to idiosyncratic presentation.

Rationale: Using a novel cell line and model compound which induces cholestasis we examine the ability to assess DILI in a real-time, non-invasive manner using an impedance based assay.

5.2 Materials and methods

5.2.1 Drug

Cpz (Chapter 2, 2.1) was stored at room temperature. A stock of 100mM in PBS buffer was aliquoted and stored at -20°C. CPZ dilutions were made in HepaRG™ Maintenance and Metabolism Medium (ADD620) according to dilutions established by Antherieu et al., 2013.

5.2.2 HepaRG™ cell culture on ibidi 8W10+E plates

The HepaRG™ cell culture method is discussed further in Chapter 2, 2.2.2. Here this method is used for HepaRG™ cells cultured on the ibidi 8 well 10+ electrode plate for ECIS ZØ. After establishment of cell culture at day 8 on the ibidi 8W10+E plate, cells were treated with CPZ, (0μM, 25μM, 50μM or 100μM C8138-5G Sigma-Aldrich) in MMM, alongside a no cell control and monitored on the ECIS platform for 24 hours. According to Antherieu, (2013), CPZ has an IC50 of 80μM after 24 hour exposure. Within his study a range of doses were used ranging from non toxic, sub toxic and toxic. Here we replicate these doses as follows; non-toxic (25μM), sub-toxic (50μM) and toxic (100μM).

5.2.3 Immunocytostaining

Immunostaining was carried out in accordance to the materials and methods discussed in Chapter 2, section 2.3.

5.2.4 Cell viability assays

Methods of measuring cell viability assays using PrestoBlue™ and Promega Cell titer-glo, total ATP, are discussed in Chapter 2, 2.5.1 and 2.5.3.

5.2.5 Electric Cell-substrate Impedance Sensing (ECIS)– Impedance assay

The ECIS Zθ system was used to measure, in real time, total impedance using a multiple frequency model. Using the ECIS-Zθ software's built-in mathematical model we were able to mathematically deconvolve the total impedance measurements, through various frequencies, to recognize electrical current pathways relating to cell-cell TJ (Rb), basolateral adhesion (z-alpha) and cell membrane capacitance (Cm) and extrapolate this into quantitative data. HepaRG™ cells were seeded in 8 well 10+ electrode (8w10E+) cultureware from ibidi. Differentiation of HepaRG™ cells into a stable and confluent co-culture of cholangiocyte-like and hepatocytes was monitored using phase microscopy alongside the ECIS–Zθ model (n=3) with measurements taken at 180s intervals over a 500Hz to 64kHz frequency range. A baseline for confluency, 8 days, had already been established within our laboratory (Gamal et al., 2017). At day 8 HepaRG™ cells were challenged with a serial dilution of CPZ as outlined above. Impedance

measurements were normalized to the values at 0 hours and modelled to a no cell control.

5.2.6 Molecular analysis

RGs for the use of normalizing GOI within the CPZ study were assessed in the same manner as the nanopattern RGs, Chapter 4, 4.2.5. The same 12 RGs; UBC, YWHA, SDHA GAPDH EIF4A1, B2M, TOP1, RPL13A, ATP5B, CYC1, 18s and ACTB were used on RNA gathered from day 8 cells before treatment with CPZ and again after 24 hrs treatment with CPZ. RNA extraction, cDNA creation and qRT-PCR analysis was carried out according to materials and methods described in Chapter 4, 4.2.5.2 and 4.2.5.3.

5.3 Results

5.3.1 Immunocytostaining

Cell/cell junctions were assessed using immunocytochemistry staining with phalloidin for F-actin cytoskeleton and specific tight junction protein Z01. After 24 hours exposure, F-actin staining appears intact at untreated and 25μM concentrations. At 50μM concentration, some degradation of cell/cell membrane and loss of confluency can be seen. While there are still some nuclei present at 100μM, evidenced by Hoescht nuclei staining (blue), there is little cellular material present and few instances of cell/cell interaction. A similar trend is seen when staining for tight junction protein ZO1. At the non-

toxic dose there is ample ZO1 illustrated with green fluorescence localised around the cell membrane giving the traditional ‘chicken wire’ appearance. Degradation of this appearance is seen at 50μM and little to no cell/cell interaction can be seen at 100μM. **(Figures 5.1 & 5.2)**

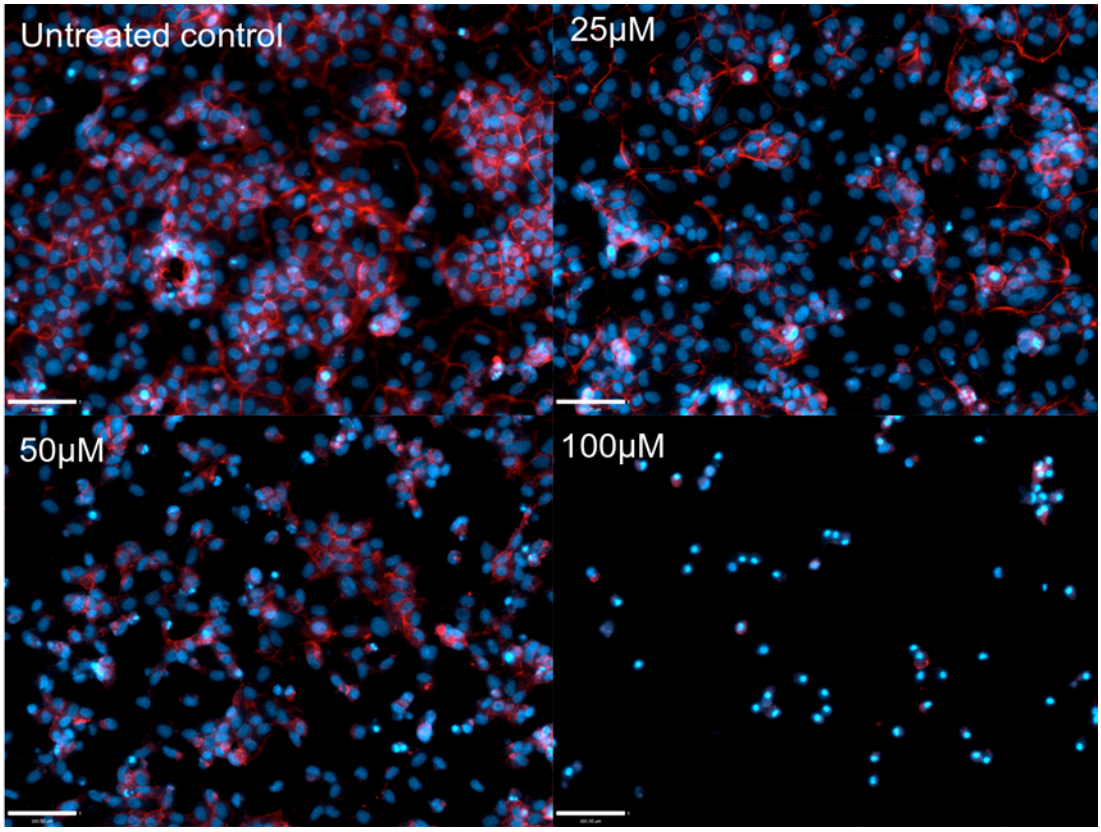

Figure 5.1 Immunocytostaining of HepaRG™ cells showing f-actin cytoskeleton after treatment with chlorpromazine: F-actin stain (red) showing cytoskeleton at day 9 after treatment with 0, 25, 50 and 100 µM Cytoskeleton indicated with arrows. Blue staining represents nuclei (hoescht). X20 magnification on EVOS Auto-flo microscope.(scale 160µm) Data representative of n=3 with 3 technical replicates. Background fluorescence subtracted across all images equally using Volocity image analysis software (Perkin Elmer). Microscopy based on 3 biological replicates with 3 technical replicates.

A

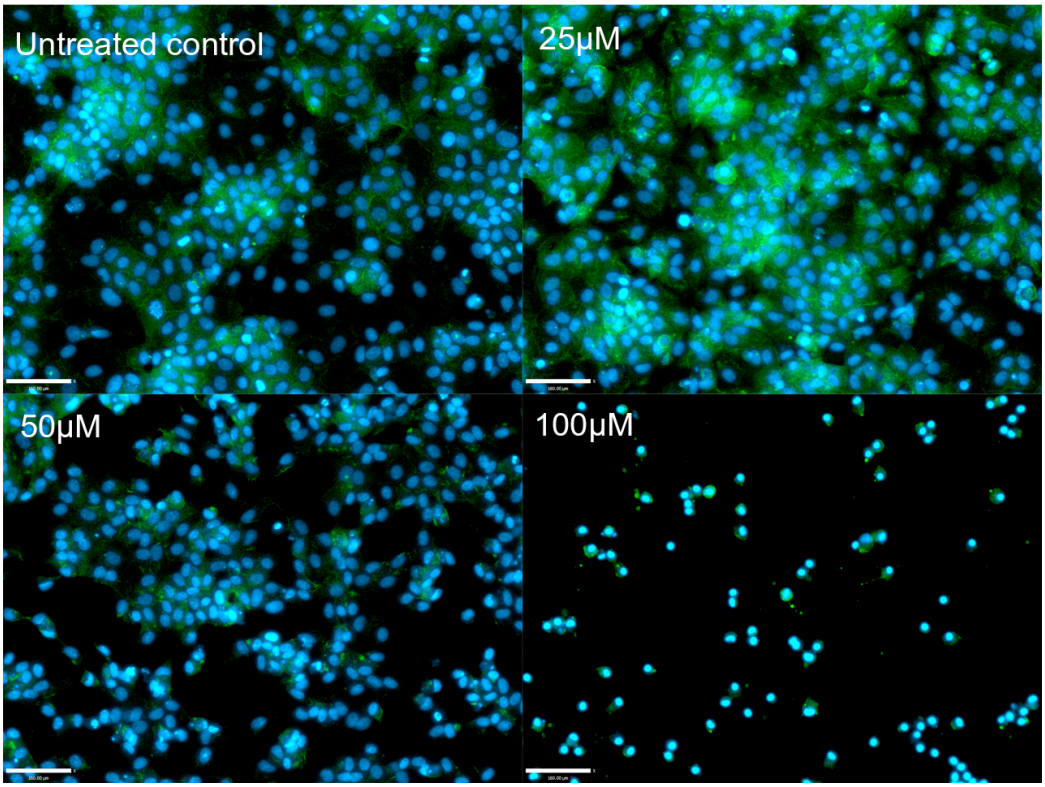

B

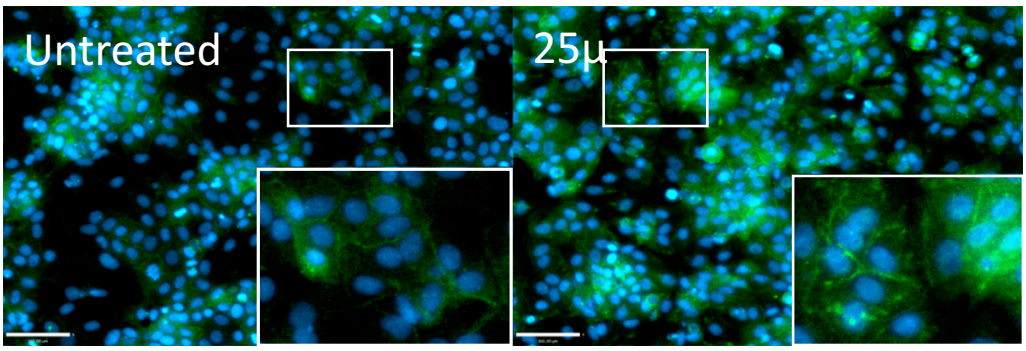

Figure 5.2 Immunocytostaining of primary antibody ZO1 on HepaRG™ cells treated with chlorpromazine: A) Chlorpromazine induced disruption of TJ protein ZO1. Green fluorescence represents ZO1 TJ protein, and nuclei are blue (hoescht) at 0 (Untreated control), 25, 50 and 100 µM. **B)** Magnified selection of 0µM (untreated control) and 25µM showing membrane bound protein. All x20 magnification on EVOS Auto-flo microscope, scale bar 160µm. Data representative of n=3 biological replicates with 3 technical replicates. Background fluorescence subtracted across all images equally using Volocity image analysis software (Perkin Elmer).

5.3.2 Measuring cell viability

5.3.2.1 Total ATP and PrestoBlue™ assays

CPZ did not compromise HepaRG™ cell viability at sub toxic concentrations as evidenced by total ATP and PrestoBlue™ assays where no statistical difference in cellular viability between treated and untreated samples was observed (n=3) **(Figure 5.3).**

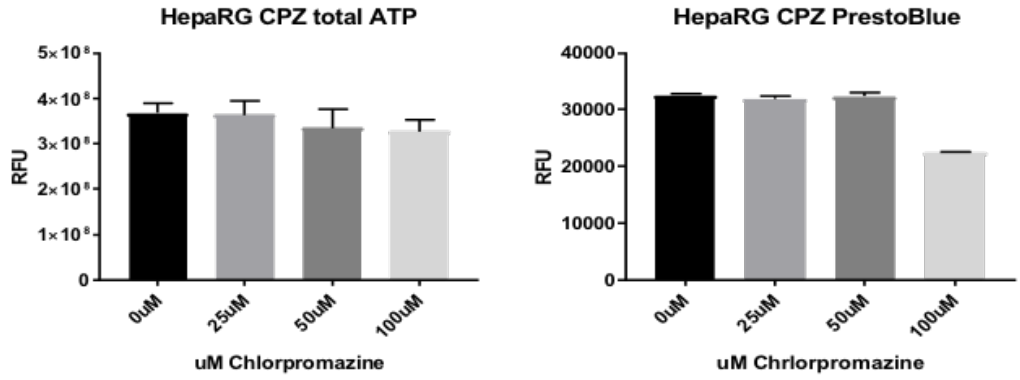

Figure 5.3 Measurement of HepaRG™ Cell Viability after treatment with chlorpromazine using total ATP and PrestoBlue™ assays: Assessment of cellular viability using A) Promega total ATP assay and B) PrestoBlue™ resazurin assay quantifying metabolic proficiency after 24 hours.(See materials and methods Chapter 2) HepaRG™ cells treated with 25μM, 50μM and 100μM of CPZ. No significant difference was detected in total ATP levels or PrestoBlue™ analysis for all conditions. (n=3, representing 3 independent experiments with 3 technical replicates each experiment).

5.3.3 Effects of CPZ on Cell to cell junctions and adhesion

5.3.3.1 ECIS

Multiple frequency measurements using ECIS Zθ allowed modelling of the following parameters: overall impedance |Z|, Tight junctions (Rb), cell-electrode adherence (α), and cell membrane integrity (Cm), and were modelled against a no cell control. Total impedance (Z) is a composite value of resistive and capacitive parts, where Rb, α and Cm measurements are deconvolved into their respective parameters corresponding to biologically significant cell behaviour.

Real time impedance |Z| monitoring showed highly-sensitive dose-response to CPZ with a decrease of impedance at all frequencies. The lowest dose, 25μM, had least effect on impedance. At 50μM impedance decreased to 0.6 after 5 hours and recovered to 0.8 after 10 hours. A CPZ concentration of 100μM shows an impedance decrease of approximately 50% within the first 2 hours of administration and continued decline thereafter.

Barrier function (Rb) tight junction & Cellular adherence (alpha) also show a dose dependant disruption. However, Cell membrane integrity (Cm) shows cells given lower concentrations of CPZ remain in-tact, and in fact impedance increases slightly and is maintained in all doses but 100μM. This give an indication to the mechanistic effect of CPZ in that, TJ and adherence has

been disrupted at low dose, whereas overall membrane capacitance has not. **(Figure 5.4)**

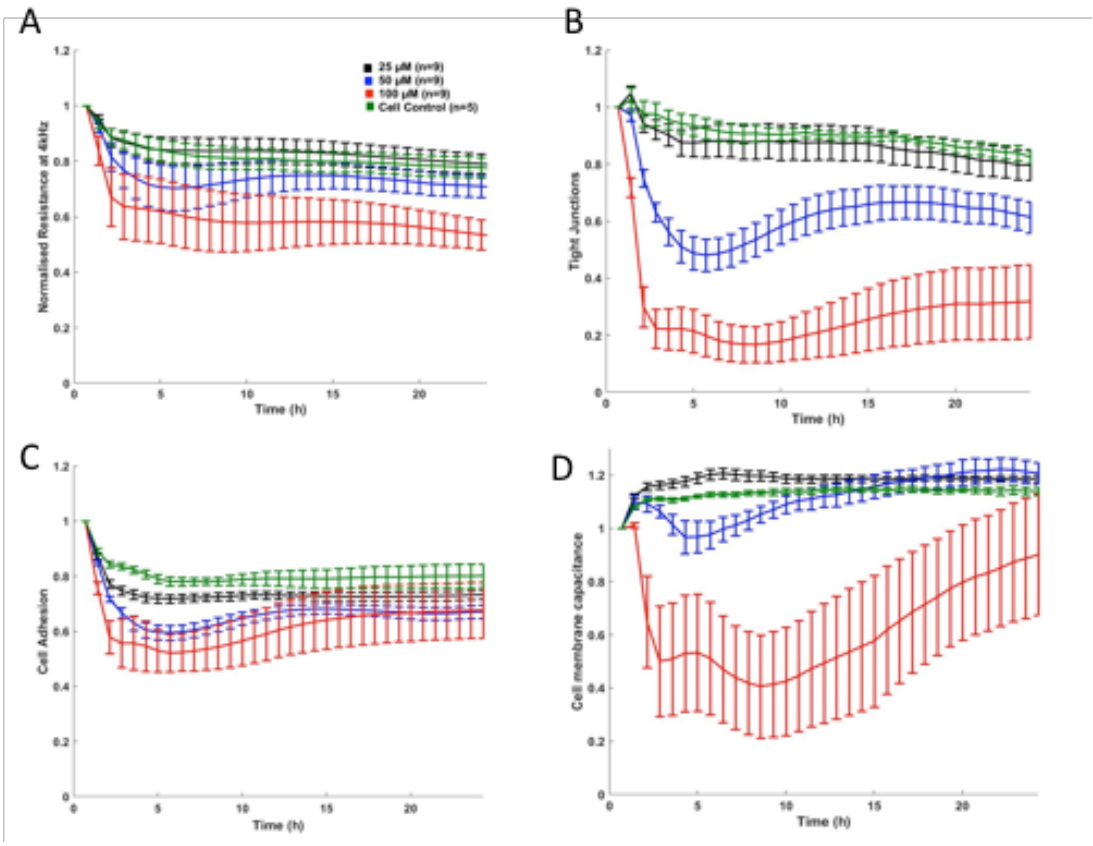

Figure 5.4 Real time impedance measurements using ECIS Zθ system A) **Post-challenge impedance kinetics showing 24 hours treatment with CPZ in confluent HepaRG cells**: CPZ caused a dose-dependent decline in normalized resistance - a global indicator of cellular status. B) **Rb (cell-cell tight junctions):** CPZ disrupted tight junctions in a concentration- and time- dependent manner; compared with control values. Subjecting HepaRg to 100µM CPZ caused Rb to decrease after 6 hours with marginal recovery around 15 hours. C) **α basolateral adhesion)**: Cell-substrate adhesion disruption was detected in a concentration dependent manner, suggesting some loosening of cells from the electrode surface. At 100µM CPZ, cell adhesiveness decreased, but showed an increase around 10 hours suggesting re-adherence of cells. D) **Cm (membrane capacitance):** membrane capacitance, reflecting cell membrane integrity, was significantly compromised at 100µM CPZ beginning at 2 hours post treatment. Some increase in Cm of 100µM CPZ was seen around 10 hours which is consistent with the basolateral adhesion (α) and further indicating some cellular compensatory effect.

5.3.4 Reference gene analysis

Analysis of RGs revealed GAPDH, UBC and TOP1 to be the most stable set for use within this study (**Figures 5.5 and 5.6 and Table 5**). Results in the following sections showing expression of GOI have all been normalised to the geometric mean of this panel.

Most stable

Least stable

Reference genes for chlorpromazine project ranked from most to least stable		
Tissue Engineering		
Ct value	**M value**	**Reference Gene**
26.0	0.37	GAPDH
26.7	>0.37	UBC
32.0	>0.40	TOP1
30.9	>0.45	SDHA
28.4	>0.47	ATP5B

Table 5: Reference gene ranking for nanopattern project Ct and M Values generated by geNorm software Reference genes for chlorpromazine treatment using HepaRG™ P cells ranked in order of most to least stable in accordance to their M value

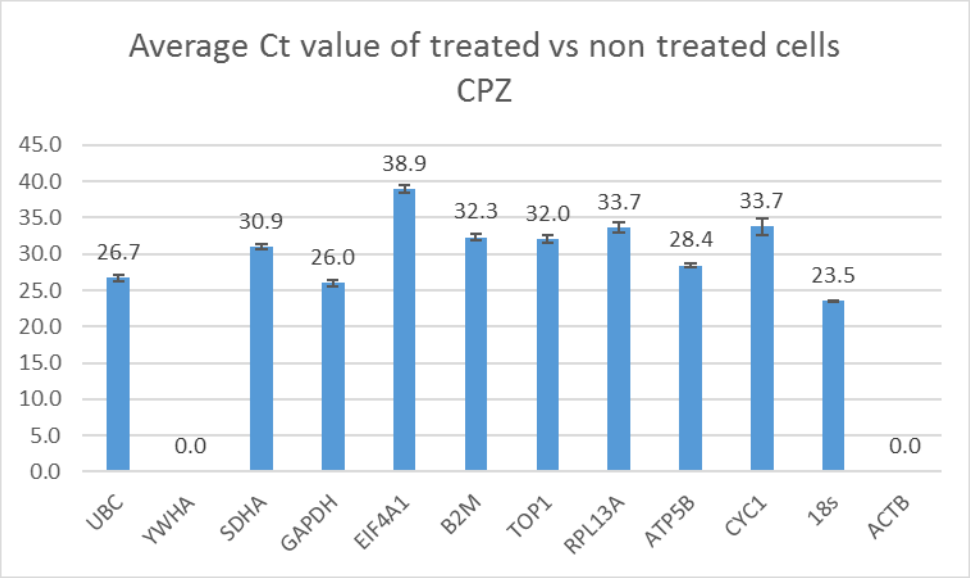

Figure 5.5: Average Ct values for chlorpromazine project reference gene selection: Graphical representation of average Ct values are shown for all 12 genes used in validating optimal reference genes. SD shown in error bars of SEM.

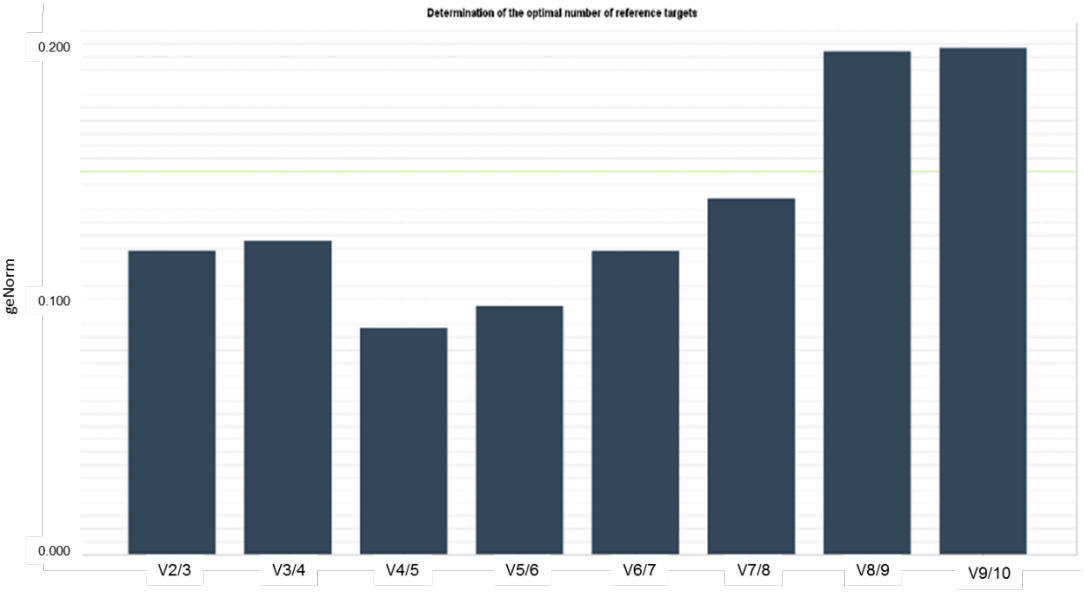

Figure 5.6: V values generated by geNorm software. The optimal number of reference genes is determined by pairwise variation known as a V value. The lower the V value the more optimal the number of reference genes for use in nomalisation. In this study a combination of 4/5 reference genes is suggested for use in normalising genes of interest. Due to cost, 3 reference genes were used in the final normalisation of genes of interest.

5.3.5 Expression of functional markers

Hepatocyte nuclear factor 4α (HNF4α) directly regulates CAR and PXR mediated expression of CYP3A4, a major metabolic enzyme within the liver. While HNF4α does not show a statistically significant increase in either 25 or 50μM, its up regulation at 25μM and low expression at 50μM correlates to the pattern seen in CYP3A4 at 25μM and 50μM. CYP3A4, is significantly up regulated at lower dose (25μM) of CPZ ($p<0.05$) when compared with untreated control. However, at 50μM CPZ, CYP3A4 expression is down regulated when compared with lower dose (25μM) **(Figure 5.7)**.

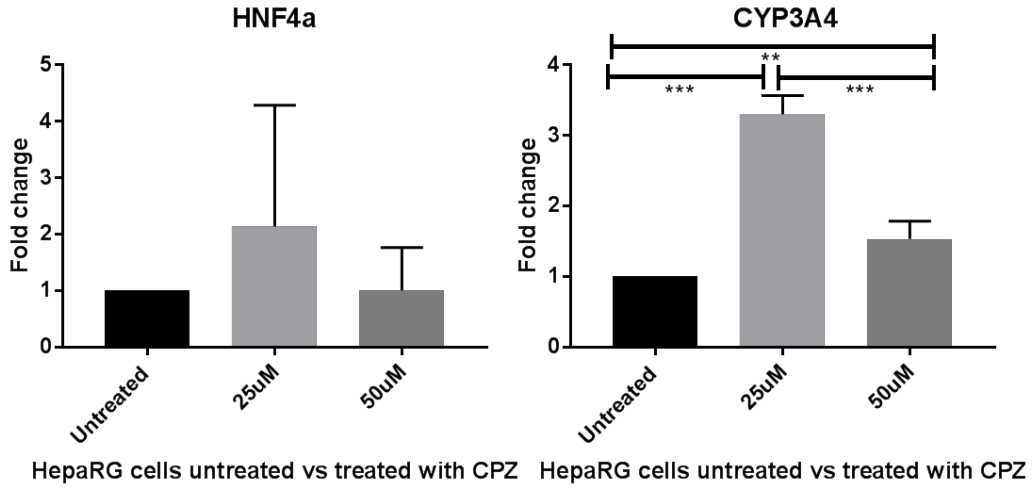

Figure 5.7 qRTPCR of nuclear factor HNF4α and gene expression of CYP3A4 on HepaRG™ cells treated with chlorpromazine: mRNA expression of **A**) nuclear factor HNF4α and **B**) CYP3A4 in the HepaRG™ cells comparing untreated, 25uM and 50uM cells treated with CPZ. Fold change is relative to untreated cells. ($p<0.05$) Results are presented as fold-changes in gene expression relative to untreated control calculated with the ΔΔCq method. (n=3, representing 3 independent experiments with 3 technical replicates each experiment).

5.3.5.1 Anti-apoptotic pathway

Further demonstration of viability can be seen in the ratio of apoptotic and anti-apoptotic markers BAX and BCL2. The statistically significant down regulation shown in this ratio indicates that apoptotic pathways are not initiated, supporting data from other viability assays. This was further supported by finding no significant changes in nuclear apoptotic (p53) marker and with the significant induction of expression of anti-apoptotic (BCL-2) in CPZ treated cells, showing that apoptotic pathway induction is not induced by CPZ treatment of HepaRG™ cells **(Figure.5.8)**.

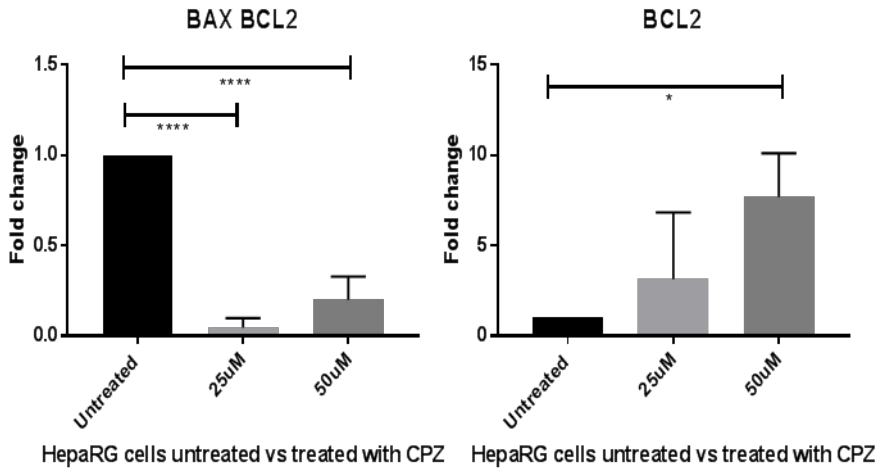

Figure 5.8 qRTPCR of Apoptotic and anti-apoptotic markers: mRNA expression (±SD) of a) ratio of apoptotic and anti-apoptotic factors Bax and Bcl2 (n=3). b) BCL2 (n=3) Statistically significant difference was seen in the BAX/BCL2 ratio indicating down regulation of apoptotic factors ($p<0.0001$). This is supported by upregulation of anti-apoptotic marker BCL2 ($p<0.0001$) Results are presented as fold-changes in gene expression relative to untreated control calculated with the ΔΔCq method. (n=3, representing 3 independent experiments with 3 technical replicates each experiment).

Statistically significant difference was seen in the BAX/BCL2 ratio indicating down regulation of apoptotic factors. This is supported by up-regulation of anti-apoptotic marker BCL2

5.3.6 Changes of biliary transport proteins

There are statistical differences in regulation of cellular membrane transporters ABCB1, ABCB4 and ABCB11 in HepaRG™ cells treated with CPZ **(Figure 5.9)**.

A statistically significant difference can be seen in the up-regulation of efflux phospholipid transporter ABCB4 between untreated HepaRG™ cells and the higher concentration of 50μM CPZ. While no statistical difference is reported between untreated and 25μM or between 25μM and 50μM, a dose dependant trend can be seen. ABCB1, responsible for xenobiotic efflux, shows a trend of down regulation at 25μM and a statistically significant up regulation between 25μM and 50μM. Whereas, bile acid export pump ABCB11 showed no detection at 25μM and down regulation at 50μM. Such increasing trends in efflux transporters can represent hepato-protective responses which aim to reduce intrahepatic accumulation of toxins while down regulation of bile acid transporters may indicate an impairment to the cellular membrane through the build-up of toxic bile acids.

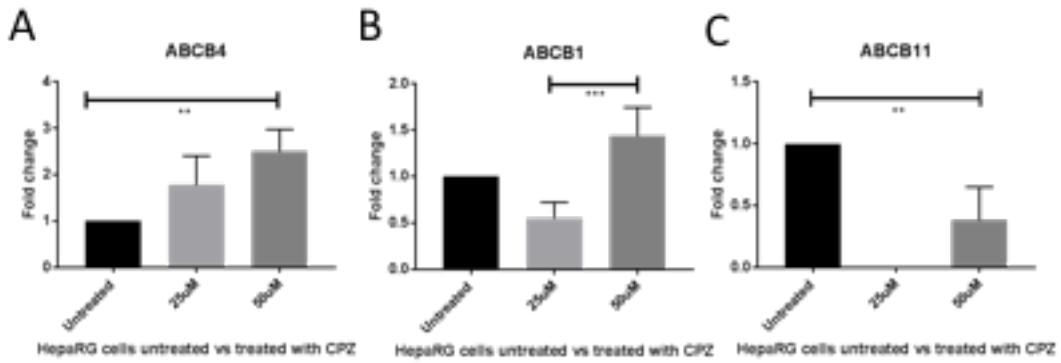

Figure 5.9 qRTPCR of membrane bound transporters ABCB4, ABCB1 and ABCB11 mRNA expression of genes related to the drug efflux and phospholipids transport (ABCB1, ABCB4) and to the bile acid transport (ABCB11) in the HepaRG™ cells of untreated, 25μM and 50μM treated cells. Fold change is relative to untreated cells. A&B) There was a dose dependent increase of membrane transporters ABCB4 (n=4) ($p<0.01$). and ABCB1 (n=4)($p<0.001$) This increase was significant between untreated control and 50μM for ABCB4 and between 25μM and 50μM for ABCB1. C) Expression of bile acid transporter marker ABCB11 (n=4) was not detected at low dose CPZ and significantly down regulated at 50μM ($p<0.01$) Results are presented as fold-changes in gene expression relative to untreated control calculated with the ΔΔCq method. (n=3, representing 3 independent experiments with 3 technical replicates each experiment).

5.3.7 Inflammatory and adaptive response

When compared with untreated control, CPZ treated cells showed an increasing and significant dose dependant response in expression of pro-inflammatory cytokines IL-6 and TNF-α. Up regulation of IL-6 at 50μM is almost a 10 fold increase compared to untreated control while TNFα showed a 2 fold increase at 25μM and a 9 fold increase at 50μM when compared to untreated control. **(Figure 5.10)**

The increase in expression of anti-oxidant regulator NRF2, with increasing concentration of CPZ, though not significant may suggest cellular activation of this defence pathway associated with cholestasis induced by CPZ (Ma, 2013)**(Figure 5.10)**.

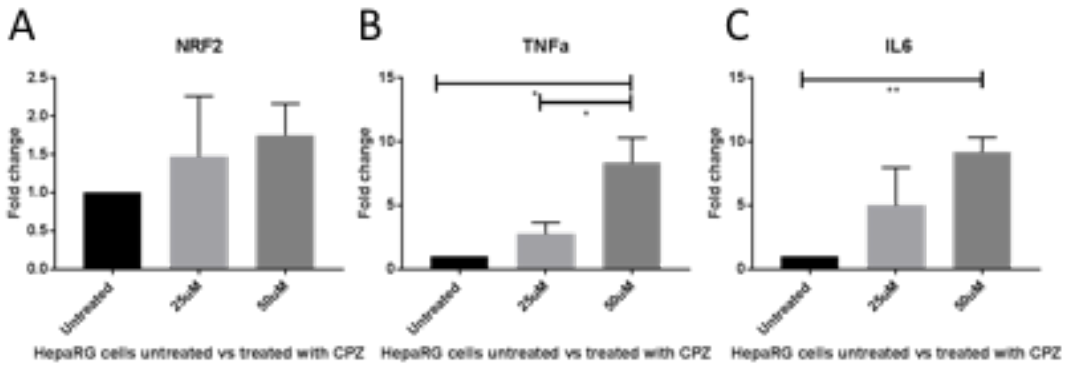

Figure 5.10 Expression of cellular defence system and pro-inflammatory markers. Expression of the oxidative defence and proinflammatory genes NRF2, TNFα and IL6 show a trend of upregulation with significant upregulation in both IL6 and TNFα

A) The mRNA expression of the oxidative defence gene NRF2 is increased in 50uM treated cells when compared to untreated control though no significant difference is reported (n=4). B) Results show significant upregulation of mRNA expression of TNFα in 25uM and 50uM treated cells ($p<0.001$) compared to untreated control. (n=3) C) IL- 6 presents dose dependent increasing trend when compared with untreated cells, showing significance at 50μM. (n=3)($p<0.005$) Results are presented as fold-changes in gene expression relative to untreated control calculated with the ΔΔCq method. (n=3, representing 3 independent experiments with 3 technical replicates each experiment (B&C), n=4 representing 4 independent experiments with 3 technical replicates each experiment (A)).

5.4 Discussion

Here, we show a novel approach forming a mechanistic view of CPZ toxicity encompassing traditional cell viability assays, impedance based quantitative measurements and mechanistic molecular techniques. This investigative method using the HepaRG™ co-culture of hepatocyte and cholangiocytes provides a unique opportunity to study the interaction of these cells when challenged with CPZ.

5.4.1 Chlorpromazine

CPZ is a neuroleptic drug used in the treatment of schizophrenia that has been known to cause acute intrahepatic cholestasis (IHC) (Antherieu et al., 2012). Up to now, an idiosyncratic view of this drug has been used to describe the variances in liver injury and cholestasis between patients. It has also been speculated whether toxicity of CPZ is due to oxidative stress or an inflammatory response which damages TJs and contributes to a more fluidic cellular membrane. Evidence from this model shows a dose dependent adaptive, inflammatory response due to oxidative stress and down regulation of membrane functional proteins with no evidence of apoptosis within this dose range. Concentrations of CPZ were based on Antherieu et al., (2013), and the determination of the IC50 value of 80μM. From this we base 25 μM and 50 μM as sub toxic doses and 100 μM as a toxic dose.

Historically, rat hepatocytes, or a sandwich culture of rat and human hepatocytes, have been the most reliable models for studying the toxic effects of CPZ (Dejanovic et al., 2016, Broeders et al., 2015, Eun et al., 2015). However, a human *in vitro* model is needed to overcome intra-species variation and better predict outcomes in pre-clinical trials where cholestasis may be an unwanted consequence. For this reason, we have employed the HepaRG™ cell line, a co-culture of hepatocytes and cholangiocytes with intrinsic CYP activity, longevity in culture and functionality akin to PHHs. Using this well-established co-culture gives the advantage of assessing membrane transport proteins in a model known to metabolise both phase I and II enzymes (Antherieu et al., 2012).

5.4.2 Tight junctions/ZO1

Tight junctions are an essential component of the cellular structure of hepatocytes and bile secretion system helping to maintain hepatic polarity by separating the basolateral and apical domains as well as providing barrier function between blood and bile. There are many elements to tight junctions consisting of adherens and occludin complexes.

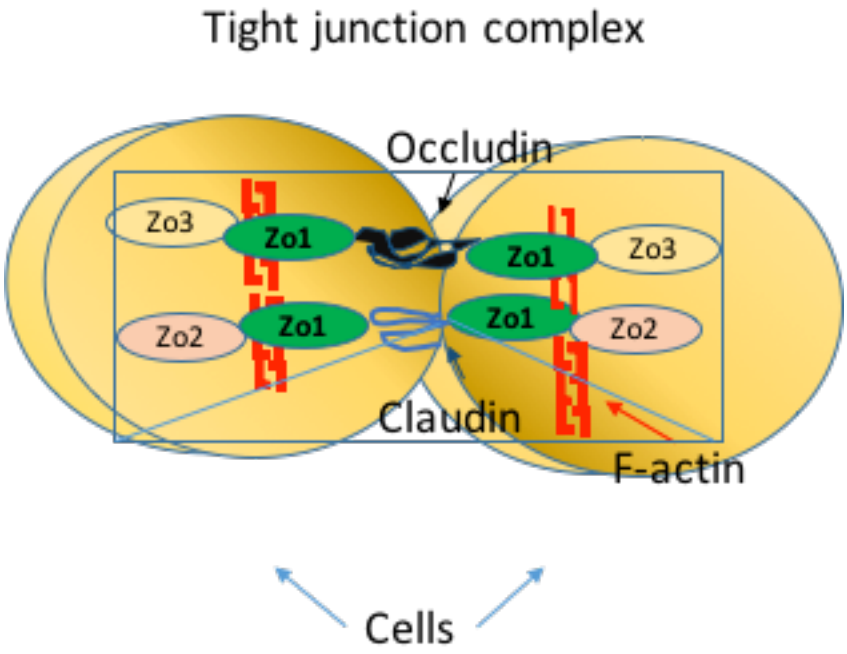

Figure 5.11 Pictoral representation of magnified tight junction complex: Tight junctions are composed of a variety of proteins including occludin, claudin and adheren complexes Zonula occludens are proteins that make up part of the complex and also anchor the tight junction complex to the F-actin cytoskeleton.

ZO1 in particular is an attractive marker as it is attached to both occludin and claudin proteins and is anchored to the F-actin cytoskeleton. For this reason, we performed parallel staining of the F-actin cytoskeleton and membrane protein ZO1 which shows a loss of F-actin and ZO1 in a dose dependent response to CPZ **(Figures 5.1 & 5.2)**.

Assays measuring total ATP and metabolic function of the cells via PrestoBlue™ have been used to assess viability (**Figure 5.3**). We did not find significant difference in cell culture viability between different concentrations of CPZ.

Although this may be in contrast with our findings of immunostaining, we speculate non-adherent cells which remain viable, would have been washed away during the staining process and would account for the discrepancy between cell survival seen in immunocytochemistry staining and viability assays.

To further understand these results, we employed a real time, label free, impedance-based assay to record changes in the cell membrane and adhesion of the culture over a 24 hour period.

5.4.3 ECIS

Cell based impedance assays are an emerging technology in drug discovery due to their high sensitivity and quantitative nature. Biological cells are

insulating particles that alter impedance when cultured on top of micro-electrodes. Therefore, an increase in impedance is a reflection of cellular growth kinetics. ECIS technology is able to decouple parameters of cell growth and cell-cell interaction through mathematical modelling and the use of multi-frequency measurements. The total impedance (encompassing resistive and capacitive components), can be deconvolved to show changes in morphology, membrane integrity, quality of basolateral adhesion and quality of cell-cell junctions (TJs), all contributing to a relative increase or decrease in impedance over time (Wegener, Giaver & Keese, 2000).

Here we demonstrate that cells treated with CPZ show alterations to cell-cell junctions, basolateral adhesion and also to total membrane integrity. This principle in correlation with our data shows that the major changes to the cell membrane happen within the first 6 hours after application of the drug (**Figure 5.4**). However, the culture was monitored for a total of 24 hours after application of CPZ and some recovery was observed. The recovery of TJ's, basolateral adhesion and cell membrane integrity after 6 hours in 25 and 50μM concentrations is significant since the half-life of CPZ is 30 hours. This suggests damage is immediate and some recovery due to adaptation occurs within the first 30 hours **(Figure 5.4)**. This highlights the usefulness of real time impedance as this may correlate to the results of cell viability assays where some viability of cells exposed to 100μM is seen at the 24 hour time point.

This result differs from impedance signatures produced using acetaminophen (APAP) as a direct hepatotoxin. We previously showed dose dependant damage to HepaRG™ TJs with no recovery when challenged with APAP (Gamal et al., 2017). As ECIS is a highly sensitive technology, it is possible that different signatures could be seen depending on the mechanism behind toxicity.

5.4.4 CYP3A4/HNF4α

Alongside viability and impedance-based assays, we also investigated functional hepatic enzyme CYP3A4 and its nuclear receptor HNF4α using qRT-PCR as a means of assessing functional viability **(Figure 5.7).** Metabolic activity and CYP functionality are important in detoxification of the cellular environment and supports adaptive processes within the cell, where CYP450 enzymes are an innate adaptive mechanism in hepatocytes when there is toxicity within the environment. Both CYP3A4 and its regulator HNF4α show a trend of up regulation at the lower dose indicating an adaptive response to low levels of toxicity within the cellular environment. The inhibition of CYP3A4 and HNF4α at the higher dose suggests the induction of a stress response causing down regulation of these markers at higher doses. Here we show an adaptive mechanism that was not seen within the APAP experiment.

5.4.5 Inflammatory and adaptive response

Inflammatory and further adaptive responses were measured though the analysis of TNFα, NRF2 and IL6. An increased dose dependent response was found in all three genes.

IL6 is an instigator of the innate and adaptive immune response. Expression is rapidly induced in instances of cellular stress and disease and is known to induce the anti-apoptotic pathway through BCL2 expression, as an adaptive response (Waxman and Kolliputi, 2009). Here we have shown up regulation of anti-apoptotic pathway by focusing on the BCL2 mRNA protein expression, indicating damage at sub toxic doses does not lead to apoptosis **(Figure 5.8)**. Up regulation of inflammatory cytokines may also go some way to explain the inhibition of CYP3A4 at 50μM within this model as CYP3A4 is down regulated in the presence of oxidative stress.

5.4.6 Bile acid and membrane bound transporters

To further understand mechanisms related to IHC we assessed several membrane transporter molecules. Decreased expression of bile acid transporter (ABCB11) suggests an impairment of this protein which is responsible for pumping toxic bile acids out of the cell. This inhibition of the bile acid transporter may compound and increase damage seen due to CPZ

as build up of bile acids are known to specifically target tight junction proteins (Raimondi et al., 2008, Chen et al., 2011)

The significant increase of genes responsible for the efflux of toxins and phospholipids (ABCB4 and ABCB1) also shows an adaptive response at the cellular level. **(Figure 5.9).**

5.4.7 Idiosyncratic presentation of CPZ induced cholestasis

Due to up regulation of membrane bound proteins, we propose a mechanism whereby the idiosyncratic presentation of CPZ injury within the liver may be explained. Mutations or variants in ABCB1 and ABCB4 may contribute to the mechanism behind CPZ toxicity. When ABCB4 is knocked out in mice, an increase of reactive oxygen species is observed alongside lipid peroxidation causing damage within the cell (Tebbi et al., 2016). Variations of ABCB4 in humans are also well documented to cause cholestatic pathologies such as intrahepatic cholestasis in pregnancy, low phospholipid associated cholelithiasis, oral contraceptive induced cholestasis and cholangiocarcinomas (Wasmuth et al., 2007, Pasmant et al., 2012, Tougeron et al., 2012). There is also a correlation between ABCB1 and drug induced cholestasis in another antipsychotic drug, risperidone. Risperidone is a second generation antipsychotic drug which is also prescribed for patients with schizophrenia. Preliminary data of a Chinese cohort suggests that phenotyping of ABCB1 may show genetic variations which influence

individual response to risperidone and aid in prescribing of the drug (Xing et al., 2006).

While we can not propose that there is a mutation or genetic variant to ABCB4 or ABCB1 within this model, we can show that any inability to regulate these efflux proteins could lead to cholestatic disease and that drugs used to treat schizophrenia are known to target these transporters. It can also be hypothesised that patients with variations or mutations of these genes may not be able to upregulate in the presence of a toxic compound and that this may provide some insight into the idiosyncratic presentation of CPZ induced IHC.

Here we describe a more mechanistic view of the damage caused by CPZ to both hepatocytes and cholangiocyte-like cells by using the HepaRG™ co-culture, real time assessment of the onset of toxicity and evidence of structural changes within the membrane which negatively impact the function of efflux transport proteins inducing inflammatory downstream effects which activate adaptive responses for cell survival.

Taken alongside viability assays, molecular data shows a dose dependent inflammatory and adaptive response induced by CPZ at non-toxic 25μM and sub-toxic 50μM concentrations. We observe an overall decrease in genes encoding proteins responsible for the initiation of apoptosis, no change in cell functionality or viability and an increase in pro-inflammatory cytokines TNFα and NRF2, which supports the hypothesis that damage caused by CPZ is

through an inflammatory pathway **(Figure 5.10).** Further evidence of an adaptive response can be seen in the up-regulation of CYP3A4 at 25μM, and membrane bound transporters ABCB1 and ABCB4 alongside dose dependant increase of IL6 and its initiation of the BCL2 anti-apoptotic pathway. Further work could be undertaken to assess oxidative stress using flow cytometry to ascertain if there is a quantitative dose dependant response that would correlate gene expression of inflammatory and adaptive markers. Down regulation of bile acid transporters are also statistically significant as it impacts the structural integrity and TJs.

To further investigate, a method using LC:MS/MS could be employed to measure bile acids within the supernatant and intracellular environment.

5.5 Conclusion

Conclusions of this study can be summarized in the following points.

1. Chlorpromazine was not directly hepatotoxic to HepaRG™ cells
2. Down-regulation of bile acid transporter (ABCB11) may be responsible for increased bile acids within the cell.
3. ECIS showed dose dependent decrease of total impedance, with clear evidence of disruption of basolateral adhesion and cell membrane integrity
4. Immunostaining confirmed disruption of adhesion (F-actin and ZO1)
5. There was dose dependant up-regulation of inflammatory cytokines (IL6 and TNFa)
6. Adaptive response was seen in upregulation of NRF2, ABCB1, ABCB4 expression with induction of anti-apoptotic marker BCL2
7. We speculate that polymorphisms of ABCB1 and ABCB4 may affect adaptive response and lead to cholestasis

Chapter 6 Discussion and future work

There is a need within the pharmaceutical sector to gain more insight into the mechanisms behind DILI and the safety and efficacy of new compounds. Hepatotoxicity is a common cause of attrition of drugs in late stage clinical trials. Therefore, a better model that mimics human liver physiology *in vitro* could help in the development of safer compounds.

There are many in vitro models of DILI, yet none that have been put forward as an industry or gold standard. One of the biggest issues within research today is reproducibility of experimentation between laboratories. To tackle this, the Innovative Medicines Initiative (IMI) set out to assess if current cell models used in safety assessment distinguish between chemicals which cause DILI. The study design used 7 laboratories across the IMI. Nine compounds were used that are known to be hepatotoxic and 4 compounds that are known to be non-toxic. All laboratories used the same reagents, cell lines and procedures to test compounds and determine if DILI could be predicted in vitro using dosing regimes of either 24 or 72 hours. Inter and intra-variability was also assessed.

The results showed inter-laboratory variation in all cells apart from HepaRG™s. They also showed that none of the cell models used was able to distinguish between DILI and non DILI compounds based on EC50. PHH and

HepG2 cells were most accurate in predicting DILI despite the variations observed.

While the design of their study was robust (7 laboratories using same protocols, reagents and cell types) it is unclear how many of these studies were combined to create the results presented. In Materials and Methods they state that inter-laboratory variation of several cell models were evaluated by at least 2 test sites. It is unclear why only 2 test sites were evaluated as 7 took part.

While all cell types were grown the same across all laboratories, HepaRG™ cells were the only line not grown on either matrigel or collagen. It is well known that collagen and matrigel coated surfaces create better adhesion than standard TCP on both 2D and 3D models using hepatocytes (Zeigerer et al., 2017, Kubo et al., 2016, Aday et al., 2011, Wang et al., 2016 & 2004, Sanchez et al., 2000,). We have also shown within this thesis the role surface substrate plays in proliferation and differentiation. Therefore, it is unclear why HepaRG™ cells were treated differently within the Sison-Young study. This may have an impact on the results showing HepaRG™ cells lacking when compared to PHH and HepG2 as we have also shown in Chapter 3 how HepaRG™ cells provide a much more relevant in vitro model when compared to HepG2/C3A's.

Another unclear point within this paper is the use of HepaRG™-P cells. Their use of Fresh HepaRG™s seemed to be based on passaging HepaRG™-P cells according to Biopredics protocol, then trypsinizing and reseeding them onto TCP as fully differentiated cells and running experiments on day 5. We know day 5 is too early to experiment on HepaRG™ fully differentiated cells due to lack of tight junctions which indicate hepatocyte polarity. This is evidenced by ECIS data shown in both APAP and CPZ experimentation (Gamal et al., 2017).

Dosing regimes within the consortium were set up for either 24 or 72 hours. 72 hour protocols take into consideration repeat dosing and is a good model to take forward, however, dosing solutions were made fresh daily. While this can be seen as a good practice, it can also introduce variability and for this reason, within our laboratory, we freeze down stock solutions so each aliquot should be directly comparable and reproducible.

The groups used the same dose for each cell type rather than an optimal dose. This creates reproducibility, but could be criticised for not considering the level of CYP enzyme activity within each cell line. Using the same dose for all cell lines may have introduced toxicity issues, thereby confounding resazurin assay. Results for the resazurin assay were not shown in the main body of the paper, but materials and methods states that cells were incubated with resazurin for 1 hour. We have shown this to be too long for HepaRG™ and HepG2/C3A cells (see Supplementary data) as secondary

fluorescent metabolite resarufin is further metabolised into hydro-resorufin, which does not fluoresce and is undetectable, meaning a loss of optimal signal.

Finally, while there are some aspects of this study which warrant further consideration (Reproducibility across various sites, multiple cell lines used, harmonized protocols and standardization) other aspects of this study fall into question. It is imperative that all cell cultures be treated the same in any DILI comparison to preserve reproducibility of results. The results of this study suggest that there was no cell model which was able to distinguish between DILI and non DILI compounds based on EC50. They also state that '...each compound varied per cell type across the relevant test sites.', HepG2 and Upcyte cells differed markedly between replicate experiments in the same laboratory, intra-laboratory analysis varied between compounds, and finally 'Importantly, we detected different degrees of inter-laboratory variation across the cell types assessed.'.

Contrary to the above study, we have shown the human hepatic HepaRG™ cell line to be a more relevant model for *in vitro* drug toxicity and development assays.

The HepaRG™ cell line exhibits better functionality than C3A models and is comparable to PHHs. However, many *in vitro* models rely on exogenous compounds for differentiation and maturation. Finding a model that differentiates cells without the use of these chemicals which also maintains

long term differentiated function could improve the outcome and high costs involved in using these models. Our first hypothesis tested whether we could improve the rate of growth, differentiation and functionality of the HepaRG™-P cells without using exogenous agents such as DMSO. By growing the HepaRG™-P cells on various nanopattern and non pattern controls we have shown that cell surface substrate/treatment can effect differentiation and function of HepaRG™-P cells without the use of exogenous chemicals. While nanopits had some effect on function and growth compared to TCP, we saw a significant difference in the rate of differentiation and functional capabilities on the UP control. This prompted us to examine the role oxygen plasma may play in the growth and function of cells. Changes in phenotype due to surface chemistry is supported within the literature. Scherthaner (2012) reported the translocation of β-catenin from cell adhesion sites to the nucleus of endothelial progenitor cells. This was more or less profound when the chemical treatment of the surface was altered by introduction of polar oxygen and nitrogen groups This highlights the complex relationship between nanopatterned surfaces/structures and the chemical composition of the substrate and their effect on cell morphology and supports further investigation into surface treatment without nanopatterning.

It has also been shown that various states of hyperoxia induce differentiation of this specific cell line (Van Wenum et al., 2018) and has also played a part in the differentiation and viability of other cell lines. This could have

implications for future work where various oxygen plasma coated surfaces could be compared to various states of hyper and hypo-oxia on HepaRG™ cells to determine its effect on differentiation and function. It may be of particular interest when assessing specific liver zonation as our model suggests a trend towards zone 3 specific cells. Future work could explore the hypothesis that oxygen plays a major role in the zonation of the liver. The oxygen gradient within the acini is well documented and experiments to replicate this *in vitro* could inform a more dynamic model of DILI. While the outcome of this study was unexpected, it is perhaps beneficial, for future manufacturing of this model, that surface chemistry, rather than nanopatterns, is key in directing earlier differentiation and function. The implications of this model based on surface treatment make it more accessible by designating a specific concentration of oxygen plasma which is easier to regulate in terms of reproducibility and keeps the cost of this model low. However, there were some results within this study that require more consideration. For instance, the immunohistochemistry was sometimes limited to one or two biological replicates. While technical replicates are important and can show variation within an experiment, biological replicates are needed to show overall reproducibility. Staining of both CPS and GS within the nanopattern project was undertaken at the end of the project on one biological replicate with three technical replicates. Repeating this experiment and any others of an n value less than 3 would be needed to discuss significance in the model overall. It was also mentioned within

Chapter 3 that there was no positive control for the staining of CPS or GS. In the absence of a signal, such as the CPS stain, a positive control should be used to verify the technique and antibody and ensure that the protocol is sound. Similarly, when considering the gene expression data for SOX9 (Figure 4.13), six biological replicates (with three technical replicates for each biological replicate) were used, but did not produce a result. Even though primers were validated by Primer Design, a positive control for SOX9 gene expression should have been tested alongside experimental conditions for verification of primers and technique.

Monitoring DILI using a real time, non-invasive and label free platform could also be beneficial, providing useful information of the time course of injury caused by compounds. The ECIS ZΘ impedance-based assay is capable of this type of monitoring and has already been used extensively in *in vitro* models of toxicity. It is interesting to note that the ECIS arrays are treated with oxygen plasma instead of the standard industry corona treatment used by companies such as Corning. This may aid in adhesion of cells to the array and warrants further investigation. Dose dependant impedance assays can shed light on the mechanisms of action of new compounds by highlighting where damage occurs and how long it takes for damage to be seen. This may then be correlated with the half-life of the compound as in the CPZ model.

Here we present a model of cholestasis using the HepaRG™ cell line. This is possible due to the unique bipotency of this cell line. As cholestasis is

described as the inhibition of bile acid secretion within the liver, one way to further establish a model of cholestasis would be to measure bile acids both intra and extracellularly. This can be done using LC:MS/MS where supernatant and cell lysates can be assessed for total concentration of primary bile acids. It is known that HepaRG™ cells typically have a similar concentration of bile acids, both intra and extracellularly, to PHHs. (Woolbright et al., 2016, Sharanek et al., 2015). Therefore, establishing a model of cholestasis using ECIS and LC:MS/MS could be directly relatable to PHHs. Using HepaRG™s in such a model would give better reproducibility than PHHs as PHHs are difficult to maintain in culture and vary phenotypically from donor to donor.

While we used qRTPCR to measure fold change of inflammatory cytokines, another option would be to measure them directly within cell supernatant. This would give more confidence in the gene expression data and may contribute further information to the model.

Further work could also look at other model cholestatic compounds to assess the impedance signature, membrane transporters and inflammatory responses and compare the results to the current study. Also, while the study on chlorpromazine assessed the regulation of key genes responsible for transporting compounds out of the cell, it did not consider membrane bound transporters responsible for influx. In future, considering genes such as

solute carrier transporters (SLCs) organic cation transporters (OCTs) and organic anion transporters (OATs) and transporting polypeptides (OATPs), coupled with a quantification of parent compound turnover, could better inform studies interested in the absorption and elimination of new compounds and other drugs known to cause cholestasis.

The HepaRG™ cell line is robust and versatile. It lends itself to many applications, and could lead to further disease in a dish models such as non-alcoholic fatty liver disease (NAFLD). Within our group we have published a model of NAFLD using C3A cells and have extensively looked at the role fat plays in the accumulation of oxidative stress (Lockman et al., 2012, Lockman et al., 2016). It would be interesting to revisit this model using the HepaRG™ cell line and compare the results to previous data.

It has also been shown that HepaRG™ cells are a good cell line for the creation of spheroids (Martucci et al., 2018). 3D cultures such as spheroids have several pros and cons. Theoretically, 3D cultures should mimic a more *in vivo*-like environment as multicellular contact promotes better cell-cell communication and confers biological relevance to a model. One of the problems with spheroids is in keeping the core cells viable. As the mass of the spheroid increases, cells at the core can die due to hypoxia and nutrient depletion. It is also difficult to find assays that will accurately assess the core viability.

It has been shown that spheroids comprised of HepaRG™ cells maintain a viable core through the measurements of Promega Cell Titer glo -3D ATP assay and optical coherence tomography (OCT).
Using HepaRG™ spheroids alongside the fat loading model used for NAFLD may give new insight into the absorbtion of fat into hepatocytes and the levels of toxicity caused by oxidative stress.

Finally, using the tool kit of viability and biochemical assays, impedance based measurements, molecular and flow cytometry techniques described in this work, it is possible to build many different models of DILI or ‘disease on a dish’ using the HepaRG™ cell line.

Chapter 7 Supplementary Data

7.1 Supplementary data to chapter 3

LC:MS/MS

Below are data sets of biotransformation used to produce chromatograms for both C3A and HepaRG™ samples.

Sample C3A

phenacetin 2

Biotransformation	Mass Shift	Expected m/z	Q1 / Q3	Retention Time. (min)	Peak Area	% Area of parent ion
Loss of 42.0 Tri demethylation	-42	138	138.0 / 110.0	3.62	2.44E+05	3.8
Loss of 28.0 Di demethylation	-28	152	152.0 / 110.0	1.74	1.67E+05	2.6
Parent	0	180.1	180.1 / 110.0	5.99	5.81E+06	89.3

Sample C3A

phenacetin 1

Biotransformation	Mass Shift	Expected m/z	Q1 / Q3	Retention Time. (min)	Peak Area	% Area of parent ion
Loss of 42.0 Tri demethylation	-42	138	138.0 / 110.0	3.62	2.44E+05	3.8
Loss of 28.0 Di demethylation	-28	152	152.0 / 110.0	1.74	1.67E+05	2.6
Parent	0	180.1	180.1 / 110.0	5.99	5.81E+06	89.3

Sample C3A

phenacetin 1b

Biotransformation	Mass Shift	Expected m/z	Q1 / Q3	Retention Time. (min)	Peak Area	% Area of parent ion
Loss of 42.0 Tri demethylation	-42	138	138.0 / 110.0	3.63	3.08E+05	5.1
Loss of 28.0 Di demethylation	-28	152	152.0 / 110.0	1.74	1.70E+05	2.8
Parent	0	180.1	180.1 / 110.0	6.01	5.24E+06	86.3

Sample C3A

phenacetin

HBSS

Biotransformation	Mass Shift	Expected m/z	Q1 / Q3	Retention Time. (min)	Peak Area	% Area of parent ion
Loss of 42.0 Tri demethylation	-42	138	138.0 / 110.0	3.6	4.18E+05	7.5
Loss of 28.0 Di demethylation	-28	152	152.0 / 110.0	1.77	1.05E+05	1.9
Parent	0	180.1	180.1 / 110.0	6.01	4.81E+06	86.1

Sample

phenacetin 1

C3A

Biotransformation	Mass Shift	Expected m/z	Q1 / Q3	Retention Time. (min)	Peak Area	% Area of parent ion
Loss of 42.0 Tri demethylation	-42	138	138.0 / 110.0	3.65	1.56E+05	3
Loss of 28.0 Di demethylation	-28	152	152.0 / 110.0	1.83	1.79E+05	3.5
Parent	0	180.1	180.1 / 110.0	6.03	4.61E+06	89.3

Sample

phenacetin 2

C3A

Biotransformation	Mass Shift	Expected m/z	Q1 / Q3	Retention Time. (min)	Peak Area	% Area of parent ion
Loss of 42.0 Tri demethylation	-42	138	138.0 / 110.0	3.6	2.34E+05	4.5
Loss of 28.0 Di demethylation	-28	152	152.0 / 110.0	1.8	1.45E+05	2.8
Parent	0	180.1	180.1 / 110.0	6.04	4.68E+06	89.3

7.1.1 HRG sample data

Sample HRG 2

Phenacetin 2

Biotransformation	Mass Shift	Expected m/z	Q1 / Q3	Retention Time. (min)	Peak Area	% Area of parent ion
Loss of 42.0 Tri demethylation	-42	138	138.0 / 110.0	3.61	2.87E+06	29.1
Loss of 28.0 Di demethylation	-28	152	152.0 / 110.0	1.81	2.10E+05	2.1
Loss of 14.0 Mono demethylation	-14	166.1	166.1 / 124.0	2.67	1.68E+05	1.7
Parent	0	180.1	180.1 / 110.0	5.99	6.37E+06	64.4

Sample HRG phenacetin 2 pbs

Biotransformation	Mass Shift	Expected m/z	Q1 / Q3	Retention Time. (min)	Peak Area	% Area of parent ion
Loss of 42.0 Tri demethylation	-42	138	138.0 / 110.0	3.59	1.15E+06	8.8
Loss of 28.0 Di demethylation	-28	152	152.0 / 110.0	1.77	1.45E+05	1.1
Loss of 14.0 Mono demethylation	-14	166.1	166.1 / 124.0	2.64	1.04E+05	0.8
Parent	0	180.1	180.1 / 138.0	6.02	1.15E+07	87.2

Sample HRG2 Phenacetin 1

Biotransformation	Mass Shift	Expected m/z	Q1 / Q3	Retention Time. (min)	Peak Area	% Area of parent ion
Loss of 42.0 Tri demethylation	-42	138	138.0 / 110.0	3.57	2.10E+06	30.3
Loss of 28.0 Di demethylation	-28	152	152.0 / 110.0	1.81	1.69E+05	2.4
Loss of 14.0 Mono demethylation	-14	166.1	166.1 / 124.0	2.63	1.15E+05	1.7
Parent	0	180.1	180.1 / 110.0	6.01	4.31E+06	62.2

Sample HRG 3.1

phenacetin

Biotransformation	Mass Shift	Expected m/z	Q1 / Q3	Retention Time. (min)	Peak Area	% Area of parent ion
Loss of 42.0 Tri demethylation	-42	138	138.0 / 110.0	3.6	1.31E+06	17.5
Loss of 28.0 Di demethylation	-28	152	152.0 / 110.0	4.17	4.59E+05	6.1
Loss of 14.0 Mono demethylation	-14	166.1	166.1 / 124.0	2.66	1.09E+05	1.5
Parent	0	180.1	180.1 / 110.0	6.04	5.47E+06	72.7

Sample HRG 3.2 phenacetin

Biotransformation	Mass Shift	Expected m/z	Q1 / Q3	Retention Time. (min)	Peak Area	% Area of parent ion
Loss of 42.0 Tri demethylation	-42	138	138.0 / 110.0	3.55	1.56E+06	21
Loss of 28.0 Di demethylation	-28	152	152.0 / 110.0	1.74	2.54E+05	3.4
Loss of 14.0 Mono demethylation	-14	166.1	166.1 / 124.0	2.61	8.88E+04	1.2
Parent	0	180.1	180.1 / 110.0	6.04	5.26E+06	70.9

7.2 Supplementary data to chapter 2 materials and methods: Characterisation of PrestoBlue™ assay for use in C3A and HepaRG™ cell lines

Very few studies have been carried out on the accuracy of PrestoBlue™ or how different plates, plate readers or cell lines react to this assay. The purpose of this supplementary section is to examine the accuracy of PrestoBlue™ to gauge cell proliferation and metabolic activity in C3A cells.

PrestoBlue™ is a resazurin based reagent capable of assessing cell proliferation, viability and metabolic activity. These three attributes run hand in hand in a given cell culture as the more proliferative your cells, the more metabolic activity you are likely to see, and if cells are metabolically active they will be viable.

PrestoBlue™ is ideal as it is not an end point assay and it is hypothesised that using PrestoBlue™ at various points during a given cell culture will not have a significant effect on the culture itself.

PrestoBlue™ works by testing mitochondrial enzyme activity (Xu et al., 2014). The blue, non-fluorescent resazurin is taken into the cytosol of viable cells

and is reduced through cellular respiration by NADPH, FAD, NADH and FMNH into resarufin which fluoresces red (Xu et al., 2014). The fluorescence or absorbance is directly proportional to the number of metabolically active or viable cells and can then be read at 520nm (Xu et al., 2014).

7.2.1 PrestoBlue™ vs Alamar Blue™

Until recently Alamar Blue™ was the industry standard in resazurin based viability assays. Little is known of the difference between Alamar Blue™ and PrestoBlue™. However, the manufacturer of PrestoBlue™ has confirmed that they contain different buffers and it has been asserted that PrestoBlue™ is faster and has a higher sensitivity than Alamar Blue™ (Xu et al., 2014)

Xu et al., (2014) used a number of incubation times and methods to assess the difference between PrestoBlue™, AlamarBlue™ and MTT™. They found that PrestoBlue™ was able to detect cells at a density of 5k after half an hour incubation while MTT could detect the same number of cells only after a 3 hour incubation.

7.2.2 Time dependency

It is important to understand the processes involved within an assay and how this related to your particular cell lines. For instance, within the PrestoBlue™

assay the dark blue resazurin salt is reduced to a red fluorescent compound called resorufin. This compound is what is measured within this assay to give you an indication of how metabolically active your cells are. However, resorufin is then further reduced to hydro-resorufin which is colourless and cannot be detected. The material safety data sheet for PrestoBlue™ recommends an incubation time of 30 minutes in order to give the cells time to reduce resazurin into resorufin. Since we are using hepatocytes which can have a high metabolic rate, it was decided to test the hypothesis of a 30 minute incubation to see if it was suitable for our particular cell line by taking a PrestoBlue™ reading once every 10 minutes for an hour. This would show the optimum time for reading by showing an increase in signal as the cells metabolize resazurin and a plateau where resorufin is visible and no further metabolism takes place. It was hypothesized that after such a plateau, a decline in signal would be apparent showing the further metabolism of resorufin to the colourless hydro-resorufin.

Figure 7.1: Schematic of resazurin metabolism Within the assay, the non fluorescent resazurin is reduced to its metabolite of resorufin which fluoresces red. Further reduction of resorufin produces hydro-resorufin which does not emit a coloric or fluorescent signal.

7.2.2.1 Day 0 seeding density readings

C3A cells were thawed from liquid nitrogen at 37C. Cells were counted using the Countess cell counter described in Chapter 2. Cells were suspended in eppendorf tubes at differing densities of 2.5k, 5k, 10k, 20k, 40k, 80k, 100k and 160k cells per tube, (n=3 for each density). Cells were spun down at 5.6k rpm for 3 mins and the supernatant was discarded. Cells were resuspended in 100ul of PrestoBlue™ for 30 mins. Cells were spun down into a pellet and the supernatant was taken into a white 96 well plate reader and read on a Glomax at 520nm.

7.2.2.2 Day 1 and 3 seeding density readings

C3A cells were seeded on a standard 96 well Corning plate at densities of 2.5k, 5k, 10k, 20k, 40k, 80k, 100k and 160k cells per well for three wells each

density. Cells were kept at 37C with 5% CO2. The PrestoBlue™ assay was performed 24 hours (Day 1) and 72 hours (Day 3) after seeding and readings were taken after cells were washed in PBS and then incubated for 30 minutes with PrestoBlue™.

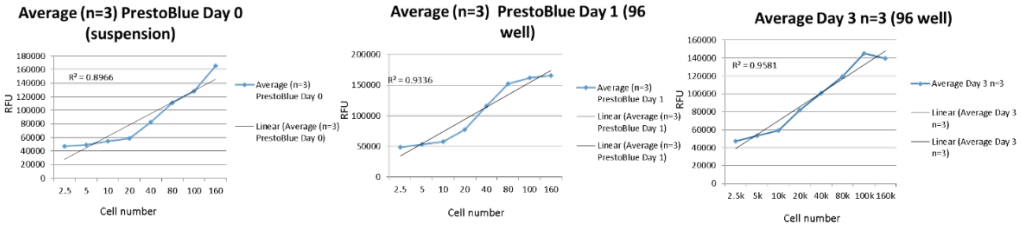

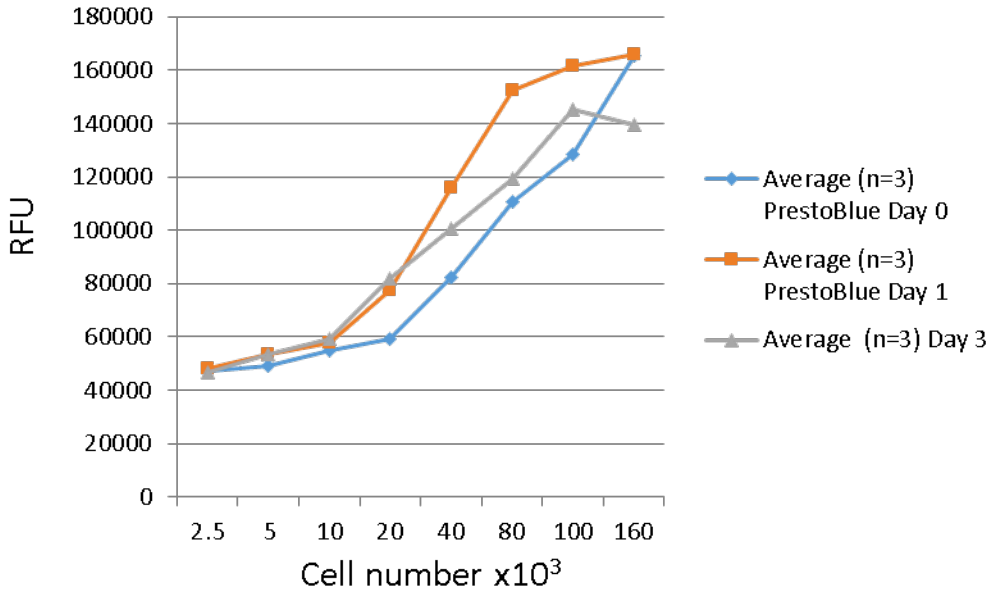

Figure 7.2: PrestoBlue™ standard curves C3A cells were seeded at 2.5, 5, 10, 20, 40, 80, 100 and 160k cells per well (n=3) and PrestoBlue™ readings were taken at day 0 in suspension then again at 24 and 72 hours. This established a standard curve which validated this technique as being sensitive enough for use with a range of cell seeding densities that may be used within future studies.

7.2.2.3 Day 3 time dependent reading

C3A cells seeded at the above densities underwent PrestoBlue™ assessment on day 3. Readings were taken every 10 minutes for one hour on the Glomax at 520nm.

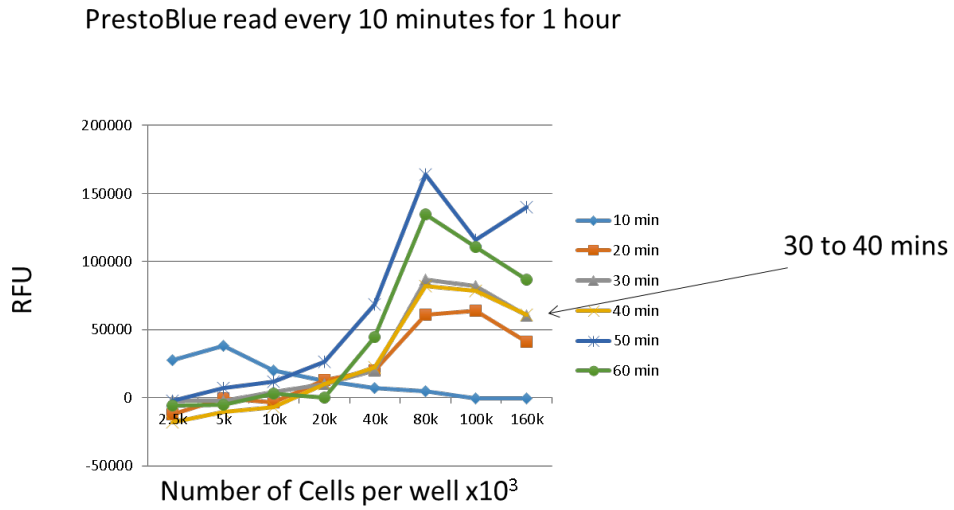

Figure 7.3 PrestoBlue™ time dependant metabolism of substrate:
Graphical representation of C3A cells grown at various seeding densities where readings were taken every 10 minutes for one hour. This shows that after 10 minutes little to no signal was detected, between 20 and 40 minutes a signal is detected and an increase is seen in metabolic proficiency up to 80k cells where signal plateaus before decline at 100k cells and beyond. Flourescent signals read at 50 and 60 minutes show increase in metabolism to 80k cells before dramatic drop 100k + indicating that after cell culture reaches 80k cells metabolic proficiency is high enough to metabolise resarufin into hydroresorufin thereby showing a loss or drop in signal.

7.3 Optimisation of Reference Genes for use in HepaRG™ cell line- raw data

MIQE guidelines were consulted throughout the processes of RG selection, sample preparation and analysis of data. Within these extensive guidelines, one of the most important factors to take into consideration is the selection of a set of three RGs that maintained stability throughout experimentation.

It was decided that the same 12 RGs would be used for analysis on both the nanopattern and CPZ projects. It was interesting then to observe that the top 3 genes recommended for the CPZ study were completely different from those selected for the nanopattern study. CYC1, SDHA and 18s were used as our panel of RGs for the nanopattern project while GAPDH, UBC and TOP1 were used for CPZ.

Within the same cell line, under different conditions, there was not one gene recommended that was the same for both cohorts. This highlights the need for stringent adherence to RG selection in accordance with MIQE guidelines and current literature, as even within the same cell line, RGs can change in accordance to experimental conditions. Keeping this in mind it would perhaps be useful to adopt a more encompassing view of the transcriptome by using a microarray or RNAseq when evaluating the stability of RGs over a particular cell line and specific experimental parameters.

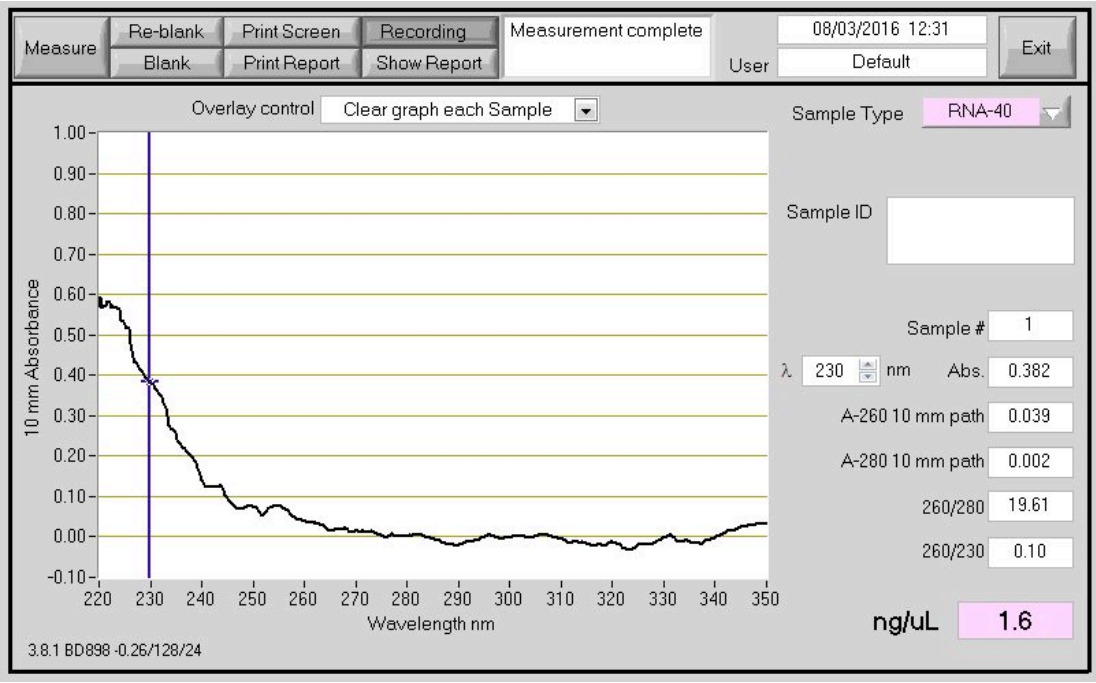

Figure 7.4 Sample screen shot of nanodrop measurement of RNA purity for HepaRG™-P cells at day 0: Nanodrop measurement of RNA from day 0 cell suspension: Graphical and quantitative representation of RNA quantity and quality of HepaRG™-P cells for us in selecting reference genes.

7.4 Supplementary data from Chapter 4

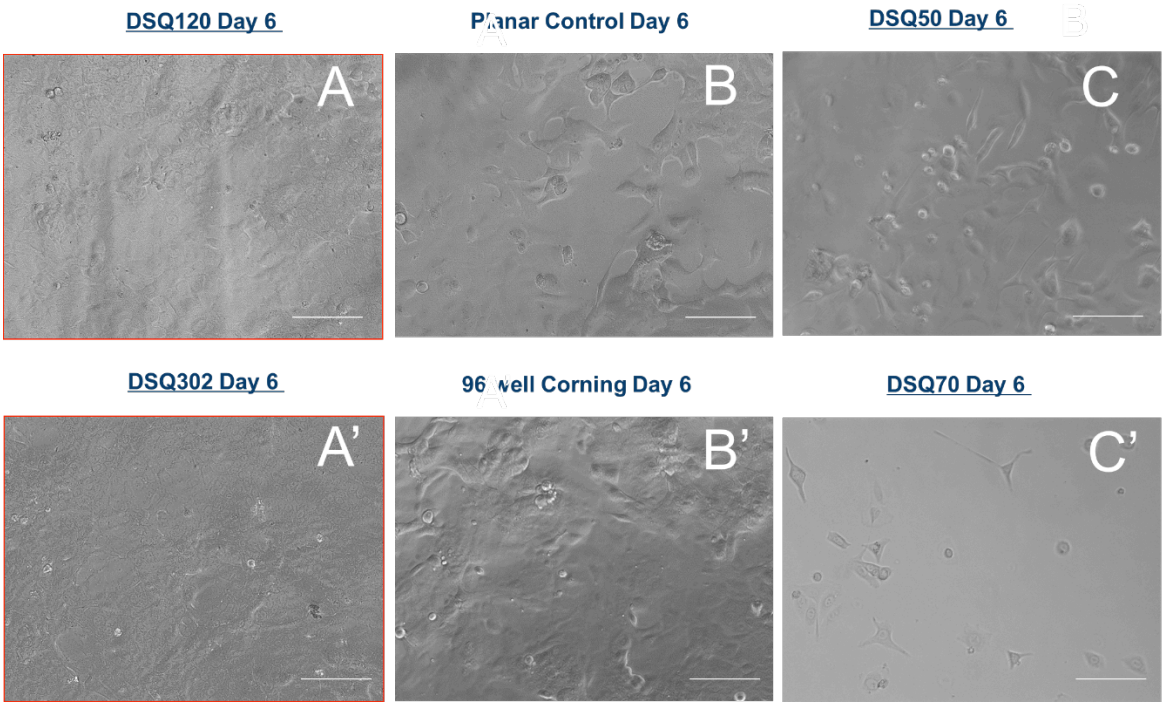

Figure 7.5 Representation of HepaRG™ cells on various different NPS and control HepaRG™ progenitors on TCP show commitment to the hepatocyte lineage ~day 14. Significantly, we identified *earlier* commitment to a hepatic lineage at day 6 on DSQ120. (**A**) – compared with both controls (**B-B'**) and all test nanopatterns (**A'**,**C, C'**).

Publications

References

1. Aday, Sezin, Ege, Hasirci, Nesrin, Middle East Technical & Deliloglu Gurhan, Ismet, Ege, 2011. A cost-effective and simple culture method for primary hepatocytes. Animal Cells and Systems, (1), pp.19–27.

2. Ahn, M., Shah, YM., Inoue, J., Morimura, K., Kim, I., Yim, S., Lambert, G., Kurotani, R., Nagashima, K., Gonzalez, FJ., Inoue, Y., 2008. Hepatocyte nuclear factor 4α in the intestinal epithelial cells protects against inflammatory bowel disease. *Inflammatory Bowel Diseases, 14*(7), 908-920.

3. Akerboom, T., Schnieder, I., vom Dahl, S., Sies, H., 1991, Cholestasis and changes of portal pressure caused by chlorpromazine in the perfused rat liver, *Hepatology*, 13: 216-221)

4. Aninat C, Piton A, Glaise D, Le Charpentier T, Langouët S, Morel F, Guguen-Guillouzo C, Guillouzo A. Drug Metab Dispose. 2006;34:75–83.

5. Anthérieu, S., Chesné, C., Li, R., Guguen-Guillouzo, C., Guillouzo A., 2012. Optimization of the HepaRG cell model for drug metabolism and toxicity studies. *Toxicol in vitro* 26:1278–85

6. Antherieu, S., Bachour-El Azz,i P., Dumont, J., Abdel-Razzak, Z., Guguen-Guillouzo, C., Fromenty, B., Robin, MA., Guillouzo, A., 2013. Oxidative stress plays a major role in chlorpromazine-induced cholestasis in human HepaRG cells. *Hepatology* 57:4:1518-1529

7. Antoniou, A., Raynaud, P., Cordi, S., Zong, Y., Tronche, F., Stanger, B.Z., Jacquemin, P., Pierreux, C.E., Clotman, F., Lemaigre, FP., 2009. Intrahepatic bile ducts develop according to a new mode of tubulogenesis regulated by the transcription factor SOX9, *Gastroenterology* 136 (7) 2325-2333

8. Babeu, JP. and Boudreau, F., 2014. Hepatocyte nuclear factor 4-alpha involvement in liver and intestinal inflammatory networks, *World Journal of Gastroenterology* Vol 20(1), p22-30

9. Bachour El-Azzia, P., Sharanek, A., Burban, A., Li, R., le Guevel, R., Abdel-Razzak, Z., Stieger, B., Guguen-Gouillozo, C., and Gouillozo, A., 2015. Comparative localization and functional activity of the main

hepatobiliary transporters in HepaRG cellsand primary human hepatocytes, *Toxicol Sci*. 145(1) 157-168

10. Ballet, F., 2015. Preventing Drug-Induced liver injury: How useful are animal models?, *Digestive diseases*, 33:477-485 DOI: 10.1159/000374093

11. Berg JM, Tymoczko JL, Stryer L. Biochemistry. 5th edition. New York: W H Freeman; 2002. Section 26.3, The Complex Regulation of Cholesterol Biosynthesis Takes Place at Several Levels. Available from: https://www.ncbi.nlm.nih.gov/books/NBK22336/

12. Bhattacharya, M., Lauren, L., Kuisma, K., Kanninen, L., Lille, M., Corlu, A., Guguen-Guillouzo, C., Ikkala, O., Laukkanen, A., Urtti, A., Yliperttula, M., 2012. Nanofibrillar cellulose hydrogel promotes three-dimensional liver cell culture. *Journal of Controlled Release, 164*(3), 291-298.

13. Biopredic International, [image] figure reference HepaRG karyotype. [online] Heparg.com. Available at https://www.heparg.com/rubrique-features [Accessed June 30, 2017]

14. Birchmeier, W., 2016. Orchestrating Wnt signalling for metabolic liver zonation, *Nature Cell Biology* 18, 463-465

15. Boncler, M., Rozalski, M, Krajewska, U., Podsedek, A., and Watala, C., 2014. Comparison of PrestoBlue and MTT assays of cellular viability in the assessment of anti-proliferative effects of plant extracts on human endothelial cells. *Journal of Pharmacological and Toxicological Methods*, 69, 9-16.

16. Bonzo, J.A., Ferry, C.H., Matsubara, T., Kim, JH. and Gonzalez, FJ., 2012. Suppression of Hepatocyte Proliferation by Hepatocyte Nuclear Factor 4α in Adult Mice, *Journal of Biological Chemistry* Vol. 287 (10) pp 7345-56

17. Broeders, JW, Parmentier, C, Truisi, GL, Jossé, R, Alexandre, E, Savary, CC., Hewitt, PG., Mueller, SO., Guillouzo, A., Richert, L., van Eijkeren, JC., Hermens, JL., Blaauboer, BJ., 2015. Biokinetics of chlorpromazine in primary rat and human hepatocytes and human HepaRG cells after repeated exposure. *Toxicology in vitro*, 30(1):52-61

18. Bustin, SA., Benes, V., Garson, JA., Hellemans, J., Huggett, J., Kubista, M., Mueller, R., Nolan, T., Pfaffl, MW., Shipley, GL., Vandesompele, J., Wittwer, Carl T., 2009. The MIQE guidelines: minimum information for publication of quantitative real-time PCR experiments. *Clinical chemistry*, Vol.55(4), pp.611-22

19. Castell, JV., Gomez-Lechon, Maria, J., Ponsoda, X., Bort, R., 1996. *in vitro* investigation of the molecular mechanisms of hepatotoxicity. *in vitro* methods in *Pharmaceutical Research*, Chapter 16:375-410

20. Caeci, T., 2018. Exercise 20: Accessory Glands of the Digestive Tract, VM8054 Veterinary Histology, Accessed March 25, 2018, Avaliable at www.doctorc.net/Labs/Lab20/LAB20.HTM

21. Cerec, V. et al., 2007. Transdifferentiation of hepatocyte-like cells from the human hepatoma HepaRG cell line through bipotent progenitor. *Hepatology*, 45(4), pp.957–967.

22. Celeen, L., De Spiegelaere, W., David M.,De Craene, J., Vinken, M., Vanhaecke, T., Rogiers, V., 2011. Critical selection of reliable reference genes for gene expression study in the HepaRG cell line, Biochemical Pharmacology, Vol 81(10), pp.1255-1261

23. Chapman KL., Holzgrefe, H., Black, LE., Brown, M., Chellman, G., Copeman, C., Couch, J., Creton, S., Gehen, S., Hoberman, A., Kinter, LB., Madden. S., Mattis, C., Stemple, HA., Wilson, S., 2013. Pharmaceutical toxicology: Designing studies to reduce animal use, while maximising human translation. *Regulatory Toxicology and Pharmacology* (66) 88–103

24. Chen, X., Oshima, T., Tomita, T., Fukui, H., Watari, J., Matsumoto, T., Miwa, H., 2001. Acidic bile salts modulate the squamous epithelial barrier function by modulating tight junction proteins, Am J Physiol Gastrointest Liver Physiol, 301(2)

25. Chesne, C., 2017 Personal Communication, Biopredic International, Rennes, France

26. Christoffels, V.M., Sassi, H.,Ruijter, J.M., Moorman, A.F.M., Grange, T., Lamers W.H., 1999. A mechanistic model for the development and maintenance of portocentral gradients in gene expression in the liver, *Hepatology* 29(4), 1180-1192

27. Christoffels, VM., Habets, PE., Das, AT., Clout, DF., Moorman, AH., Lamers, WA., Van Roon, M., 2000. A single regulatory module of the carbamoylphosphate synthetase I gene executes its hepatic program of expression. *Journal of Biological Chemistry, 275*(51), 40020-40027

28. Curtis, ASG., Gadegaard, N., Dalby, MJ., Riehle, MO., Wilkinson, CDW., Aitchison, G., 2004., Cells react to nanoscale order and symmetry in their surroundings. *NanoBioscience, IEEE Transactions on*, 3(1), pp.61-65

29. Czysz, K., Minger, S., and Thomas, N., 2015. DMSO efficiently downregulates pluripotency genes in human embryonic stem cells during definitive endoderm derivationand increases the proficiency of hepatic differentiation. *PLOS one*, 10(2): e0117689

30. Dalby, M., Gadegaard, N., Tare, R., Andar, A., Riehle, P H., Wilkinson, C., and Oreffo, R., 2007. The control of human mesenchymal cell differentiation using nanoscale symmetry and disorder. *Nature Materials*, doi:10.1038/nmat2013

31. Daly, A.K., 2007. *Phase II metabolism*, London: Henry Stewart Talks

32. Dejanovic, B., Stevanovic, I., Ninkovic, M., Stojanovic, I., Lavrnja, I., and Radicevic, T., 2016. Protective effects of agmatine against chlorpromazine-induced toxicity in the liver of wistar rats, *Acta facultatis medicae naissensis* DOI: 10.1515/afmnai-2016-0002

33. Dorsemus, D., George, E., Dealy, C., and Nukavarapu, S. 2017. Harnessing external cues: development and evaluation of an in vitro culture system for osteochondral tissue engineering. Tissue engineering Part A. vol. 23(15-16):719-737

34. Elkayam, T., Amitay-Shaprut, S., Dvir-Ginzberg, M., Harel, T., Cohen, S., 2006. Enhancing the drug metabolism activities of C3A–a human hepatocyte cell line–by tissue engineering within alginate scaffolds. Tissue Eng, 12:1357–68

35. Ellis, AJ, Hughes, RD, Wendon, JA, Dunne, J, Langley, PG, Kelly, JH., Gislason, GT., Sussman, NL., Williams, R., 1996. Pilot-controlled trial of the extracorporeal liver assist device in acute liver failure. *Hepatology* 24:1446–51. [PubMed]

36. Eun, JW, Bae, HJ, Shen, Q., Park, SJ., Kim, HS, Shin, WC., Yang, HD., Jin, CY., You, JS., Kang, HJ, Kim, H., Ahn, YM., Park, WS., Lee, JY., Nam, SW., 2015. Characteristic molecular and proteomic signatures of drug-induced liver injury in a rat model. *Journal of Applied Toxicology 35*(2):152-164.

37. Fantin, VR., St-Pierre, J., Leder, P. 2006 Attenuation of LDH-A expression uncovers a link between glycolysis, mitochondrial physiology, and tumor maintenance. *Cancer Cell* Vol 9, Issue 6 pp425-434

38. Filipp,i C., Keatch, SA., Rangar, D., Nelson, LJ., Hayes, PC., Plevris, JN., 2004. Improvement of C3A cell metabolism for usage in bioartificial liver support systems. *J Hepatol* ;41:599–605.

39. Galli, C., Piemontese, M., Lumetti, S., Ravanetti, F., Macaluso, G.M., and Passeri, G., 2012. Actin cytoskeleton controls activation of Wnt/B-catenin signalling in mesenchymal cells on implant surfaces with different topographies. *Acta Biomaterialia* (8): 2963-2968

40. Gamal, W (2015) Real-time bioimpedance measurements of stem cell based disease models on a chip, PhD., The University of Edinburgh

41. Gamal, W., Treskes, P., Samuel, K., Sullivan, G., Siller, R., Srsen, V., Morgan, K., Bryans, A., Kozlowska, A., Underwood, I., Smith, S., Del-Pozo, J., Moss, S., Thompson, AI., Henderson, NC., Hayes, PC., Plevris, JN., Bagnaninchi, PO., Nelson, LJ., 2017. Low-dose acetaminophen induces early disruption of cell-cell tight junctions in human hepatic cells and mouse liver. *Scientific Reports, 7*, 37541.

42. Gerich, J., Meyer, C., Woerle, HJ., and Stumvoll, M. 2001. Renal gluconeogenesis - Its importance in human glucose homeostasis. *Diabetes Care*, 24(2), pp.382–391.

43. Germain, T., Favelier, S., Cercueil, JP., Denys, A., Krause, D., Guiu, B., 2014. Liver segmentation: Practical tips. *Diagnostic and Interventional Imaging*, 95(11), pp.1003–1016.

44. Gerets, H., Tilmant, J., Gerin, K., Chanteux, B., Depelchin, O., Dhalluin, S., Atienzar, FA., 2012. Characterization PHHs, including expression of primary human hepatocytes, HepG2 cells, and HepaRG cells at the mRNA Level and CYP activity in response to inducers and their predictivity for the detection of human hepatotoxins. *Cell Biol Toxicol* 28:69–87. [PubMed]

45. Giaever, I. and. Keese, CR., 1984. *Monitoring Fibroblast Behaviour in Tissue Culture with an Applied Electric Field.* Proceedings of the National Academy of Sciences of the United States of America, **81**(12): p. 3761-3764.

46. Giaever, I. and Keese CR., 1991. Micromotion of mammalian cells measured electrically. *Natl. acad Sci* 88:7896-7900

47. Giancotti, FG. And Ruoslahti, E., 1999. Integrin signalling. *Science* 285:1028–32. [PubMed]

48. Gómez-Lechón, MJ., Laho,z A., Gombau, L., Castell, JV., Donato, MT., 2010. *in vitro* evaluation of potential hepatotoxicity induced by drugs. *Current Pharmaceutical Design*, (16), 000-000 1

49. Gov.uk, Guidance on Animal testing and research published 2013, Animals for Scientific Procedures Act updated March 2018, (Retrieved 02/04/18) 1986 Ref https://www.gov.uk/guidance/research-and-testing-using-animals)

50. Grime, K., Ferguson, D., Riley, R., 2010. The use of HepaRG and human hepatocyte data in predicting CYP induction drug-drug interactions via static equation and dynamic mechanistic modelling approaches. *Curr Drug Metab* 11:870–85.

51. Gripon, P., Rumin, S., Urban, S., Le Seyec, J., Glaise, D., Cannie, I., Guyomard, C., Josette,Lucas,. Christian, T., Guguen-Guillouzo, C., 2002. Infection of a human hepatoma cell line by hepatitis B virus. Proceedings of the National Academy of Sciences of the United States 99.24; 15655.

52. Guguen-Gouillozo, C., Corlu, A., and Gouillozo, A., 2010. Stem cell derived hepatocytes and their use in toxicology, Toxicology 270(1) 3-9

53. Guguen Guilliozo, C., 2014 Personal Communication, Biopredic International, Rennes, France

54. Guillaume F. and Otto SP., 2012. Gene Functional Trade-Offs and the Evolution of Pleiotropy. *Genetics*. 192(4):1389-1409. doi:10.1534/genetics.112.143214.

55. Gunness, P., Mueller, D., Shevchenko, V., Heinzle, E., Ingleman, MS., Noor, F., 2013. 3D Organotypic cultures of human HepaRG cells: a tool for toxicity studies. *Toxicol Sci* 133:67–78.

56. Hariparsad, N., Carr, B., Evers, R., & Chu, X., 2008. Comparison of drug disposition gene exression between FA2N-4 immortalized cells and human hepatocytes: evaluation of FA2N-4 as an *in vitro* model for cytochrome p450 induction. *Drug Metabolism Reviews, 40*, 87.

57. Hart, S., Li, Y., Nakamoto, K., Subileau, E., Steen, D., & Zhong, X., 2010. A comparison of whole genome gene expression profiles of HepaRG cells and HepG2 cells to primary human hepatocytes and human liver tissues. *Drug Metabolism and Disposition: The Biological Fate of Chemicals, 38*(6), 988-94.

58. Hine, R., & Martin, E., (Eds.), 2016. A Dictionary of Biology: Transferrin. Oxford University Press. Retrieved 12 Apr. 2018, from http://www.oxfordreference.com.ezproxy.is.ed.ac.uk/view/10.1093/acref/9780198714378.001.0001/acref-9780198714378-e-4498.

59. Izdebska, J., 2015. Corona Treatment. In *Printing on Polymers: Fundamentals and Applications* (pp. 123-142). Elsevier.

60. Jaggessar, A., Shahali, H., Mathew, A., & Yarlagadda, P., 2017. Bio-mimicking nano and micro-structured surface fabrication for antibacterial properties in medical implants. *Journal Of Nanobiotechnology, 15*(1), 64.

61. Jemnitz K, Veres Z, Monostory K, Kobori L, Vereczkey L., 2008. Interspecies differences in acetaminophen sensitivity of human, rat, and mouse primary hepatocytes. *Toxicol in vitro*; 22:961–967

62. Kanebratt, K., & Andersson, T., 2008. Evaluation of HepaRG cells as an *in vitro* model for human drug metabolism studies. *Drug Metabolism and Disposition: The Biological Fate of Chemicals, 36*(7), 1444-52.)

63. Keitzmann, T. (2017). Metabolic zonation of the liver: The oxygen gradient revisited. Redox biology, 11, 622-630.

64. Kim, M., Lee, B., Yang, K., Park, J., Jeon, S., Um, S., Kim, D., Im, S., and Cho, S., 2013. BMP-2 peptide-functionalized nanopatterned substrates for enhanced osteogenic differentiation of human mesenchymal stem cells. *Biomaterials* 34 7236-7246

65. Kobayashi, K., Oshima, K., Chiba, K., Nakajima, M., Yokoi, T., & Shimada, N. (1999). Involvement of CYP2E1 as a low-affinity enzyme in phenacetin O- deethylation in human liver microsomes. *Drug Metabolism and Disposition, 27*(8), 860-865.

66. Krasowska A, Sigler K., 2014. How microorganisms use hydrophobicity and what does this mean for human needs? *Frontiers in Cellular and Infection Microbiology*, 4:112. doi:10.3389/fcimb.2014.00112.

67. Kubo, T., Kuroda, Y., Hojvo, M., Kim, SR., Horiuchi, S., Sekino, Y., Morel, F., Corlu, A., and Ishida, S. (2016) Maintenance of Hepatic Progenitor-like Characteristics of HepaRG Cells by Cultivation on VECELL Inserts, AATEX 21(2), 71-79

68. Kumar, A., 2018 Sweet Biochemistry: Remembering structures, cycles and pathways by mnemonics, Academic Press, pp1-5 https://doi.org/10.1016/B978-0-12-814453-4.00001-7

69. Lackie, J., 2010. islets of Langerhans. *A Dictionary of Biomedicine*, pp.A Dictionary of Biomedicine.

70. Le Vee, M., Jouan, E., Stieger, B., & Fardel, O., 2013. Differential regulation of drug transporter expression by all-trans retinoic acid in hepatoma HepaRG cells and human hepatocytes.(Report). *European Journal of Pharmaceutical Sciences, 48*(4-5), 767.

71. Lee, L.C.Y., Gadegaard, N.,de Andres, M.C., Turner, L.A., Burgess, K.V., Yarwood, S.J., Wells, J., Salmeron-Sanchez, M., Meek, D., Oreffo, R.O.C., and Dalby, M.J., 2017. Nanotopography controls cell cycle changes involved with skeletal stem cell self-renewal and multipotency. *Biomaterials*, 116, 10-20

72. Leite, S.B. et al., 2012. Three-Dimensional HepaRG Model As An Attractive Tool for Toxicity Testing. *Toxicological Sciences*, 130(1), pp.106–116.

73. Lemaigre, F. P., & Rousseau, G. G. 1994. Transcriptional control of genes that regulate glycolysis and gluconeogenesis in adult liver. *The Biochemical journal*, *303 (Pt 1)*(Pt 1), 1-14.

74. Lin, L., Wang, H., Ni, M., Rui, Y., Cheng, T., Cheng, CK., Pan, X., Li, G., Lin, C., 2014. Enhanced osteointegration of medical titanium implant with surface modifications in micro/nanoscale structures. *Journal of Orthopaedic*
Translation, 2(1), 35-42.

75. Lockman, KA., Baren, JP., Pemberton, HB., Burgess, KE., Plevris-Papioannou, N., Lee, P., Howie, F., Beckett, G., Pryde,A., Jaap, AJ., Hayes, PC., Filippi, C., Plevris, JN., 2012. Oxidative stress rather than triglyceride accumulation is a determinant of mitochondrial dysfunction in *in vitro* models of hepatic cellular steatosis, *Liver Int'l,* Vol 32, issue 7, pp. 1079-1092

76. Lockman, KA., Htun, V., Sinha, R., Treskes, P, Nelson, J., Martin, SF., Rogers, SM., Le Bihan, T., Hayes, PC., Plevris, JN., 2016. Proteomic profiling of cellular steatosis with concomitant oxidative stress *in vitro*, *Lipids Health Dis*. 15:114

77. Lu Y., Cederbaum AI., 2008. CYP2E1 and oxidative liver injury by alcohol. *Free Radic Biol Med,* 44:723–38.

78. Lübberstedt et al., 2011. HepaRG human hepatic cell line utility as a surrogate for primary human hepatocytes in drug metabolism assessment in vitro. *Journal of Pharmacological and Toxicological Methods*, 63(1), pp.59–68.

79. Lunt SY.and Vander Heiden, MG. 2011.Aerobic Glycolysis: Meeting the Metabolic Requirements of Cell Proliferation Annual Review of Cell and Developmental Biology 27:1, 441-464

80. Ma, Q., 2013. Role of NRF2 in oxidative stress and toxicity, Annu Rev Pharmacol *Toxicol.* 53: 401-426

81. Ma, Xin et al., 2017. Expression of glutathione S-transferase A1, a phase II drug-metabolizing enzyme in acute hepatic injury on mice. *Experimental and therapeutic medicine*, 14(4), pp.3798–3804

82. Magnon, C., and Frenette, PS., 2008. Hematopoietic stem cell trafficking, StemBook, ed. The Stem Cell Research Community, doi/10.3824/stembook.org

83. Martignoni, M., Groothuis, G., & De Kanter, R., 2006. Comparison of mouse and rat cytochrome P450-mediated metabolism in liver and intestine. *Drug Metabolism and Disposition: The Biological Fate of Chemicals, 34*(6), 1047-54.

84. Martines, E., Seunarine, K., Morgan, H., Gadegaard, N., Wilkinson, C.D.W., and Riehle, M.2005. Superhydrophobicity and superdhydrophilicity of regular nanopatterns. *Nano Letters* 5 (10), 2097-2103

85. Martucci, NJ., Morgan, K., Anderson, GW., Hayes, PC., Plevris, J., Nelson, LJ., Bagnaninchi, PO., 2018. Nondestructive Optical Toxicity Assays of 3D Liver Spheroids with Optical Coherence Tomography *Adv. Biosys*, 2, 1700212. https://doi.org/10.1002/adbi.201700212

86. Marx, V., 2013. PCR: living life amplified and starndardized, *Nature Methods* 10(5), 391-395 doi:10.1038/nmeth.2443

87. Matsuo, S., Ogawa, M., Muckenthaler, M.U., Mizui, Y., Sasaki, S., Fujimura, T., Takizawa, M. Ariga, N., Oaki. H., Sakaguchi, M., Gonzalez, F.J., and Inoue, Y., 2015. Hepatocyte Nuclear Factor 4α Controls Iron Metabolism and Regulates Transferrin Receptor 2 in Mouse Liver. *J Biol Chem*. 290(52): 30855-30865

88. Micholt, L., Gartner, A., Prodanov, D., Dotti, C.G., and Bartic, C., 2013. Substrate topography determines neuronal polarization and growth *in vitro, PLOS ONE* 8(6): e66170. https://doi.org/10.1371/journal.pone.0066170

89. Moedas et al., 2017. Advances in methods for characterization of hepatic urea cycle enzymatic activity in HepaRG cells using UPLC-MS/MS. *Analytical Biochemistry*, 535(C), pp.47–55.

90. Moradpour, D., Altorfer, J., Flury, R., Greminger, P., Meyenberger, C., Schmid, M., 1994. Chlorpromazine-induced vanishing bile duct syndrome leading to biliary cirrhosis. *Hepatology* 1994:20:1437–1441. doi:10.1002/hep.1840200610

91. Morgan, K., 2014. Evaluation of C3A and HepaRG cells and their ability to metabolise the drug phenacetin in vitro for reduction/replacement of animals in pharmaceutical applications, BSc Hons, Edinburgh Napier University.

92. Mohan, C., Sreerekha, P., Divyarani, V., Nair, S., Chennazhi, K., & Menon, D., 2012. Influence of titania nanotopography on human vascular cell functionality and its proliferation *in vitro*. *Journal Of Materials Chemistry, 22*(4), 1326-1340.

93. National Center for Biotechnology Information, SOX9, U.S. National Library of Medicine_8600 Rockville Pike, Bethesda MD, 20894 USA, Accessed March 18, 2018 at https://www.ncbi.nlm.nih.gov/gene?Db=gene&Cmd=ShowDetailView&TermToSearch=6662

94. Nebela, O., Slepicka, P., Svorcik, V., 2017. Surface Modification of Polymer Substrates for Biomedical Applications, *Materials*, 10(10) 1115 doi:10.3390/ma1010115

95. Nelson, LJ., Navarro, M., Treske,s P., Samuel, K., Tura-Ceide, O., Morley, S., Hayes, P., and Plevris, J., 2015. Acetaminophen cytotoxicity is ameliorated in a human liver organotypic co-culture model, *Scientific Reports*, (5):17455

96. Nelson, L., Morgan, K., Treskes, P., Samuel, K., Henderson, C., LeBled, C., Homer, N., Grant, HM., Hayes, PC., Plevris, J., 2017. Human Hepatic HepaRG Cells Maintain an Organotypic Phenotype with High Intrinsic CYP450 Activity/Metabolism and Significantly Outperform Standard HepG2/C3A Cells for Pharmaceutical and Therapeutic Applications. *Basic & Clinical Pharmacology & Toxicology, 120*(1), 30-37.

97. Newsome, PN., Plevris, JN., Nelson, LJ., Hayes, PC., 2000. Animal models of fulminant hepatic failure: a critical evaluation. *Liver Transpl* 6:21–31. [PubMed]

98. Oinonen, T. & Lindros, K.O., 1998. Zonation of hepatic cytochrome P-450 expression and regulation. The Biochemical journal, 329 (Pt 1), pp.17–35.

99. Olin, P., Lindstrom, S.B., Pettersson, T. and Wagberg, L., (2013) Water drop friction on superhydrophobic surfaces (29), 9079-9089DOI: 10.1021/la401152b

100. Pal, R., Marmidi, K., Kumar Das, A., Bhonde, R., 2012. Diverse effects of dimethyl sulfoxide (DMSO) on the differentiation potential of human embryonic stem cells, *Archives of Toxicology*, 86 (4) 651-661

101. Park, Y., Smith, R.D., Combs, A.B., Kehrer, J.P., 1988. Prevention of acetaminophen-induced hepatotoxicity by dimethyl sulfoxide, *Toxicology* 14;52(1-2): 165-75

102. Pasmant, E., Goussard, P., Baranes, L., Laurendeau, I., Quentin, S., Ponsot, P., Consigny, Y., Farges, O., Condat, B., Viduad, D., Viduad, M.,.Chen, JM., Parfait, B., (2011). First description of ABCB4 gene deletions in familial low phospholipid-associated cholelithiasis and oral contraceptives-induced cholestasis. *European Journal of Human Genetics, 20*(3), 277-82.

103. Poncy, A., Antoniou, A., Cordi, S., Pierreux, C.E., Jacquemin, P., Lemaigre, F.P. 2015. Transcription factors SOX4 and SOX9 cooperatively control development of bile ducts, *Developmental Biology*, Vol 4 (2) 136-148

104. Prot, JM, Aninat, C, Griscom, L, Razan, F, Brochot, C, Guillouzo, CG., Legallais, C., Corlu, A., Lecler, E., 2011. Improvement of HepG2/C3a cell functions in a microfluidic biochip. *Biotechnol Bioeng* 2011;108:1704–15.

105. Qian, T. and Wang, Y., 2010. Micro/nano-fabrication technologies for cell biology, *Med Bio Eng Comput* 48:1023-1032

106. Raimondi, F., Santoro, P., Barone, MV., Pappacoda, S., Barretta, ML., Nanayakkara, M., Apicella, C., Capasso, L., Paludetto, R., 2008. Bile acids modulate tight junction structure and barrier function of Caco-2 monolayers via EGFR activation, Am J Physiol Gastrointest Liver Physiol 294(4)

107. Ramsey, W., Hertl, W., Nowlan, E., Binkowski, N., 1984. Surface treatments and cell attachment. *in vitro, 20*(10), 802-808.

108. Rang, H.P. & Dale, M.M., 2007. Rang and Dale's pharmacology Sixth., Philadelphia, Pa.: Churchill Livingstone/Elsevier.

109. Rappaport AM., 1958. The structural and functional unit in the human liver (liver acinus). *Anat Rec*; 130: 673–689.

110. Rines, A. K., Sharabi, K., Tavares, C. D., & Puigserver, P. (2016). Targeting hepatic glucose metabolism in the treatment of type 2 diabetes. *Nature reviews. Drug discovery*, *15*(11), 786-804.

111. Sanchez, A. et al. Fibronectin regulates morphology, cell organization and gene expression of rat fetal hepatocytes in primary culture. J. Hepatol. 32, 242–250 (2000).

112. Schernthaner, M., Reisinger, B., Wolinski, H., Kohlwein, S., Trantina-Yates, A., Fahrner, M., Romanin, C., Itani, H., Stifter, D., Leitinger, G., Groschner, K., and Heitz, J., 2012. Nanopatterned polymer substrates

promote endothelial proliferation by initiation of B-catenin transcriptional signalling. *Acta Biomaterialia* 8 : 2953-2962

113. Schevchenko, V., 2014. Personal Communication, Biopredic International, Rennes, France.

114. Sharanek, A., Burban, A., Humbert, L., Bachour-El Azzi, P., Felix-Gomes, N., Rainteau, D., & Guillouzo, A., 2015. Cellular Accumulation and Toxic Effects of Bile Acids in Cyclosporine A-Treated HepaRG Hepatocytes. *Toxicological Sciences, 147*(2), 573-587.

115. Shin, Dae-Seop et al., 2018. Quantitative Evaluation of Cytochrome P450 3A4 Inhibition and Hepatotoxicity in HepaRG 3-D Spheroids. *International Journal of Toxicology*, 37(5), pp.393–403.

116. Stolwijk, J., Hartmann, C, Balani, P., Alberman, S., Keese, C.R., Giaever, I., and Wegener, J,. 2011 Impedance analysis of adherent cells after in situ electroporation: Non-invasive monitoring during intracellular manipulations*, Biosensors and Bioelectronics* 26, 4720-4727

117. Stormonth-Darling, JM., Gadegaard, N., 2012. Injection moulding difficult nanopatterns with hybrid polymer inlays, *Macromolecular Materials and Engineering*, Vol.297(11), pp.1075-1080

118. Spears Graber, T., 2018. Main segments of liver, [Water color, gouache] personal illustration

119. Szabo, M., Veres, Z., Baranyai, Z., Jakab, F., and Jemnitz, K. (2013) Comparison of Human Hepatoma HepaRG cells with Human and Rat Hepatocytes in Uptake Transport Assays in Order to Predict a Risk of Drug Induced Hepatotoxicity, PLOS one, March 2013 vol 8 issue 3

120. Takiya, CM., Diaz Paredes, B., de Mesquita, L., Dias, GS., Faccioli, L., Takami,T., Terai, S., Sakaida, I., Santos Goldenberg, RC., 2013. Chapter 10 - Liver Resident Stem Cell, Editor(s): Regina Coeli dos Santos Goldenberg, Antonio Carlos Campos de Carvalho,Resident Stem Cells and Regenerative Therapy, Academic Press, , Pages 177-203, ISBN 9780124160125

121. Tebbi, A., Levillayer, F., Jouvion, G., Fiette, L., Soubigou, G., Varet, H., Boudjadja, N., Cairo, S., Hashimoto, Suzuki, A., Carninci, P., Carissimo, A., Di Bernardo, D., Wei, Y., 2016. Deficiency of multidrug resistance 2 contributes to cell transformation through oxidative stress, Carcinogenesis, Vol .37(1), pp39-48

122. Tonge et al., 1998. Role of CYP1A2 in the Hepatotoxicity of Acetaminophen: Investigations UsingCyp1a2Null Mice. Toxicology and Applied Pharmacology, 153(1), pp.102–108.

123. Tougeron, D., Fosting, G., Barbu, V., Beauchant, M., 2012. ABCB4/MDR3 gene mutations and cholangiocarcinomas. *Journal of Hepatology, 57*(2), 467-468.

124. Tsiaoussis, J., Newsome, PN., Nelson, LJ., Hayes, PC., Plevris, JN., 2001. Which hepatocyte will it be? Hepatocyte choice for bioartificial liver support systems, *Liver Transpl,* 7:2–10. [PubMed]

125. Turpeinen, M., Ghiciuc, C., Opritoui, M., Tursas, L., Pelkonen, O., Pasanen, M., 2007 Predictive value of animal models for human cytochrome P450 (CYP)-mediated metabolism: a comparative study *in vitro Xenobiotica*, 37, pp. 1367-1377

126. Vandesompele, J., De Preter, K., Pattyn F., Poppe, B., Van Roy, N., De Paepe, A., and Speleman, F. 2002. Accurate normalization of real-time quantitative RT-PCR data by geometric averaging of multiple internal control genes. *Genome Biology* 3(7) Research 0034.1-0034.11

127. Van Wenum, MA., Adam, AA., Van der Mark, VC., Chang, JE., Wildenberg, MP., Hendriks, EJ., Jongejan, A., Moerland, PD., van Gulik, TM., Oude Elferink, RP., Chamuleau, RAFM., Hoekstra, R., 2018. Oxygen drives hepatocyte differentiation and phenotype stability in liver cell lines. *Journal of Cell Communication and Signaling,* 1-14.

128. Vermeir, M., Annaert, P., Mamidi, RN., Roymans, D., Meuldermans, W., Mannens, G., 2005. Cell-based models to study hepatic drug metabolism and enzyme induction in humans. *Expert Opin Drug Metab Toxicol*, 1:75–90. [PubMed]

129. Vieu, C., Carcenac,F, Pepin, A., Chen, Y., Mejias, M., Lebib, A., Manin-Ferlazzo, L., Couraud, L., Launois, H., 2000. Electron beam lithography: Resolution limits and applications. *Applied Surface Science, 164*, 111-117.

130. Wasmuth, HE., Glantz, A, Keppeler, H., Simon, E., Bartz, C., Rath, W., Mattsson, LA., Marschall, HU., Lammer, F., 2007. Intrahepatic cholestasis of pregnancy: the severe form is associated with common variants of the hepatobiliary phospholipid transporter ABCB4 gene, *Gut*, 56(2), pp.265-270

131. Wang, Y. et al., 2016. ECM proteins in a microporous scaffold influence hepatocyte morphology, function, and gene expression. Scientific Reports, 6(1), p.37427.

132. Wang, Ying-Jie et al., 2004. Primary hepatocyte culture in collagen gel mixture and collagen sandwich. World journal of gastroenterology, 10(5), pp.699–702.

133. Waxman, AB. and Kolliputi, N., 2009. IL-6 protects against hyperoxia-induced mitochondrial damage via BCL-2-induced Bak interactions with mitofusins. *Am J Respir Cell Mol Biol.* 41(4):385-96

134. Wegener, J, Keese, CR, Giaever, I., 2000. Electric cell-substrate impedance sensing (ECIS) as a noninvasive means to monitor the kinetics of cell spreading to artificial surfaces. *Experimental Cell Research* 259:158-166

135. Wei, C. J., Pan, W. S., & Hung, M., 2013. The effects of substrate roughness and associated surface properties on the biocompatibility of diamond-like carbon films. *Surface and Coatings Technology, 224*, 8-17.

136. Wiśniewski, JR., Vildhede, A., Norén, A., Artursson, P., 2016. In-depth quantitative analysis and comparison of the human hepatocyte and hepatoma cell line HepG2 proteomes. *Journal of Proteomics, 136*, 234-247.

137. Woolbright, BL., McGill, MR., Yan, H., Jaeschke, H., 2016. Bile Acid-Induced Toxicity in HepaRG Cells Recapitulates the Response in Primary Human Hepatocytes. *Basic Clin Pharmacol Toxicol*. 118(2):160-7. doi: 10.1111/bcpt.12449.

138. Xiao, C. and Luong, J., 2003. On-line monitoring of cell growth and cytotoxicity using Electric Cell-Substrate Impedance Sensing (ECIS), Biotechnology Progress, Vol.19(3), pp1000-1005

139. Xing, Q., Gao, R, Li, H., Feng, G., Xu, M., Duan, S., Meng, J., Zhang, A., Qin, S., He, L., 2006. Polymorphisms of the ABCB1 gene are associated with the therapeutic response to risperidone in Chinese Schizophrenia patients, *Pharmacogenomics*, Vol 7(7), pp.987-93.

140. Xu, C., Li, C. & Kong, Y.-T., 2005. Induction of phase I, II and III drug metabolism/transport by xenobiotics. Archives of Pharmacal Research, 28(3), pp.249–268.

141. Xu, M., McCanna, D., and Sivak, J. (2014) Use of the viability reagent PrestoBlue in comparison with alamarBlue and MTT to assess the

viability of human corneal epithelial cells *Journal of Pharm and Tox Meth* 71 1-7

142. Yim, E.K.F., Reano, R.M., Pang, S.W., Yee, A.F., Chen, C.S. and Leong, K.W., 2005. Nanopattern-induced changes in morphology and motility of smooth muscle cells. *Biomaterials* 26(26): 5405-5413

143. Yoon, CJ., Puigserver P, Chen, G., Donovan, J., Wu, Z., Rhee, J., Adelmant, G., Stafford, J., Kahn, RC., Granner, DK., Newgard, CB., and Spiegelman, BM. 2001. Control of hepatic gluconeogenesis through the transcriptional coactivator PGC-1, *Nature*, 413, 131-138

144. Yu, W., Hawley, TS., Hawley, RG., Qu, C., 2002. Role of the docking protein Gab2 in beta (1)-integrin signalling pathway-mediated hematopoietic cell adhesion and migration, Blood, 99(7),pp2351-9

145. Yu, Y., Fisher, JE., Lillegard, JB., Rodysill, B., Amiot, B., Nyberg, SL., 2012. Cell therapies for liver diseases. *Liver Transpl* 18:9–21. [PubMed]

146. Zanger & Schwab, 2013. Cytochrome P450 enzymes in drug metabolism: Regulation of gene expression, enzyme activities, and impact of genetic variation. Pharmacology and Therapeutics, 138(1), pp.103–141.

147. Zareidoost, A., Yousefpour, M., Ghaseme, B. and Amanzadeh, A., 2012. The relationship of surface roughness and cell response of chemical surface modification of titanium. *J Mater Sci Mater Med* 23(6): 1479-148

148. Zeigerer et al., 2017. Functional properties of hepatocytes in vitro are correlated with cell polarity maintenance. Experimental Cell Research, 350(1), pp.242–252.

149. Zhang, W., 2017. Gluconeogenesis. Introductory Chapter InTech Gluconeogenesis. http://dx.doi.org/10.5772/intechopen.6980, DOI:10.5772/63700

150. Zimmerman, HJ., Lewis, JH., 1987. Drug-induced cholestasis. Medical Toxicology 2:2:112-160